EVALUATING THE IMPACT OF SURFACE CHEMISTRY ON ADHESION OF POLYMERIC SYSTEMS UNDERWATER BY MEANS OF CONTACT MECHANICS

by

NASIM RAHMANI

B.S., Iran University of Science and Technology, 2004
M.S., KN Toosi University of Technology, 2006

AN ABSTRACT OF A DISSERTATION

submitted in partial fulfillment of the requirements for the degree

DOCTOR OF PHILOSOPHY

Department of Mechanical and Nuclear Engineering
College of Engineering

KANSAS STATE UNIVERSITY
Manhattan, Kansas

2015

Abstract

The overall goal of this study was to assess the effects of surface chemistry on adhesion of polymeric systems underwater. The adhesion is quantified by the thermodynamic work of adhesion (W) when two surfaces are approached and the energy release rate (G) when the surfaces are separated. For some polymeric systems there is a difference between W and G, referred to as adhesion hysteresis. For this study an experimental approach based upon Johnson-Kendall-Roberts (JKR) theory of contact mechanics was utilized to evaluate how surface chemistry affects the adhesion behavior (both W and adhesion hysteresis) in the presence of water. The interfacial interactions were also studied in air and contrasted to those obtained underwater.

To accomplish the overall goal of this research, this study was divided into two phases where smooth model surfaces with disparate surface chemistries were used. The model surfaces in the first part included poly(dimethysiloxane) (PDMS), glass surfaces chemically functionalized to display hydrophilic to medium to hydrophobic characteristics, and thin films of wood-based biopolymers. The functionalities used to modify glass surfaces included polyethylene oxide (PEO) with hydrophilic nature; amine, carbomethoxy, and mercapto (thiol) with intermediate characteristics; cyclohexyl, fluorocarbon, and methyl with hydrophobic behavior. In addition to these surfaces, flat PDMS and clean glass surfaces were also used for means of comparison. The wood-derived polymers included two different cellulose types (natural cellulose and regenerated cellulose) as well as one lignin surface (from hardwood milled lignin). These surfaces were probed with native PDMS hemispheres, which are hydrophobic. The results showed that in air the value of W for all model surfaces was independent of the surface chemistry, except fluorocarbon which was lower. Underwater W was significantly

affected by the surface hydrophilicity/ hydrophobicity. The adhesion hysteresis both in air and underwater was significantly dependent on the structure of the probed surface.

For the second phase PDMS hemispheres were chemically modified with amine functionality to probe model surfaces with hydrophilic and intermediate behavior. These surfaces included glass surfaces functionalized with PEO and amine as well as PDMS sheets that were functionalized with amine. Native PDMS flat surfaces were also used for means of comparison. The results showed that for the selected surfaces both W and hysteresis were affected by the surface chemistry in both media.

EVALUATING THE IMPACT OF SURFACE CHEMISTRY ON ADHESION OF POLYMERIC SYSTEMS UNDERWATER BY MEANS OF CONTACT MECHANICS

by

NASIM RAHMANI

B.S., Iran University of Science and Technology, 2004
M.S., KN Toosi University of Science and Technology, 2006

A DISSERTATION

submitted in partial fulfillment of the requirements for the degree

DOCTOR OF PHILOSOPHY

Department of Mechanical and Nuclear Engineering
College of Engineering

KANSAS STATE UNIVERSITY
Manhattan, Kansas

2015

Approved by:

Major Professor
Kevin B. Lease

Copyright

Abstract

The overall goal of this study was to assess the effects of surface chemistry on adhesion of polymeric systems underwater. The adhesion is quantified by the thermodynamic work of adhesion (W) when two surfaces are approached and the energy release rate (G) when the surfaces are separated. For some polymeric systems there is a difference between W and G, referred to as adhesion hysteresis. For this study an experimental approach based upon Johnson-Kendall-Roberts (JKR) theory of contact mechanics was utilized to evaluate how surface chemistry affects the adhesion behavior (both W and adhesion hysteresis) in the presence of water. The interfacial interactions were also studied in air and contrasted to those obtained underwater.

To accomplish the overall goal of this research, this study was divided into two phases where smooth model surfaces with disparate surface chemistries were used. The model surfaces in the first part included poly(dimethysiloxane) (PDMS), glass surfaces chemically functionalized to display hydrophilic to medium to hydrophobic characteristics, and thin films of wood-based biopolymers. The functionalities used to modify glass surfaces included polyethylene oxide (PEO) with hydrophilic nature; amine, carbomethoxy, and mercapto (thiol) with intermediate characteristics; cyclohexyl, fluorocarbon, and methyl with hydrophobic behavior. In addition to these surfaces, flat PDMS and clean glass surfaces were also used for means of comparison. The wood-derived polymers included two different cellulose types (natural cellulose and regenerated cellulose) as well as one lignin surface (from hardwood milled lignin). These surfaces were probed with native PDMS hemispheres, which are hydrophobic. The results showed that in air the value of W for all model surfaces was independent of the surface chemistry, except fluorocarbon which was lower. Underwater W was significantly

affected by the surface hydrophilicity/ hydrophobicity. The adhesion hysteresis both in air and underwater was significantly dependent on the structure of the probed surface.

For the second phase PDMS hemispheres were chemically modified with amine functionality to probe model surfaces with hydrophilic and intermediate behavior. These surfaces included glass surfaces functionalized with PEO and amine as well as PDMS sheets that were functionalized with amine. Native PDMS flat surfaces were also used for means of comparison. The results showed that for the selected surfaces both W and hysteresis were affected by the surface chemistry in both media.

Table of Contents

List of Figures

List of Tables

Acknowledgements

First and foremost, I am very grateful to my major advisor, Dr. Kevin Lease. This work would not have been possible without all his genuine supports throughout the years I was at Kansas State University. I appreciate him for letting me grow on a personal basis as well as giving me the freedom and support to become an independent researcher. I felt very fortunate to have him as my advisor.

I would like to thank Dr. Christopher Culbertson for his involvement in this project and helping me interpret and explain the results. He also allowed me to work in his lab and use the resources therein. He also arranged for using other equipment on campus if needed.

Also thank to my dissertation committee members (in the alphabetical order): Dr. Christer Aakeroy, Dr. Amy Betz, Dr. Christopher Culbertson, Dr. Xiuzhi Susan Sun, and Dr. Jack Xin.

I thank the past and current members of Dr. Culbertson's research laboratory; Dr. Eve Metto, Dr. Neluni Perrera, Shu Jia, Damith Patabad, Kathleen Sellens, and Jay Sibbitts for their help, for instructing me on using the equipment in their lab or acquiring the chemicals I needed from other labs in the Chemistry Department at KSU.

Thanks to Mr. James Hodgson, the glassblower specialist in the Chemistry Department at KSU, for his initial suggestions on the zigzag arm design, making it, and fixing it when it would break.

I would also like to thank the Mechanical and Nuclear Engineering Department at Kansas Student University and the faculty members who supported me financially in the form of GTA/GRA.

Last, but not least, special thanks to my family and friends that supported and encouraged me throughout my studies.

Chapter 1 - Introduction

Adhesion of polymeric systems in air has been studied extensively during the past several decades. Understanding the adhesion behavior and interactions of these systems underwater, however, is less developed even though water is present in many biochemical and biological applications. A broader understanding of the adhesion interactions developed underwater can benefit several application areas where an aqueous environment is present, e.g. underwater adhesives (synthetic or bio) [1], anti-fouling coatings [2], protein adsorption [3], development of bacterial biofilms, drug delivery applications, durability of artificial implants [4], and tribological applications (friction and lubrication) in biological systems [5, 6].

The broad motivation behind this research laid in the interest to understand how the interfacial interactions of polymeric systems are altered in the presence of water as compared to those in air. This specific research project focused on one aspect of this overall goal: *the use of model systems to study (at the mesoscopic level) the interfacial interactions of polymeric systems underwater as a function of surface chemistry in a systematic manner.* In order to assess the interactions in a principal manner and merely as a function of surface chemistry, only smooth model surfaces were used in this study to eliminate any contributions from surface roughness or other geometric complexities. Even though model systems may not reproduce the performance of real systems in practical applications, they are widely used in many applications to gain an insight into the fundamental issues of a system and study the potential influence of those fundamental issues on the behavior of the system.

Typically two different categories of experimental techniques are used to evaluate the interfacial interactions between two surfaces [7]. The first consists of nano-scale spectroscopies, such as surface force apparatus (SFA) and atomic force microscopy (AFM). In both of these

methods, the interaction forces are measured as a function of the distance between two surfaces as they approach or retract (both the force and the distance are in the nano-scale). The results of these studies disclose the nature of the interfacial forces as being attractive or repulsive over a range of distances. The second category of test techniques is based on contact mechanics, and is typically used to determine adhesion characteristics in the mesoscopic range. As noted earlier, this is the range focused on in this study. For the purpose of this study an experimental approach based upon the Johnson-Kendall-Roberts (JKR) theory of contact mechanics [8] is used. In the JKR experimental approach a hemisphere (typically made out of a compliant polymeric material) is used to probe other surfaces, referred to substrates. The JKR theory of contact mechanics and its corresponding experimental approach are discussed in more detail in subsequent chapters. But in brief, the JKR theory [8], developed in 1971 by Johnson, Kendall, and Roberts, has made it feasible to determine the thermodynamic work of adhesion and chemical interactions of smooth solid surfaces in a direct manner, as compared to contact angle measurements with different liquid probes. In general, the JKR method (which is based upon the JKR theory) consists of a loading and an unloading process. In the loading process the hemispherical probe and the substrate are pressed together successively while developing a circular contact area. This contact area recedes upon withdrawing the probe and vanishes upon separation. The relationship between the contact area and the applied load during the loading process determines the thermodynamic work of adhesion, which is an indication of the surface forces upon approaching. The adhesion hysteresis (denoted as the difference between the loading and unloading process), if present in a system, can reveal more information regarding other interfacial interactions that may develop [9] or frictional properties [10-12] at the interface of the two surfaces in contact.

The JKR technique has been shown to be a powerful tool to determine the effects of polymer structure variation and/or different surface structures on adhesion of polymeric materials.

The experiments performed to accomplish the goal of the current study were broken down into two phases. In phase I, first a basic yet discriminating set of model surfaces were identified. These surfaces were selected based on the fact that they span a broad spectrum of surface chemistry ranging from hydrophilic to hydrophobic while showing simple and well-studied chemical structures. These basic model surfaces included several functional groups that were chemically applied to glass surfaces and were used as the substrates in the JKR approach. In the second part of phase I, three more advanced model surfaces based upon wood-derived bio-polymers were used as substrates in the JKR experiments to verify whether the results of the basic set could be exploited to prefigure and/or interpret the behavior of more complex systems. Moreover, studying these wood-derived surfaces underwater can benefit several areas, such as papermaking industries or composites and hydrogels that are developed based on wood-derived polymers. It should be noted that in the first phase the polymeric probe was used in its native (un-functionalized) form. For the second phase, and in order to further advance our understanding of the interactions underwater, the probe was chemically modified and used along with a number of chemically modified substrates which were used in the first phase. For means of comparison, the adhesion studies for all surfaces in both phases were carried out in air under lab environment, too.

The remainder of this chapter provides a detailed discussion of “adhesion” and its related topics as well as an overview of the scope of this research. At the end, this chapter terminates with the outline of this document.

Adhesion

Adhesion, despite its broad use in science and technology is a complex phenomenon that has different definitions. In general, "adhesion" can be perceived in three disparate perspectives [13]: (1) basic or fundamental adhesion, (2) thermodynamic or reversible adhesion, and (3) practical adhesion.

Fundamental adhesion is associated with the nature and strength of intermolecular interactions between two materials at the molecular scale. Such interactions include ionic, covalent, metallic, hydrogen bonds or van der Waals forces. The magnitude of these forces, however, cannot be directly measured or calculated for practical systems.

Thermodynamic adhesion is the change in Gibbs free energy when creating a unit area. The adhesion level in this manner is quantified in terms of thermodynamic work of adhesion (W) and surface energy (γ) between two surfaces. Surface energy is a property of the surface that quantifies the reversible energy required to create a unit surface area in a solid. The surface energy of a solid reflects the nature of the bonds between the atoms which constitute it. Based on the definition given by the International Union of Pure and Applied Chemistry (IUPAC), the work of adhesion is defined as the energy required to reversibly separate a unit area of two condensed phases forming an interface (see Figure 1.1). According to the Dupre equation [14], the thermodynamic work of adhesion is expressed in the following form:

$$W = \gamma_1 + \gamma_2 - \gamma_{12} \tag{1}$$

where γ_1 and γ_2 are surface energies of the materials 1 and 2, respectively, and γ_{12} is the interfacial energy between the two surfaces. If the two materials are identical, the reversible work is the work of cohesion expressed as:

$$W_c = 2\gamma \tag{2}$$

Thermodynamic work of adhesion is correlated to surface chemistry and is indicative of physical attractions developed between two surfaces in close proximity or in contact. Here, physical attractions refer to the forces, interactions or bonds that are formed between molecules of two surfaces when they are close to each other, for example dipole-dipole interactions, van der Waals forces or hydrogen bonds (H-bonds).

Figure 1.1 Work of adhesion for two different surfaces

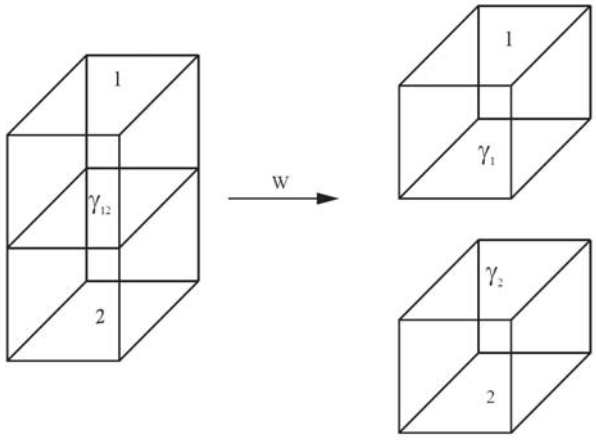

Practical adhesion (typically measured by destructive tests at the macro level) signifies adhesion in practical situations where two solids are bonded by some type of glue or adhesive. In this manner, practical adhesion (or the adhesive strength) is defined as the force or work needed to separate the bonded joint and determines the load-bearing capacity of the bonded system under stress. This separation does not necessarily need to occur at the interface of the bonded materials.

These arguments suggest that adhesion is concerned with both formation and breakage of bonds created at the interface of two objects depending on the point of view. It should be noted here that the strength of the bonds formed between two bodies is dependent on the strength of the molecular interactions that are developed at the interface upon contact of two bodies. In other words, in order to have strong and durable adhesive bonds, it is a necessary (but not always

sufficient) condition that strong intermolecular interactions are formed between the components of an adhesive joint. This simply means that obtaining large values of practical adhesion requires high values of W. It has been shown, however, that the measured practical adhesion of an adhesive bond might be several orders of magnitude larger than the thermodynamic work of adhesion [15]. This implies that surface forces (indicated by the thermodynamic work of adhesion) cannot be the only factor affecting practical adhesion. The other factors include dissipation of energy in terms of plastic or viscoelastic deformations, surface roughness, and other mechanisms. It should be pointed out here that the value of practical adhesion in itself is not a physical property. Because this value is different from one measurement technique to another or when different measuring conditions (e.g. rate, temperature, etc.) are used. Therefore, this quantity is mostly used as a qualitative comparison with reference to a specific type of test technique, rather than a material constant whereas, surface energy is a constant physical property.

Adhesion Mechanisms

Several separate mechanisms may contribute to the overall adhesion between two bodies, including wetting behavior or adsorption, chemical bonding, mechanical interlocking, electrostatic interactions, and diffusion of molecules across the interface. A combination of these mechanisms may contribute to the adhesion between two objects depending on the system. Therefore, no single theory is adequate to describe all aspects of adhesion in a comprehensive manner. Moreover, it's not possible to quantitatively discriminate these mechanisms in the adhesion of two objects.

The adsorption or wetting mechanism suggests that adhesion occurs when two materials are brought very close, and involves forces of attraction developed between the atoms or

molecules of the two surfaces [16]. These forces include relatively weak attractions occurring at short length scales including van der Waals forces or hydrogen bonds. It is assumed that van der Waals forces are one of the main factors contributing to adhesion of many polymeric materials. The chemical bonding mechanism involves the primary chemical bonds (such as ionic or covalent bonds) that may form across the interface [16]. In these cases the adhesive and the substrate merge and hence, form a chemical compound at their interface. Mechanical interlocking is associated with surface irregularities. In practical situations where glue (or liquid adhesive) is used to bind two solid materials at their surfaces, the adhesive can penetrate into the pores and irregularities of the substrates and hold them together with mechanical interlocking [16]. The penetration depth depends on the roughness of the surface, viscosity of the adhesive, and the time the adhesive and the substrate are in contact. It should be noted here that for optimum adhesion the adhesive must first maintain a close contact with the substrate and wet its surface to maximize the contact area and attractive forces between the adhesive and the substrate. For a liquid adhesive to wet the surface, the surface energy of the adhesive should be equal to or lower than surface energy of the adherent. Based on the electrostatic mechanism, adhesion is associated with the difference in electronegativities of the adhering surfaces or the attractions between positive and negative charges that are produced because of electron transfer from one surface to another. This mechanism is present in adhesion of charged materials, such as capacitors. The basis of the diffusion mechanism is the inter-penetration of polymeric chains at the interface [16]. This process is likely to happen if the molecules of both materials are mobile and soluble in each other. More in depth discussions of these mechanisms can be found elsewhere [16]. It should be emphasized again that no unifying mechanism or theory can describe adhesion phenomena inclusively.

Adhesion Underwater

The interfacial interactions of polymeric materials have typically been studied in the ambient conditions. In most cases, the interactions for polymeric systems have been reported as van der Waals forces or weak hydrogen bonds when the two objects are in contact in air. Understanding of the adhesion behavior in a liquid environment, especially when two surfaces are submerged underwater, on the other hand, is less developed. It is believed that the presence of water reduces van der Waals forces and hence, adhesion at the interface. For non-polar surfaces, however, it has been reported that the thermodynamic work of adhesion underwater is larger than that in air [17]. This behavior, typically referred to as "hydrophobic interactions", is caused by the change in the enthalpy and entropy of the reaction rather than intermolecular forces [18]. Once the hydrophobic molecules are introduced to water, hydrogen bonds between water molecules are broken to make room for nonpolar molecules. The disruption of hydrogen bonds is an endothermic reaction. Since nonpolar molecules are unable to form hydrogen bonds with water, the distorted water molecules rearrange around the nonpolar molecules so that they can form new hydrogen bonds [18]. The rearrangement of water molecules forms a cage-like structure around nonpolar molecules which is referred to as a "clathrate cage". This orientation of water molecules increases the entropy of the reaction and hence, stronger hydrophobic interactions are formed underwater compared to other weak intermolecular interactions present between two surfaces in air (e.g. van der Waals forces or hydrogen bonds). The hydrophobic interactions have been shown to be dependent on several factors, such as temperature, structure, shape and/or size of the hydrophobic molecule [18].

The Scope of This Work

As noted before, this study was driven by the interest to understand the effects of surface chemistry on adhesion interactions underwater. To accomplish this, the JKR method of contact mechanics was selected because the JKR technique and its corresponding experimental part (the set-up and sample preparation) are less complicated compared to SFA and AFM techniques. In addition, the JKR loading and unloading parts can be used to infer different information regarding the interactions at the interface. As mentioned earlier, during the JKR loading part the thermodynamic work of adhesion is determined, whereas the unloading part can reveal information regarding specific/non-specific interactions as well as frictional behavior at the interface of two surfaces. Moreover, only a limited number of studies using the JKR method underwater can be found in literature although it has been numerously used for measurements in air.

As mentioned earlier, this study encompasses two phases, which are discussed in subsequent chapters. For both phases the JKR experiments on model surfaces were performed both in air and underwater. In the first part of phase I model surfaces included glass slides functionalized with PEO (as a hydrophilic group), amine, mercapto (thiol), and carbomethoxy (as intermediate groups), methyl, cyclohexyl, and fluorocarbon groups (as hydrophobic groups). These surfaces were probed with hemispheres made out of poly(dimethylsiloxane) (PDMS). In the second part of phase I, wood-based biopolymers, specifically cellulose and lignin were probed with PDMS probes. As mentioned earlier, the probes in the first phase were used in their native (un-functionalized) form. Native PDMS has a hydrophobic nature. For this phase native PDMS self-adhesion and adhesion of native PDMS to clean glass surfaces were also evaluated both in air and underwater. For phase II PDMS probes were functionalized with a non-hydrophobic group. Because of its wide application in nature, amine functionality was selected

for treating PDMS probes in the second phase. The amine-treated PDMS probes were used to evaluate substrates functionalized with hydrophilic or intermediate groups. The substrates here included glass surfaces treated with PEO and amine as well as amine-functionalized PDMS flat sheets. For means of comparison the adhesion of amine-treated PDMS hemispheres with native PDMS was also evaluated. As mentioned earlier, all of these tests were performed both in air and underwater to determine the thermodynamic work of adhesion as well as the adhesion hysteresis in both media.

Based on the literature review that is covered later, there are multiple unique aspects of this study. First, this study exploits the full loading/unloading JKR experiments on a systematic and comprehensive set of model systems underwater ranging from hydrophilic to medium to hydrophobic. The results of these systems can enhance our understanding of the general trend of adhesion interactions underwater and pave the way in engineering surfaces with desired properties as related to adhesion or friction based on the end application. The second is that this is the first study to evaluate adhesion of cellulose and lignin underwater using the JKR technique. In addition, the majority of the studies using the JKR technique underwater have used native PDMS probes. The only study using non-hydrophobic PDMS probes [19] has reported the JKR results in terms of only adhesion hysteresis and not W as in the current study. Based on the results, they mentioned that their functionalization technique could have roughened the PDMS samples, and hence the reported results may not truly reflect the interactions underwater. The current study uses PDMS hemispheres that were treated with a non-hydrophobic functional group with a technique that did not impose significant roughness as shown by the JKR results.

Document Outline

The remainder of this document is organized in the following form:

Chapter 2 reviews the JKR theory of contact mechanics which is the basis of the JKR technique. This chapter also shows how fracture mechanics can be combined into the JKR theory to link adhesion behavior with molecular properties. As is shown in literature, studying the system behavior in terms of fracture mechanics provides the opportunity to infer the specific or non-specific interactions that are formed between two surfaces [9].

Chapter 3 introduces the experimental techniques that are used in this study for adhesion evaluation of the polymeric systems studied in the current research. These techniques include contact angle measurements and JKR method. A brief overview regarding the experimental considerations of these techniques is given in this chapter.

Chapter 4 provides a review of prior works performed to assess adhesion of polymeric materials. The majority of this chapter focuses on the studies which used the JKR method as the main experimental approach. The review includes the results of previous JKR studies related to PDMS self-adhesion, chemically modified PDMS surfaces, special applications of the JKR technique, the adhesion between PDMS and cellulose/lignin surfaces, JKR underwater, and the studies that have utilized SFA or AFM to study either functionalized surfaces or cellulose/lignin mostly underwater.

Chapter 5 discusses the two different phases that are carried out in this study to accomplish the goal of this project.

Chapter 6 begins with the description of the materials that are used in this study, such as PDMS, functional groups, cellulose, and lignin and continues with an overview of the different techniques that are used for surface treatment of glass and PDMS. A brief overview is also presented for preparing PDMS and smooth surfaces of cellulose and lignin.

Chapter 7 shows the wettability and the JKR results obtained for the first phase. The results of native PDMS probes with the basic model surfaces (functionalized glass surfaces) are presented and discussed first. Following that, the results obtained for cellulose and lignin surfaces are displayed and discussed.

In Chapter 8 the results of the second phase (functionalized PDMS probes) are presented and discussed.

Chapter 9 provides a detailed summary for this study.

There is also an appendix at the end, which contains the procedure and the JKR results related to one of the approaches (the hydrosilylation technique) carried out in this study to functionalize PDMS surfaces.

Chapter 2 - JKR Theory of Contact Mechanics

The subject of contact mechanics is to study stresses and deformations of solids that touch each other at one or more points. These deformations are caused by the forces acting between bodies, such as external loads or surface forces, and are related to the elastic properties of the materials in contact. The original work in this field dates back to 1882 by Hertz [20]. Hertz studied the behavior of two glass spheres pressed together by an external load (P), depicted in Figure 2.1(a). By using the interference pattern of Newton's rings developed between two glass spheres, illustrated in Figure 2.1(b), Hertz found that the pressure distribution in the area of contact for two spheres is elliptical; see Figure 2.1(c). Based on the elliptical distribution of pressure and using the theory of elasticity and continuum mechanics, he formulated the relationship between the circular contact area and the applied force for elastic, frictionless contact of two spheres (or equivalently between a sphere and a plane).

Figure 2.1 (a) Two spheres under an external load, (b) illustration of Newton's rings, and (c) pressure distribution, p(x,y), inside the circular Hertzian contact area

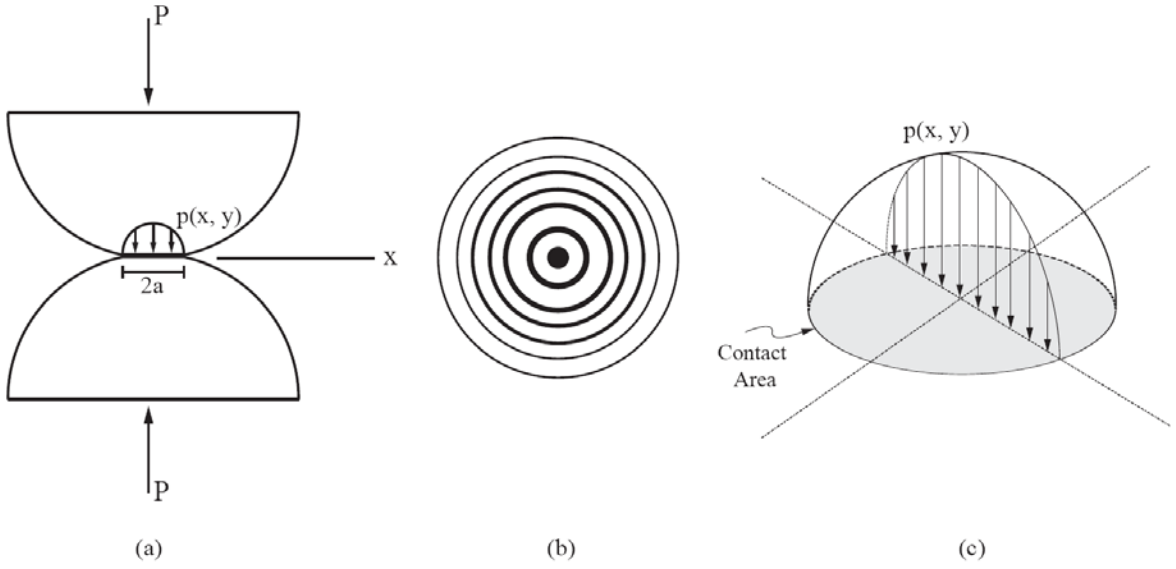

When two spheres with radii R_1 and R_2 are brought into contact with an external load (P), the centers of two spheres approach by a quantity referred to as the penetration depth (δ). Based on the Hertzian theory, the radius (a) of the resulting circular contact region and the penetration depth (δ) are given as:

$$a_H^3 = \frac{PR}{K} \tag{3}$$

$$\delta_H = \frac{a^2}{R} = \left(\frac{P^2}{RK^2} \right)^{\frac{1}{3}} \tag{4}$$

where R is the equivalent radius of curvature expressed as:

$$\frac{1}{R} = \frac{1}{R_1} + \frac{1}{R_2} \tag{5}$$

and K is the reduced bulk modulus which is in general form expressed in terms of the elastic modulus (E) and Poisson's ratio (ν) of each sphere as:

$$\frac{1}{K} = \frac{3}{4}\left(\frac{1-\nu_1^2}{E_1} + \frac{1-\nu_2^2}{E_2} \right) \tag{6}$$

As can be seen in equation (3) and (4), the elastic deformations in the Hertz theory are caused solely by external forces and therefore, the contact area reduces to zero when the external force is removed. Typically, the Hertz theory is only applicable to elastic bodies with high stiffness at large external loads, such as bearings, where surface interactions can be neglected.

Since Hertz' initial development further extensions to the Hertz theory have been proposed to explain the behavior of other, more complex systems. An extension to the Hertzian model was given in 1971 by Johnson, Kendall, and Roberts [8]. Johnson et al. [8] found that the Hertzian theory underestimates the size of the contact area for spheres made out of compliant materials. They also noted that for these lower stiffness materials the contact area does not tend

to zero when the external load vanishes. Therefore, a tensile force is required to separate the two bodies. They attributed these effects to surface attractions between the solid objects caused by surface forces. They used the Hertz theory as a basis and developed their theory, referred to as the JKR theory, to obtain the relationship between circular contact radius and the applied load in the presence of surface forces. This theory has since found applications in the study of adhesion of solid polymeric materials. In 1975, Derjaguin, Muller and Toporov [21] developed another model for adhesion of high elastic modulus bodies, referred to as the DMT model. Similar to the JKR theory, the DMT model also considered surface forces acting between two bodies, but the tensile force required to pull-off the two objects in contact was found to be greater than that predicted by the JKR theory. At first it was thought that this was a contradiction between the JKR and DMT models. As a result, the DMT model was not fully accepted until 1977, when Tabor [22] noted that the discrepancy between the JKR and DMT models arises from the different assumptions considered to derive these models. According to Tabor's work, the error in the JKR theory is to consider surface forces only inside of the contact zone and being zero outside. This assumption, as will be seen later in this chapter, produces an unphysical infinite stress at the edge of contact. Similarly, the DMT model assumes that surface forces act only in a circular zone outside of the contact area. This assumption will cause a non-continuous stress profile close to the edge (just inside and outside of the contact area). Tabor resolved the discrepancy between the JKR and DMT models by defining a dimensionless parameter (μ), noted as Tabor's parameter, as the ratio of elastic deformations to the range of adhesive forces. He showed that there is a continuous transition from the DMT to the JKR model when μ is increased. According to Tabor's work, the JKR model is mostly applicable to solid systems where at least one material is compliant (having a low stiffness) whereas, the DMT model is

appropriate for surfaces with higher elastic modulus. Later in 1992, Maugis [23] used the analogy between adhesion and fracture mechanics and assumed that the edge of the contact zone can be considered as a circumferential mode I crack that recedes or advances when the contact area is increased or reduced, respectively. He developed a general model based upon the Dugdale model used in fracture mechanics, referred to as the Maugis-Dugdale model. Dugdale analysis assumes that all plastic deformation concentrates in a strip in front of the crack tip [23]. Likewise, Maugis assumed that the adhesive forces are constant in an annular region around the contact area. The stress distribution in the Maugis-Dugdale model is the superposition of the Hertzian stress inside the contact area and the Dugdale stress. The Dugdale stress itself is composed of an adhesive stress inside the contact area and the constant adhesive stress in the annular region around the area of contact. The Maugis model uses a transition parameter similar to the Tabor parameter to provide generalized parametric equations for contact area and the penetration depth. The Maugis-Dugdale model confirms that JKR and DMT models are two extremes of a single model and the JKR-DMT transition can be achieved analytically.

Due to the fact that the present study is focused on adhesion studies of polymeric systems and the probe that is used for this study is a low-stiffness material, the JKR theory of contact mechanics is the most applicable approach and will be the basis of theoretical and experimental framework of this study. Thus, only the JKR theory development will be reviewed in the next section. For more information on contact mechanics and different theories, please see [21, 23].

JKR Theory

In 1971 Johnson, Kendall and Roberts [8] showed that for two spheres made out of an elastic low-stiffness material (rubber) at low loads the contact area is larger than that predicted by the Hertz theory. They also noted that when the load is reduced to zero, the contact area

between these compliant bodies becomes a constant finite value rather than zero and a tensile force is required to separate the surfaces. Johnson et al. [8] concluded that these differences are caused by surface forces and developed their contact mechanics theory to incorporate these effects.

To obtain the relationship between the applied load and contact area when surface forces are present, Johnson et al. assumed the relationship between the contact area and the applied load remains Hertzian, namely, $a^3 = \frac{P_1 R}{K}$ where P_1 is the apparent Hertzian load that corresponds to the contact area of a in the presence of surface forces. They obtained P_1 by means of an energy balance approach. They assumed that the total energy of the system (U_T) is made up of three terms: the elastic energy stored in two surfaces caused by their deformation (U_E), the potential energy associated with the displacement of the applied load (U_P), and the surface energies of the bodies (U_S) in the following form:

$$U_T = U_E + U_P + U_S \tag{7}$$

where

$$U_E = \int P d\delta \tag{8}$$

$$U_P = -P\delta \tag{9}$$

$$U_S = -\pi a^2 W \tag{10}$$

where P is the load, δ is the displacement of the center of the spheres, a is the contact radius, and W is the energy per unit area of contact, referred to as the work of adhesion between two bodies.

In the JKR theory, it is assumed that the equilibrium is obtained when:

$$\frac{dU_T}{da} = 0 \tag{11}$$

where a is the contact radius. The elastic energy (U_E) is determined from the energy of the system in initial and final states by using the load-displacement curve. In the initial state, where

energy is denoted by U_1, surface forces are neglected. Here, the system is loaded with P_1 to give the contact radius a, and hence, the displacement is expressed by δ_H. In the final state of the system the contact area is kept constant while the load is reduced from P_1 to P. This increases the energy of adhesion up to W. The displacement at this state is given by the Boussineq's flat punch displacement ($\delta_B = \frac{2P'}{3aK}$) [24] and letting P'=P (the applied load). Here, K is the reduced bulk modulus given in equation (6). The elastic energy is, therefore, given as following:

$$U_E = U_1 - U_2 = \frac{Pa^2}{3R}\left(\frac{P_1}{P} + \frac{P}{P_1}\right) \tag{12}$$

In order to obtain the potential energy (U_P) of the applied load, Johnson et al. considered that the total displacement is composed of the Hertzian displacement, δ_H given in equation (4), and displacement of a Boussineq's flat punch by letting $P'=P_1- P$. Thus, the potential energy is given by:

$$U_P = -\frac{Pa^2}{3R}\left(1 + \frac{2P}{P_1}\right) \tag{13}$$

here R is the equivalent radius of curvature of the spheres given in equation (5). Johnson et al. assumed that surface forces are only present in the area of contact. Using equation (10) and the Hertzian contact area, the surface energy (U_S) can be expressed by the following:

$$U_S = -\pi W\left(\frac{RP_1}{K}\right)^{\frac{2}{3}} \tag{14}$$

By inserting equations (12), (13), and (14) into equation (7) and applying the equilibrium condition of equation (11), the resulting JKR relationship between the applied force, P, and contact radius, a, which is referred to as the JKR equation, is obtained as [8]:

$$a^3 = \frac{R}{K}\left[P + 3\pi RW + \sqrt{(3\pi RW)^2 + (6\pi RPW)}\right] \tag{15}$$

Note that the phrase expressed in brackets is P_1. It is obvious that if we set W to zero (no adhesion) in equation (15), the Hertzian solution (equation (1)) is recovered. Equation (15) also indicates that the attractive forces included in the JKR theory produce a larger contact area than that predicted by the Hertz theory alone.

Here it should be noted the JKR equation can be extended to two hemispheres in contact or a (hemi)sphere in contact with a flat sheet. In the case of an elastic (hemi)sphere in contact with a flat, elastic half space, the equivalent radius of curvature in equation (5) is reduced to the (hemi)sphere radius, $R=R_1$, since $R_2 \to \infty$. If one of the two bodies is rigid (modulus is essentially infinite), then the reduced elastic modulus in equation (6) will be dominated by the soft sample.

If we set the applied force to zero in equation (15) while the materials are still in contact, the contact radius at zero load can be expressed as:

$$a_0^{\,3} = \frac{6\pi RW}{K} \tag{16}$$

As can be seen, a_0 is a non-zero value due to the work of adhesion; this is in contrast with Hertzian theory prediction.

The difference between the Hertzian and JKR contact profile for two spheres is illustrated in Figure 2.2. It should be pointed out here again that the JKR model best suits low elastic modulus materials (i.e. soft samples) at low external loads where surface forces are comparable to the force required to detach those bodies. For cases involving materials with high stiffness or large external loads, the surface attractive forces are negligible compared to the applied load and the JKR theory reduces to the Hertz theory [8].

Figure 2.2 Schematic view of the contact area between two spheres comparing Hertzian and JKR models (reproduced from [8])

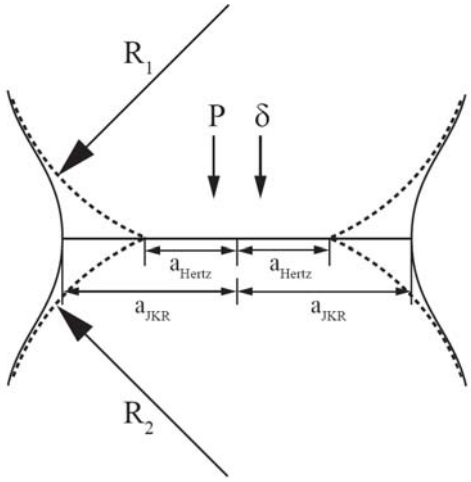

In the JKR model the distribution of normal stresses inside the contact area is given by a superposition of the compressive Hertzian stress and a tensile stress caused by surface forces. The resulting relation is given in equation (17) where r is the radial distance in the contact region [15]. The first right hand side term in equation (17) is the Hertzian stress profile and the second right hand side term is the stress caused by the tensile force (P_1-P) due to the flat punch movement (this term displays the effect of surface forces). In working with contact mechanics theory the sign convention defines compressive stress as positive (+) and tensile stress as negative (-). As can be seen in equation (17), at the boundary of the contact region (where r=a) the JKR theory predicts a theoretically infinite stress. This is similar to the mathematical model of the stress field near a crack tip in linear elastic fracture mechanics where the stress field near the crack tip is proportional to $1/r^2$, r is the location of a point measured from the crack tip. According to the linear elastic fracture mechanics theory, stresses at the crack tip (where $r \to 0$) are infinite. Physically, a plastic zone is developed near the crack tip to relieve this unphysical infinite stress. Analogous to this, the contact area of two curved surfaces also deforms at the edge in the form of "necking", illustrated in Figure 2.2, to attain the equilibrium dictated by surface

forces outside the contact area [15]. The stress distribution of the Hertzian and JKR models are depicted in Figure 2.3. As stated earlier, the stress distribution in Hertz theory is elliptical whereas, surface forces included in the JKR model produce an infinite stress at the edge of the contact area. The stress outside of the contact area is zero for both Hertz and JKR models.

$$\sigma(r) = \frac{3K}{2\pi R}\sqrt{a^2 - r^2} - \sqrt{\frac{3WKa}{2\pi\left(a^2 - r^2\right)}} \tag{17}$$

Figure 2.3 The stress distribution in (a) the Hertz theory and (b) the JKR theory

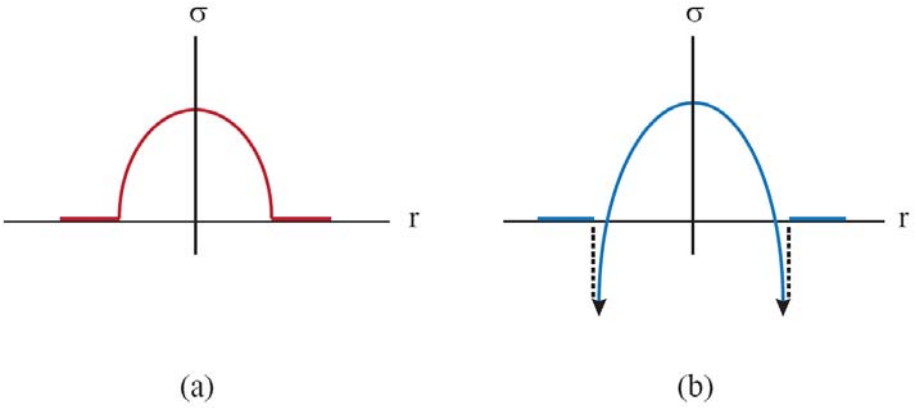

The experimental technique based upon the JKR theory, which is referred to as the "JKR Experiment" will be discussed in the next chapter. It should be noted here, however, that the JKR experiment consists of two portions; loading and unloading. In the loading process a hemispherical probe and surface of another material (flat or curved) are brought into contact followed by pushing the probe against that surface. When two samples are brought close enough together two surfaces leap into contact and a circular area is developed which is getting larger by increasing the applied force in the loading portion. This contact area recedes when the two samples are withdrawn in unloading. The diminishment of the contact area in the unloading regime can be seen as a well-mannered crack advancing through the interface of contact, illustrated in Figure 2.4. By using principal concepts of fracture mechanics, an extension to the

standard JKR model has been developed by Maugis [25]. This extension is described in the next section.

Figure 2.4 The contact edge can be seen as a crack emanating through the interface

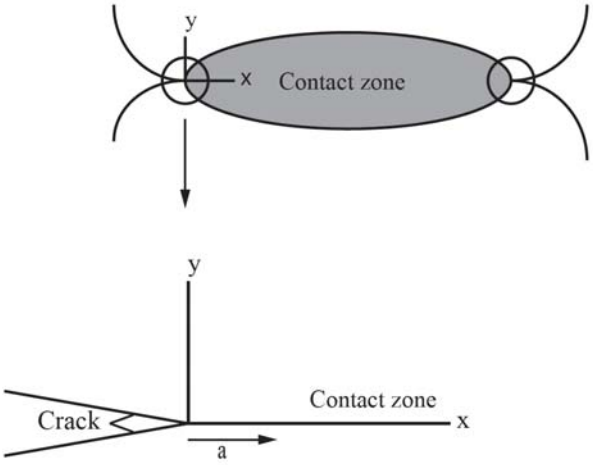

Incorporating Fracture Mechanics into the JKR Model

Fracture mechanics describes the strength of cracked bodies subjected to stresses and strains. The first successful analysis in this area dates back to the 1920's where Griffith explained the propagation of cracks in glass [26]. Griffith, using an energy balance criterion, assumed that crack propagation is a tradeoff between the reduction of the elastic strain energy and the increase in surface energy (or the energy required to create new crack surfaces) [26]. In 1950, Irwin [27] extended the Griffith's theory for ductile materials by introducing the concept of "energy release rate" or "crack driving force" (G) as the total energy dissipated per unit length of crack when crack moves. According to the Griffith's equilibrium condition, the critical energy required to propagate the crack along the periphery (G_c) is expressed as:

$$G_C = 2\gamma \tag{18}$$

where γ is the surface energy of a material. Griffith's theory states that if the energy release rate (G) is larger than the critical value (G_c), the crack will propagate.

According to the basic principles of fracture mechanics, the strain energy release rate is expressed in terms of the stored energy and the mechanical potential energy as following [24]:

$$G = \frac{\partial}{\partial A}\left(U_E + U_P\right) \qquad or \qquad dU_E = Pd\delta + GdA \tag{19}$$

where dA is the change in crack area when the crack moves. To derive the energy dissipated while two bodies are in contact, the same energy approach can be utilized. According to equation (10), the work of adhesion (W) is defined as:

$$W = -\frac{\partial U_S}{\partial A} \tag{20}$$

The total energy given in equation (7), therefore, can be rewritten as the following:

$$dU_T = (G - W)dA \tag{21}$$

where GdA is the mechanical energy released when the crack is extending by an area dA, and WdA is the energy required for breaking the bonds. The difference between G and W (G-W) is the crack extension force per unit length of crack, which is zero at equilibrium. If G<W, the area must increase so that the potential energy reduces. That means the crack recedes and the contact area enlarges. When G>W the mechanical energy is enough to break the bonds hence, the crack advances and the contact area reduces in size.

Differentiating U_E in equation (19) and introducing U_P given in equation (13), the strain energy release rate for two bodies in the JKR model provided by Maugis and Barquins [25] is given as the following:

$$G = \frac{\left(P_1 - P\right)^2}{6\pi a^3 K} = \frac{\left(\frac{Ka^3}{R} - P\right)^2}{6\pi a^3 K} \tag{22}$$

where K is the bulk modulus defined in equation (6). According to the Griffith's criterion of equilibrium, at constant temperature the energy release rate is equal to the work of adhesion ($G = W$).

Although the loading and unloading processes in the JKR theory are assumed to be reversible, some polymeric systems violate this condition because they dissipate energy by plastic or viscoelastic deformation in a region near the crack tip during unloading [28]. For these systems the standard JKR equation (equation (15)) describes the behavior of the system in the loading regime, but fails to explain the unloading behavior. Based on work by Maugis and Barquins [25], for the unloading regime the thermodynamic work of adhesion can be replaced by the strain energy release rate (equation (22)) because of the non-equilibrium situation associated with polymeric systems. The discrepancy between W during loading and G measured in unloading is referred to as adhesion hysteresis, schematically depicted in Figure 2.5. It should be noted here that the energy release rate is equal to the thermodynamic work of adhesion (W) in the loading regime where adhesion is mostly caused by weak van der Waals forces [29]. In the unloading process, however, short-range interactions may occur such as hydrogen bonding or rearrangements of surface molecules [9]. For breaking these bonds additional energy is required. Therefore, although $G \approx W$ in the loading regime, G in the unloading regime might be orders of magnitude higher than W. Here it should be noted that the rate at which the two surfaces are withdrawn can influence values of the energy release rate (G). Therefore, the results of energy release rate are usually used as a qualitative tool to determine the strength of the bonds that are formed between different surfaces rather than a constant fixed value.

Figure 2.5 JKR loading/unloading adhesion hysteresis

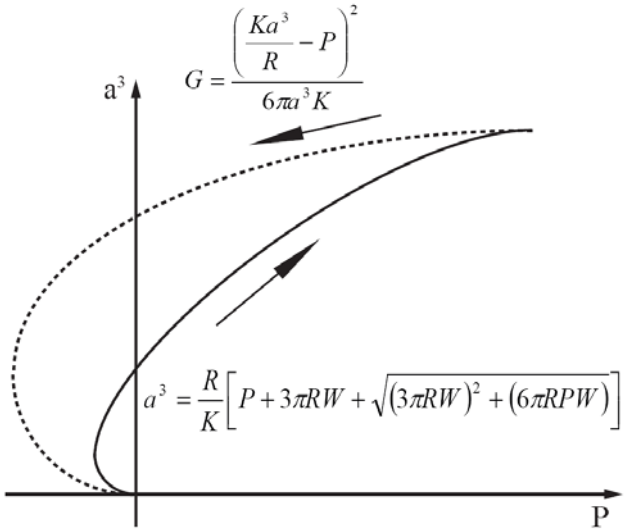

Figure 2.6 illustrates typical data for adhesion of PDMS to itself (self-adhesion) reproduced from [30]. As can be seen, the energy release rate (G) shows a stable behavior during the loading process and its value is equal to the value of W obtained from the standard JKR equation. During the unloading, however, G is larger than the thermodynamic work of adhesion (W) and increases until two surfaces are separated. The difference between W and G in a system can be related to the strength of the bonds that are formed between two surfaces. In other words, if strong bonds are formed between two surfaces, a large force is required to break the bonds and separate the two surfaces. This simply means that the difference between G and W would be large.

Figure 2.6 Typical loading unloading data from a JKR experiment showing stability of G in loading regime and hysteresis in unloading in self-adhesion of PDMS (reproduced from [30])

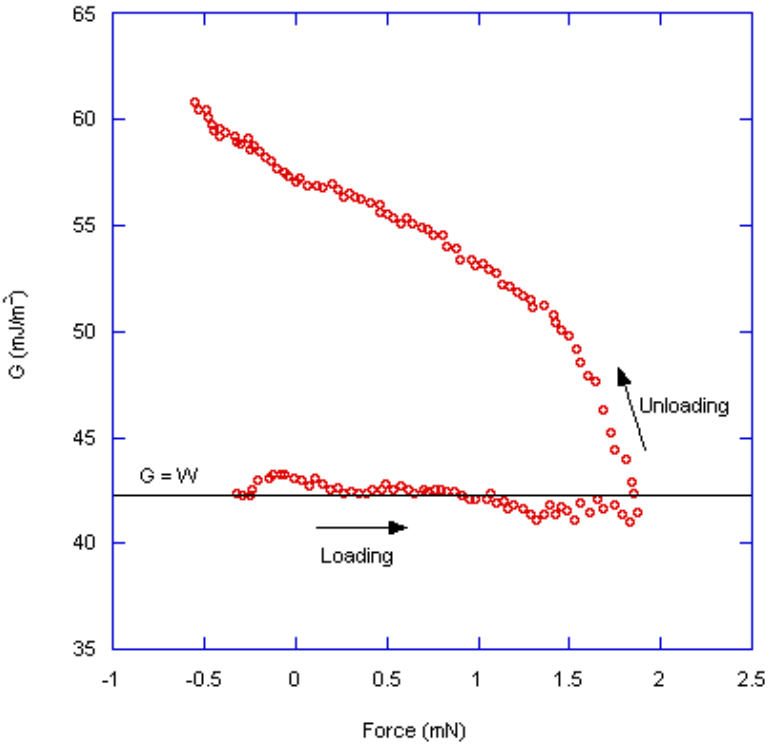

Adhesion Hysteresis in Polymers

As discussed in the previous section, adhesion hysteresis of polymeric materials may arise from different mechanisms such as bulk viscoelastic losses, or from a mechanical and/or chemical change of the materials at their interface [16]. Increasing surface roughness is one of the mechanical factors that can enlarge the adhesion hysteresis. The chemical sources of adhesion hysteresis may include formation of H-bonds [9], and entanglement or interdigitation of surface molecular chains [31]. Another adhesion hysteresis source is plastic deformations [32].

It has been shown that in elastomeric materials showing viscoelastic behavior (and viscoelastic energy losses, such as pressure sensitive adhesives), the energy release rate (G) is dependent on the velocity of crack advancement [33]. Gent and Schultz [34] and then Andrews and Kinloch [35] using a fracture mechanics approach, showed that this velocity dependence of

G can be described by the Williams-Landell-Ferry (WLF) equation [36]. In the WLF model the results at different temperatures can be shifted to a reference temperature by the WLF factor a_T. According to this model, the relation between the energy release rate (G) and work of adhesion (W) is expressed in the following empirical form:

$$G = W\left(1 + \Phi\left(a_T V\right)\right) \tag{23}$$

where Φ is a dimensionless function representing the bulk dissipation of the viscoelastic material near the crack tip and V is the rate at which the contact radius decreases. V is defined as:

$$V = -\frac{da}{dt} \tag{24}$$

Equation (23) shows that the energy release rate between two surfaces is composed of an elastic term (W) plus an energy dissipation term. If the system follows the empirical relation given in equation (23), the dissipation function is given by:

$$\Phi\left(V\right) = \frac{G - W}{W} \tag{25}$$

One of the suggested forms for Φ is the power law form as the following:

$$\Phi = \left(\frac{V}{V^*}\right)^n \tag{26}$$

where V* and n are obtained from fitting experimental results. The exponent, n, varies between 0.2 [37] and 0.7 [38] depending on the materials that are in contact. The Gent-Schultz relationship (equation (23)) can distinguish between the interfacial and bulk contributions to the adhesion energy measured by adhesion tests [25].

Chapter 3 - Adhesion Measurement Techniques

As mentioned previously in Chapter 1, “adhesion” is related to a variety of phenomena depending on the point of view. Moreover, adhesion is used in many disciplines and hence, different methodologies and experimental techniques have been developed to measure adhesion in air and aqueous environments. These techniques include atomic force microscopy (AFM) and surface force apparatus (SFA) to determine adhesion at a molecular level, contact angle measurements to determine wetting behavior, contact-mechanics-based experiments (such as the JKR technique) to determine the thermodynamic work of adhesion, micro-droplet method and single fiber fragmentation test at the micro-level as well as lap-shear test at the macro-level to measure practical adhesion or the adhesive strength.

For the purpose of the current research, contact angle measurements and the JKR experimental technique (in air and underwater) are used to study adhesion (or surface interactions) of the material systems used in this study. The contact angle measurements are typically used to estimate liquid-solid “wetting” (or wettability) of a solid surface against a liquid probe. The surface free energy of the solid surface can be calculated based upon the contact angles that are measured against several liquid probes. The JKR experiment provides input on the thermodynamic work of adhesion (which is equivalent to solid-solid “wetting”) during the loading portion, as well as information on the interactions that are developed between two surfaces during the unloading portion. This chapter gives an overview of these experimental techniques and the details about the JKR test set-up developed for this study.

Contact Angle Measurements

In general, contact angle measurements are used to infer characteristics of a surface. The contact angle is the angle that forms at the interface of a solid/liquid system, denoted by θ in

Figure 3.1. The contact angle is indicative of the molecular interactions that are developed at the interface of the solid/liquid surface. Low values of contact angle imply that there is a strong affinity between the solid surface and the liquid drop at the interface. Thus, the droplet wets the solid surface to increase the contact area. On the other hand, a high contact angle is indicative of a weak affinity between the solid and liquid at their interface. For this case, the liquid drop beads up to minimize the contact area instead of wetting the surface. In the case of using a water drop as the liquid, the surface is referred to as hydrophobic if the contact angle is larger than 90º and hydrophilic if the contact angle of water is lesser than 90º, see Figure 3.1.

Figure 3.1 Contact angle of a water drop on a solid surface

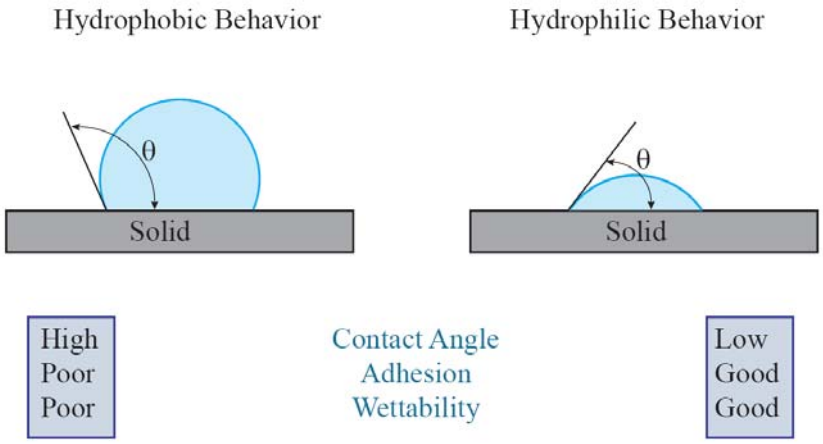

Contact angles are typically divided into static and dynamics angles. For a static contact angle the boundary of the solid/liquid/vapor is not moving. Namely, a droplet is deposited on a surface and the angle is measured by looking at the drop. For the dynamic angle the boundary is changed by increasing/reducing the volume of the droplet without changing the liquid/solid interface. Dynamic contact angles are measured during advancing (increasing the volume) and receding (decreasing the volume) of the droplet. The difference between advancing and receding

contact angles is referred to as contact angle hysteresis and is indicative of surface roughness, surface heterogeneity, adsorption of solution impurities on the surface, or swelling [39].

Contact angle measurements are typically used in either a qualitative or quantitative manner. In the qualitative manner, contact angles are used as a direct method to determine wetting behavior of a particular solid-liquid surface. The qualitative measurements are performed as a basic tool to verify hydrophilic or hydrophobic nature of a surface after chemical modification of the surface. The quantitative manner involves measuring contact angles of several reference liquid probes with known surface characteristics on the surface of a solid material to characterize the surface in terms of surface energy (γ). The surface energy of the solid object is calculated based upon the thermodynamic equilibrium between the liquid, solid, and ambient gas phases (Young's equation) [40]. The most common models developed to calculate surface energy of a solid using reference probes are the Good-Van Oss model [41] or the Owens-Wendt model [42]. For most polymeric materials with weak van der Waals forces among their molecules, the surface energy is very low (less than 80 mJ/m^2) compared to ionic solids with intermediate surface energies (in the range of 0.1 to 0.5 J/m^2), and solids with metallic and covalent bonds with high surface energies (in the range of 1-3 J/m^2) [24]. It should be noted that the application of contact angle measurements in the quantitative manner is limited because the surface energy values obtained in the quantitative manner are dependent on the liquid probe selection as well as the equations used to analyze the results of contact angle [41, 42]. In this study static contact angles are measured as a screening method for the purpose of quality control to assess the wettability degree of a surface after a chemical modification.

JKR Technique

The "JKR technique" is based upon the Johnson-Kendall-Roberts (JKR) theory of contacts mechanics [8] discussed in the previous chapter. As mentioned before, the JKR theory is an extension of the classical Hertz theory [20] and takes into account the surface and interfacial energies especially at low loads where surface forces are comparable to the applied load. The JKR test method has been commonly used to directly measure the thermodynamic work of adhesion (W) in the loading portion and energy release rate (G) in the unloading portion. As mentioned in the previous chapter, the JKR theory and therefore, test method requires that at least one of the materials (either the probe or the substrate) have low elastic modulus. In general, the JKR test consists of two portions; loading and unloading. In loading, a small hemispherical probe is brought close to the surface of another material, typically a flat substrate as depicted in Figure 3.2(a), followed by bringing the probe into contact and then pushing the probe against the surface by increasing the load. The resulting contact radius (a) and the displacement of the lens (δ) are shown in Figure 3.2(a). It is noteworthy here to mention that as the distance between two surfaces is reduced, two objects leap into contact and a circular contact area, illustrated in Figure 3.2(b), is formed. When the probe is compressed against the substrate, this circular area is getting larger and larger with increasing the load. After the load reaches a pre-determined value, the loading portion is halted. The unloading portion then begins by reversing the motion and withdrawing the two samples. In unloading, when the load is decreased the contact area diminishes until the two surfaces are separated. During both the loading and unloading portions the applied load and images of the contact area are captured for later processing. For typical JKR experiments, the radius of the probe is 1-3 mm while the maximum applied load is in the range of mN (e.g. 4-5 mN [43] or 25-30 mN [44]). The resulting contact radius (shown in Figure 3.2(b)) is typically in the range of 50-250 μm.

Typically, in the JKR experiment, the loading and unloading modes can be carried out in two primarily different manners: (1) quasi-static (or step-wise) or (2) continuous. In the quasi-static approach the system is allowed to relax for a period before the next increment is imposed. This time can vary from 30 sec [45] to 5 min [46] for loading and 1 min [47] to 20 min [45] for unloading increments. For polymeric systems with visco-elastic behavior, the step-wise loading/unloading experiments reveal stress relaxation over time related to these polymers. In the continuous approach the probe is moved progressively without letting the system reach the equilibrium state. During the quasi-static process in the unloading mode, the adsorption ability of the polymer chains can be investigated, while during the continuous mode, the velocity dependence of G can be studied [48, 49].

Figure 3.2 (a) Schematic representation of a hemisphere in contact with a flat substrate, (b) a typical image of the contact area

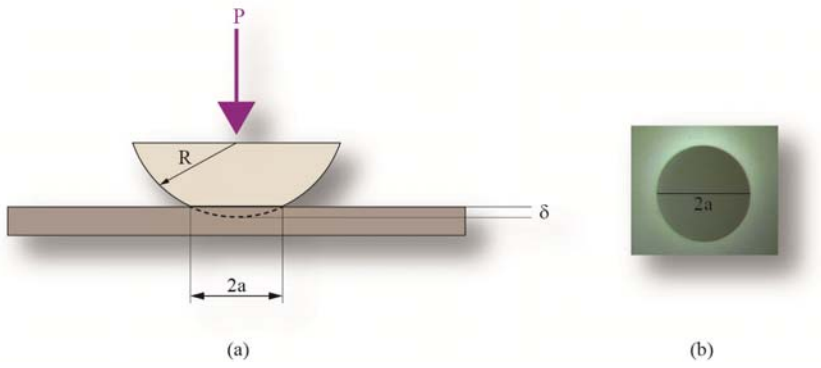

During both the loading and unloading portions of the JKR test, the raw data obtained is the load (P) and the contact radius (a). The bulk modulus (K) and work of adhesion (W) can be deduced by fitting the loading data to the standard JKR equation given in equation (2.14). As discussed in the previous chapter, for systems showing hysteresis there is a discrepancy between loading and unloading portions which is indicative of specific interactions at the interface. The

unloading data is generally used to infer the ability of the system to form specific or non-specific interactions.

An alternative method to obtain K and W from the loading raw data is to use a linearized form of the energy release rate equation given in equation (2.19). Assuming that the loading process has been carried out under equilibrium conditions and letting G=W, the linearized form can be rearranged as following [50]:

$$\frac{P}{\sqrt{6\pi}\, a^{3/2}} = K\left(\frac{a^{3/2}}{\sqrt{6\pi}\, R}\right) - \sqrt{WK} \tag{27}$$

In equation (27) the reduced bulk modulus (K) is the slope while the work of adhesion (W) is calculated from the X-intercept. The equilibrium condition can be verified by replacing back the values of K and W obtained from the linearized form and the experimental values of P into the standard JKR equation (2.14) to obtain the corresponding contact area values and compare these values with the experimental contact area results.

The radius of curvature of the lens (R) is calculated from the side image of the cured lens on a glass slide taken with the microscope from the following equation after an experiment:

$$R = \frac{h}{2} + \frac{r^2}{2h} \tag{28}$$

where h is the height of the lens and r is half of its base width measured from the side profile of the lens, illustrated in Figure 3.3. The radii of the curvature of the lenses used in the current study were typically in the range of 1.4-2.5 mm.

Figure 3.3 Lens geometry

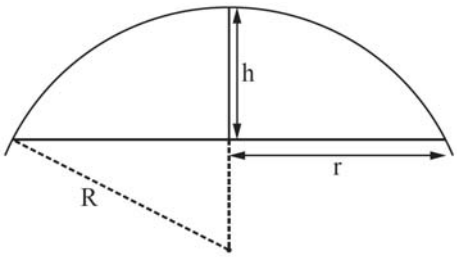

The schematic view of the JKR set-up developed for the purpose of this study is depicted in Figure 3.4. The main components of this system are a microscope and a camera to capture the image of the contact area, a motorized translation stage to control the relative motion of the probe and the substrate, a 0.5 N load cell to measure the load, and a vibration isolation table. The PDMS hemisphere is mounted directly on a zig-zag shaped arm which was inspired by the design described by Loskofsky et al. [51]. The zig-zag arm is made out of glass rods (with circumference of about 10 mm to reduce the capillary forces for underwater measurements) and thin disks (with 25.4 mm diameters). The glass arm holding the PDMS hemisphere is fixed to a vertical post. The glass slide (which is functionalized or coated and used as the substrate) is secured to the bottom of a plastic container by means of a piece of double sided tape. A piece of black tape is also used in between the back of the slide and the double-sided tape to increase the contrast underwater. It should also be noted that a clear plastic wrap with a small opening covering the top of the plastic container was used to minimize the evaporation rate of water during underwater measurements. The water evaporation rate in the lab environment was about 0.7-1.0 mg/min over 30 min for the loading/unloading portions.

The container is placed on a TEDS-integrated 0.5 N load cell calibrated by the manufacturer (Interface®). The calibration is further verified by standard calibration weights. This load cell is connected to a TEDS hand-held display. The hand-held display is connected to the host computer via an RS-232 serial port. The load readout shown on the hand-held display is

imported to the host computer through MATLAB®. The load cell is attached to a motorized translation stage (M-111.2 DG from PI®) through a 90-degree angle bracket. The total travel range of the motorized stage is 15 mm. The motorized stage, that is used to approach or withdraw the substrate to/from the fixed hemispherical probe, is linked to a controller which is connected to the host computer via an RS-232 serial port. The motorized stage can be controlled by the PI software provided with this stage through the linked controller. The motorized stage itself is secured to an XYZ manual translation stage with 1" travel in each direction. This manual stage is used to adjust the XY position or the height of the load cell and hence, the substrate with respect to the location of the probe. The manual stage is placed on an adapter plate which is screwed to the vibration isolation table.

The camera, used to capture and transfer the image of the contact area to the host computer, is mounted on a stereoscopic microscope with a magnification of up to 140X. A heavy duty manual XY translation stage, which is screwed to the vibration isolation table, holds the circular post used to sustain the microscope and the camera. The manual XY translation stage for the microscope gives more flexibility to view and position the contact area in the field of view of the microscope especially when the magnification is increased. The scale for each magnification zoom of the microscope is calibrated by a reticle when the camera was installed for the first time. The images of the contact area are captured through the software that comes from the vendor at the end of each step size right before the next increment is applied in both loading and unloading modes. The images are saved for later image analysis. All images are analyzed with a custom written routine in MATLAB® to find the radius of the contact region. This routine uses the edge detection functions to determine the area of the contact.

In order to observe the contact area discernibly, a light source focused on the contact zone is also needed. For this purpose an illuminator with fiber optic light and variable intensity is used. The light of the illuminator is transferred to the microscope through a flexible goose-neck light. A 90-degree adapter attached to the microscope holds the light pipe. The light beam is reflected to the contact zone by two slant lenses inside the microscope.

For any hemisphere/glass surface the JKR experiment is first performed in air (with the plastic wrap covering the container) under quasi-static condition for both loading and unloading portions. In the quasi-static condition, the substrate and the lens are approached or withdrawn in small displacements (δ) step by step and the system is allowed to relax between each step. In the quasi-static method only the last a(t) and P(t) are captured before the next increment is imposed for both loading and unloading portions. The incremental jumps for stepwise loading/unloading are kept small (0.6-0.8 μm) in order to minimize the force that is exerted on the glass arm during the loading or unloading portion underwater. A wait time of 60 sec is also used during unloading before the next increment is applied. Once the test is carried out in air, the container is filled with deionized water and the JKR test is performed underwater for the same hemisphere and glass slide in the same quasi-static condition for both loading and unloading portions. Typical plots of load-contact radius for JKR experiment are shown in Figure 2.5 and Figure 2.6.

Figure 3.4 Schematic of the JKR apparatus used for JKR measurements

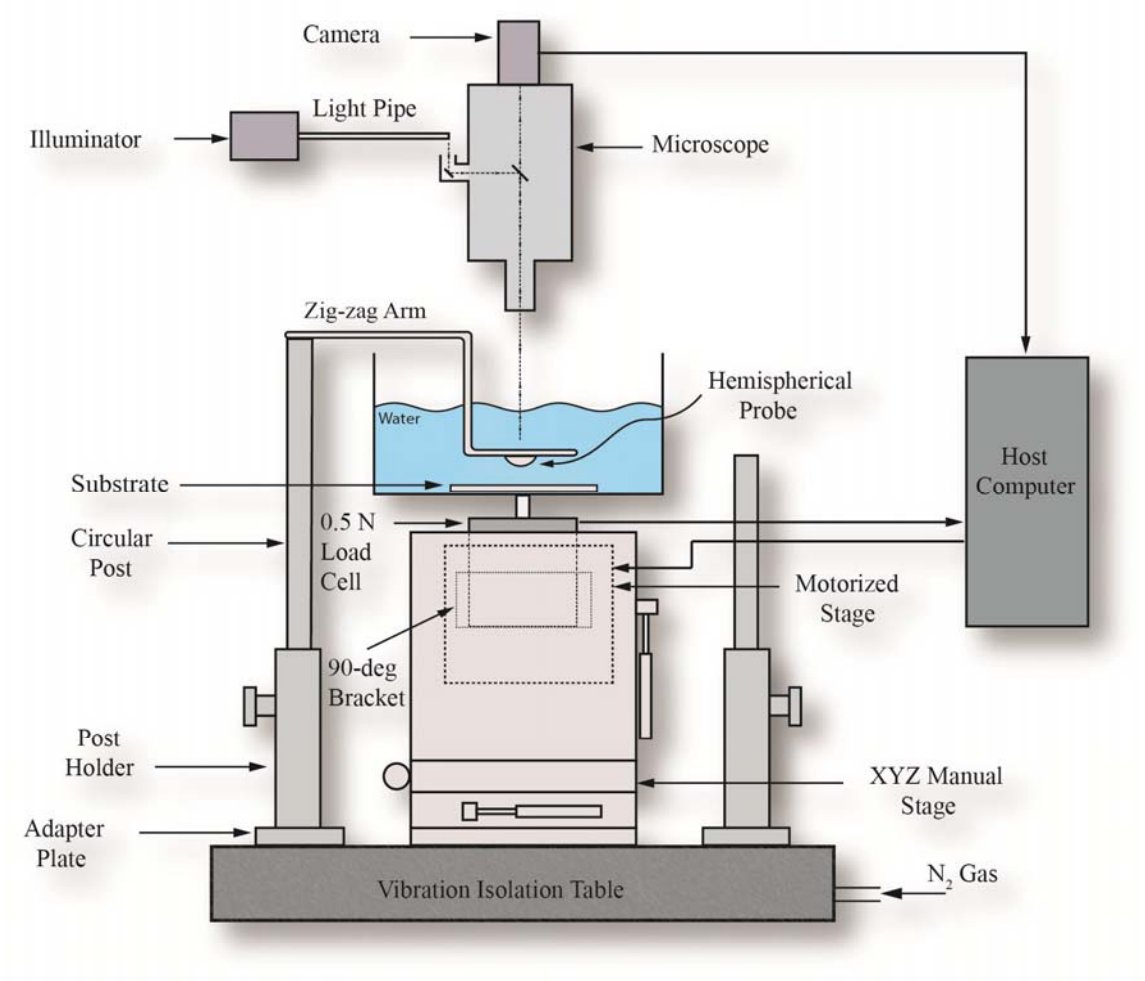

Chapter 4 - Literature Review

Numerous studies have exploited the JKR technique to investigate fundamental aspects of adhesion for different systems in air. Very few studies, however, can be found in the open literature where the JKR technique has been used for adhesion characterization underwater. This chapter deals with the review of prior works which used the JKR technique both in air and underwater to evaluate adhesion at the interface of two surfaces where at least one surface is a polymer.

In JKR experiments, hemispheres are typically made out of PDMS to probe the adhesion behavior at the interface. PDMS has a low elastic modulus that deforms measurably in the range of the JKR experiments. Moreover, it is optically transparent with a smooth and homogenous surface. All of these properties have made PDMS an appropriate probing material for JKR measurements. In the current study, we are also using PDMS as a probe to investigate the adhesion of various model surfaces in the presence of water. These model surfaces include PDMS, cellulose, lignin, and a variety of functionalized surfaces. This chapter provides a review of the literature concerning the JKR technique used for PDMS self-adhesion (as a baseline), adhesion between PDMS and chemically modified substrates, special applications of JKR experiments, and PDMS with cellulose and lignin. It also provides a review of several studies where the JKR technique has been used to perform adhesion measurements underwater. In addition, the results that are obtained using other contact-based experimental approaches (e.g. AFM and SFA) are also included in the final subsection.

PDMS Self-Adhesion

After the emergence of the JKR theory of contact mechanics in 1971 [8] for soft materials, many studies [15, 28, 44, 52-56] exploited the JKR measurements to study adhesion at

interfaces directly. Chaudhury and Whitesides [52] are believed to be the first researchers that developed and implemented the "modern" JKR technique to obtain the thermodynamic work of adhesion (in 1991). They used small hemispheres (radius ca. 1-2 mm) of cross-linked PDMS (Sylgard 170) in contact with flat PDMS sheets. The work of adhesion (W) for PDMS self-adhesion was reported to be 42-44 mJ/m^2. These values are in close agreement with the values of surface energy of PDMS (γ_{PDMS}= 20-22 mJ/m^2) obtained by contact angle measurements. This study showed no hysteresis for PDMS self-adhesion.

After Chaudhury and Whitesides [52], various research groups [15, 29, 53, 57] advanced the JKR apparatus by incorporating a stepper motor, a balance or a load cell, temperature controlling chamber, and anti-vibration table into the system for more accurate measurements. In the majority of the studies that exploit the JKR test set-up, typically the loading/unloading JKR experiments for PDMS self-adhesion is performed prior to any testing to determine the accuracy of the system. The calculated value of W for PDMS self-adhesion in general, using the loading portion of the JKR experiment, has been reported in the range of 37-53 mJ/m^2. Please note that the specific value of W is dependent on a number of factors including PDMS manufacturer/type or the synthesis method, time and temperature of curing, mixing ratio, etc. For Sylgard 184 with the mixing ratio of 10:1 the value of W in the literature has been reported as 52.5 ± 1.3 mJ/m^2 [58], 43.6 mJ/m^2 [59], and 43 mJ/m^2 [60] where the latter two are close to the mostly accepted value of W for PDMS self-adhesion (42-44 mJ/m^2). No published values, however, have been reported for 10:2 mixing ratio. The values obtained in the current study (where 5:1 mixing ratio was used) are in the range of 41-44 mJ/m^2, which is in good agreement with the previous results for PDMS self-adhesion.

Although Chaudhury and Whitesides [52] didn't observe any adhesion hysteresis for PDMS self-adhesion in their initial study, various studies have seen adhesion hysteresis during self-adhesion of PDMS samples made with different PDMS base or synthesis methods. Significant research has been carried out to assess the underlying reasons of adhesion hysteresis for PDMS self-adhesion, although the reasons provided in the literature for hysteresis are sometimes contradictory. The following paragraphs discuss the studies focusing on hysteresis observed in PDMS self-adhesion.

Choi et al. [61] observed that adhesion hysteresis increased by extracting PDMS samples in toluene where free chains of the PDMS network were removed. The PDMS samples in their study were prepared with different stoichiometric ratios between the cross-linker (r) and the base. The results also showed that the adhesion hysteresis reduced by increasing the amount of cross-linker. Choi et al. [61] rejected the idea proposed by Silberzan et al. [62] that the adhesion hysteresis of extracted PDMS is caused by H-bonding from Si-OH groups of PDMS because in that way the hysteresis should have increased by increasing the cross-linking ratio. Choi et al. attributed the adhesion hysteresis to the entanglement of PDMS tethered chains and their interdigitation with cross-linked PDMS network at the interface because the number of tethered chains increases when r decreases [61]. Deruelle et al. [53] assessed the adhesion hysteresis between elastomeric PDMS hemispheres and silicon wafers grafted by a layer of monodisperse PDMS as a function of the molecular weight and surface density of the grafted chains. The adhesion hysteresis in their study was attributed to physical bridging and interpenetration of dangling chains from the grafted layer to the opposite surface.

In another study to determine the origin of adhesion hysteresis, Perutz [54] found that hysteresis of PDMS networks (prepared by means of hydrosilylation) was increased by adding

excess amounts of cross-linker to PDMS networks. In this study it was shown that by "poisoning" the platinum (Pt) catalyst with a thiol the hysteresis could be lowered significantly, or removed in some cases. Perutz et al. [54] rejected the role of dangling chains interpenetration on adhesion hysteresis proposed by Deruelle et al. [53] and attributed the adhesion hysteresis of elastomer-elastomer systems to surface reconstruction caused by the formation of complexes between silane groups and the Pt catalyst. Perutz et al. [54] also observed that the hysteresis during unloading was rate dependent. They rejected the hypothesis given by Maugis and Barquins [25] that bulk viscoelastic losses could be one possible reason for adhesion hysteresis because in that case both loading and unloading should be dependent on the rate of increase or decrease in contact area, respectively while in the Perutz' study only unloading G was rate dependent and the loading G was equal to the thermodynamic work of adhesion ($W= 44\ mJ/m^2$). Recall that Maugis used the analogy between fracture mechanics and the diminishment of the contact area during the unloading portion of the JKR experiments. Based on this, Maugis and Barquins [25] claimed that the adhesion hysteresis seen in a polyurethane/glass system arises from the viscoelastic losses right at the crack tip. In the study performed by Perutz et al. [54], however, the crack velocities were much lower than those achieved by Maugis and Barquins [25]. Another possible reason given for adhesion hysteresis by Perutz et al. [54] was the chemical changes at the interface. They claimed that methyl surface functional groups (CH_3) could reconstruct in such a way as to interact with the (SiH) functional groups on opposite sides of the interface.

In a work performed later by Amouroux and Leger [45], the role of chain interpenetration on adhesion hysteresis was again confirmed for elastomer-elastomer systems. They [45] used the JKR test to investigate the interactions between tailored PDMS elastomers with identical

chemistry but different amount of dangling chains. PDMS networks were prepared by hydrosilylation of vinyl-terminated pre-polymer and a catalyst. These systems exhibited time-dependent adhesion hysteresis that increased with the amount of dangling chains. Similar to Deruelle et al. [53], the adhesion hysteresis of elastomer-elastomer systems was attributed to the progressive bridging of the interface by pendant chains present in the network [45].

In the study performed by Mason et al. [56] only the hemispheres that were extracted in toluene showed hysteresis. It was shown that for the system involving the extracted hemispheres and tethered polystyrene substrates no hysteresis was present. Based on this, they concluded that hysteresis was caused by surface interactions rather than bulk viscoelastic properties. In their work, adhesion hysteresis was observed only for PDMS networks with a high molecular weight; whereas tightly cross-linked networks did not show any hysteresis, even at extended contact times [56]. They attributed the hysteresis to the chemical cross-links across the interface because the hysteresis could be prevented by inhibiting the hydrosilylation reaction between residual vinyl and silane groups.

In summary, for PDMS self-adhesion it has been shown that during loading W is in the range of 37-53 mJ/m^2, resulting in surface energy of 18.5-26.5 mJ/m^2. Where, as discussed above, several factors attribute to this range. The widely accepted value of surface energy, however, is in the range of 21-22 mJ/m^2. The hysteresis observed for PDMS self-adhesion has been attributed to a variety of effects including irreversible chemical interactions at the interface, reorganization, entanglement or interdigitation of surface molecular chains, and viscoelastic energy loss caused by plastic deformation.

Chemically Modified PDMS Surfaces

Chaudhury and Whitesides [63] employed JKR measurements to measure surface energies of a variety of self-assembled monolayers (SAMs) of alkylsiloxane on PDMS surfaces. The end chemical functionalities of these monolayers were CF_3, CH_3, OCH_3, $COOCH_3$, and Br groups. PDMS surfaces were first modified by exposing PDMS sheets and hemispheres to an oxygen plasma source to produce a silica-like layer (SiOH) on the surface. Monolayers were then generated by chemisorptions of alkyltrichlorosilanes [$Cl_3Si(CH_2)_nR$] onto oxidized PDMS sheets and hemispheres, where R is the functional groups mentioned earlier. The results of the JKR measurements were compared to the values of surface energies obtained from contact angle measurements. The values of W varied from 31 mJ/m^2 for self-adhesion of CF_3 SAMs to 39 mJ/m^2 for CH_3 SAMs to 53 mJ/m^2 for OCH_3 SAMs to 65 mJ/m^2 for $OCOCH_3$ SAMs, and 72 mJ/m^2 for Br SAMs. For non-polar groups, such as CF_3 and CH_3, there was a good agreement between surface energies obtained from the JKR experiments and those predicted from the contact angle measurements. For polar groups (OCH_3, $COOCH_3$, and Br) JKR measurements underestimated the values of surface energies compared to contact angle measurements. The values of surface energies determined from the JKR measurements were, however, close to the non-polar component of surface energy predicted from contact angle measurements [63].

Using the JKR method, Kim et al. [9] investigated the adhesion of cross-linked PDMS hemispheres with a variety of functional groups on gold substrates. These monolayers were prepared on the surface of gold by means of thiol-based solutions terminated with CF_3, COOH, CH_3, and F. They also conducted JKR experiments between PDMS lenses and oxidized silicon wafers. Experiments with different waiting times between maximum loading and the beginning of unloading showed that there is a time-dependent adhesion hysteresis between PDMS and oxidized wafer. This adhesion hysteresis was attributed to H-bonding between OH groups

present on surface of silicon wafer and Si-O-Si groups of PDMS. The interactions between PDMS and monolayers also demonstrated that the adhesion hysteresis was dependent on the chemical composition of the surface and the strength of the bonds that were formed between the two surfaces. For instance, the COOH group showed significant adhesion hysteresis which was attributed to the formation of hydrogen bonds. This was compared to negligible adhesion hysteresis observed for CF_3- or F-terminated surfaces where van der Waals forces are dominant. Based on these results they concluded that the distinction in the unloading portion of the JKR is an indication of non-specific (van der Waals, dipolar) or specific interactions (H-bond, acid-base, donor-acceptor) developed at the interface of the two surfaces. In the graph superimposing G vs. normal stress for the loading/unloading portions, the loading trend for all the functionalized surfaces were similar, indicating that W was almost the same for all the functionalities. Although they obtained $W = 42 \pm 1$ mJ/m^2 for PDMS self-adhesion, no values for functionalized surfaces were reported. However, by scaling the G vs. normal stress graph the value of W was approximately 30 mJ/m^2.

Mason and Koberstein [64] used the JKR technique to study the interfacial interactions between PDMS hemispheres and various functionalized substrates. PDMS hemispheres were prepared by hydrosilylation reactions between silane (SiH) and vinyl groups in the presence of a Pt catalyst to produce silane or vinyl functionalities. Functionalized substrates included poly(styrene-b-butadiene) (PS) copolymers with vinyl functionality, vinyl-terminated trimethoxysilane SAMs, and α,ω-functional PDMS brushes terminated with either monomethoxy or hydroxyl groups. The molecular weights of the interfaces used in this study were kept below the entanglement molecular weight to minimize the effects of chain interpenetration on adhesion. The results showed that hydrosylilation and silicone reactions that occurred at the interface

enhanced adhesion significantly. Systems with hydroxyl (OH), methoxy (CH_3), and silanol (SiH_3OH) functionality provided considerable adhesion improvements by forming stronger interfacial bonds [64]. Using the values of the surface energies for PDMS and polystyrene, they calculated the value of W for this system as 57.4 mJ/m^2, which agreed well with the value obtained from the JRK theory. For all other systems G_0 (the zero-rate fracture energy) was determined from the fracture toughness vs. crack velocity and reported. At zero velocity, the viscoelastic dissipation energy is ignored [29] and in the absence of interfacial chemical reactions, G_0 should be equal to the work of adhesion.

Special Applications of JKR Experiments

Shanahan and Michel [65] investigated the adhesion of polyisoprene rubber to glass surfaces near equilibrium when the cross-link density of the rubber is changed. In addition to the standard JKR approach, another experimental protocol was also used in their study to ensure that equilibrium is achieved. In this approach, a glass slide (0.1 g) was placed on the hemisphere and a force of 50 g imposed for 5 minutes and then removed. The evolution of the contact area after load removal was observed as a function of time for 15 days. The JKR measurements showed that for the material system used the adhesion hysteresis was considerably dependent on the cross-link density.

Li et al. [55] exploited the JKR technique to investigate surface and interfacial energies of glassy or semi-crystalline polymeric materials. In their study, cross-linked PDMS hemispheres were coated with a thin layer of various glassy polymers with a polyethylene backbone. The PDMS surface was modified by oxygen plasma before the thin layer was deposited. Coated PDMS probes were then brought into contact with silicon wafer substrates coated with the same polymer. The results showed that in the case of the coated lens and/or substrate, the surface and

interfacial properties were governed by the coating material while the elastic modulus of the soft material let the system deform sufficiently under small forces which is essential for probing surface forces. By comparing the results of surface energies measured by the contact angle measurements and the JKR technique, Li et al. [55] concluded that the JKR technique is more reliable to determine surface energy of solid polymers because the results of contact angle measurements are dependent theoretical approach used to analyze the data.

Pickering et al. [66] exploited the JKR method to determine the effects of contact time, humidity, and surface roughness on the adhesion hysteresis of PDMS. The results showed that by increasing the contact time between PDMS and various substrates, adhesion hysteresis was increased. In order to study the effects of roughness, glass and mica substrates were used. Mica has a negligible surface roughness compared to glass. The results showed that the hysteresis for PDMS/mica in ambient air was smaller than the hysteresis of PDMS/glass. The authors attributed this to the smaller surface roughness of mica. The experiments performed in dry nitrogen revealed the same results for hysteresis of PDMS with glass and mica, although considerably less hysteresis was observed in dry nitrogen (no humidity). The lower adhesion hysteresis in dry nitrogen was attributed to the lower capillary forces and hydrostatic interactions at the interface. The authors stated that in the presence of water layers on a glass surface in ambient air PDMS can rearrange to form weak hydrogen bonds with the water layer. Therefore, a larger adhesion hysteresis was observed for PDMS/glass in ambient air. Hydrophilic surfaces also showed a larger hysteresis compared to hydrophobic surfaces. This was associated with the ability of PDMS networks to establish H-bonds with hydrophilic surfaces.

Woerdeman et al. [67] demonstrated the feasibility of the JKR testing method to probe the effects of surface contamination on adhesion of inorganic substrates. They exploited the JKR

approach to assess the interactions between a diglycidyl epoxy elastomer and an aluminum oxide substrate in the presence of an organic contaminant (hexadecane). The hexadecane contamination was shown to decrease the adhesion hysteresis.

Dillow and coworkers [43] used the JKR approach to study adhesion of biomimetic membrane substrates and $\alpha_5\beta_1$ receptors. The membrane substrates were constructed from peptide and polyethylene glycol (PEG) amphiphiles by means of the Langmuir-Blodgett (LB) technique. In this technique a thin film is deposited from a liquid into a solid surface by immersing the solid substrate in the liquid. PDMS hemispheres were used to immobilize the integrin receptors because of the well-behaved characteristics of PDMS. In this work, the effects of membrane composition, density, temperature, and peptide conformation on adhesion to activated integrins were determined. The results demonstrated that the JKR technique can be used as a simple, yet robust method to measure adhesion strength of bio-systems.

Falsafi and co-workers [68] used JKR measurements to study the influence of composition on surface energetics and mechanical performance of cross-linked 2-ethylhexyl acrylate acid (2EH-co-AA) elastomers as model pressure sensitive adhesives (m-PSAs) by means of the JKR technique. Measurements of surface energy showed that, for these materials, the surface energy was dominated by the methylene group (γ=30 mJ/m^2). The adhesion hysteresis was also shown to be independent of the acrylic acid content implying that viscoelastic dissipations are the main mechanism contributing to adhesion of un-cross-linked or lightly cross-linked versions of these types of PSAs. The results of contact of PDMS hemispheres coated with un-cross-linked PSA showed cavitation and fibrillation of the material around the edge of the contact area. The cavitation and fibrillation were attributed to visco-elastic dissipation in adhesion of PSAs.

Adhesion properties of acrylic pressure sensitive adhesive-like networks (PSA-LNs) were examined by Garif and coworkers [37]. The JKR measurements showed that acid- or amino-modified samples of PSA-LN displayed substantial hysteresis while the unmodified version showed no hysteresis. The amino-modified PSA showed a larger hysteresis compared to acid-modified surfaces because of the ability of the amine group to form acid-base interactions at the interface. The acid-base interactions of amine groups are stronger compared to the hydrogen bonds formed at the interface of the acid-modified PSA with carboxylic acid side groups. For the three PSA versions the results of G vs. the fracture velocity (v) showed that there was a transition from weak to strong dependence in adhesion behavior of commercial acrylic PSAs [37]. The rate-dependent behavior showed a power-law form with the power changing from 0.2 to 0.5. The amino-modified surfaces revealed a more rate-dependent behavior because of the stronger interactions at the interface of these PSA modified systems.

Leger et al. [38, 45, 48] investigated the adhesion of MQ resins (silica-like nano-particles) incorporated in PDMS elastomers and acrylic adhesives in a three-part work. In the first study [45], they used elastomers with various concentrations of MQ resin and PDMS layers made of densely grafted short chains to characterize how the resin content influences the dissipation behavior in the elastomeric layer. In order to determine the role of resins and their effects on enhanced interactions in the interfacial adhesion of elastomeric layers thin-surface-anchored acrylic layers were used. The thickness of acrylic layers were kept minimal so that the dissipation in the acrylic layer could be disregarded [45]. The results obtained during JKR loading for acrylic adhesives showed K increased as the amount of MQ resin was increased while W displayed an inverse dependence. The values of W also showed a rate dependency for the 40% MQ resin. The results during the unloading showed that G_0, the adhesive strength at zero

fracture velocity, and G(v), the velocity-dependent energy release rate, were dependent on the MQ resin content and contact time. The dissipation energy (Φ) for various MQ resin amounts followed the empirical power law expression described in Chapter 2.

In the second work of Leger et al. [48], the adhesion between silicon elastomers containing various amounts of MQ resin and model substrates made of self-assembled monolayers (SAM) of thiol molecules with various amounts of carboxylic terminations was investigated. The interfacial adhesion was shown to be a trade-off between increased interactions and decreased chain mobility associated with the amounts of the resin inside the elastomer. By increasing the amount of the MQ resin the oxygen content of the adhesive was increased which would favor the hydrogen bond formation. But at the same time replacing the flexible chains of PDMS with rigid nano particles reduced the mobility and reorganization of the polymer chains.

The third work [38] compared the behavior of polybutylacrylate (PBA) hemispheres on (1 mm thick) PDMS layers with or without MQ resins, thin PDMS layers made from α,ω-OH terminated PDMS melt, and pure MQ resin layer deposited on silicon wafer. The results showed that G_0 was dependent on the MQ resin and increased with the resin amount in a non-linear manner. The authors attributed this to an extraction process of the PnBA chains attached to the elastomer surface from the PnBA hemispheres or to the fracture of these chains attached to the surface. The MQ resins present at the interface showed to slow down fracture propagation and preventing the PnBA chains from leaving the surface, hence producing a larger deformation of PnBA lenses.

Ahn et al. [69] used the JKR technique to study UV-curable PSAs derived from acrylated epoxidized soybean oil (AESO). The PSAs were prepared by 3 to 9 UV scan cycles until the AESO polymer lost its tackiness. The JKR experiments, however, were performed on samples

with 6 and more UV scans. The JKR loading/unloading experiments were carried out for AESO self-adhesion and PDMS-AESO adhesion. During the JKR loading the values of W and K were determined whereas during the unloading portion G(V) was obtained. No values for self-adhesion of samples cured with 6 UV cycles were reported, however, as the authors observed fingers around the contact area during both loading and unloading portions. The fingering effect observed for viscoelastic materials such as PnBA chains in contact with adsorbed resin layers [38], glucose above its glass transition temperature [70], and self-adhesion of uncross-linked PSAs [68] has been attributed to viscoelastic dissipation. For the samples cured with 7, 8, and 9 UV cycles, the evolution of the adhesion energy (G) as a function of crack velocity (v) for AESO self-adhesion showed different kinetic laws during the relaxation steps and deviated from the power law trend described in Chapter 2. The authors attributed this to the hydrogen bonds developed between AESO surface and that these bonds fail through a series of catastrophic "bursts" of energy as the bonds are broken [29]. For PDMS-AESO adhesion the different relaxation step contributed to a unique G(v) curve except the last step before separation. The authors attributed the relaxation behavior of PDMS-AESO to the purely physical interactions that were formed between PDMS and AESO.

These studies show that the JKR technique can be adjusted in different manners to examine the interfacial behavior of any combination of polymeric surfaces or to mimic the adhesive properties of two surfaces that are hard to study directly. PDMS has also been shown to be a commonly used material for the JKR measurements because its surface can be modified to represent different chemical functionalities without altering its bulk properties.

PDMS/Cellulose-Lignin

The work performed by Rundlof et al. [71] is believed to be the first study using the JKR method to measure adhesion of cellulosic surfaces. Rundlof et al. [71] conducted JKR measurements to determine adhesion between PDMS and Langmuir-Blodgett (LB) cellulose surfaces as well as hydrophobic mica, bare mica and glass. The results for self-adhesion of PDMS and self-adhesion of oxidized PDMS were also presented as a reference. Cellulose surfaces were prepared by depositing trimethylsilyl cellulose (TMSC) on hydrophobized mica surfaces by means of LB method. TMSC was then converted to cellulose by exposing the surface to humid HCl. The work of adhesion (W) for PDMS self-adhesion for three measurements was 48.6 ± 3 mJ/m^2, 50.6 ± 4 mJ/m^2, and 44.6 ± 1 mJ/m^2, although no reason was given for the discrepancies. The values of W for other surfaces were 47.6 ± 1.5 mJ/m^2 for self-adhesion of oxidized PDMS, 58.9 ± 2.3 mJ/m^2 for PDMS-mica, 39.8 ± 1.2 mJ/m^2 for PDMS/hydrophobic mica, 49.5 ± 3 mJ/m^2 for PDMS-cellulose, and 44.8 ± 2.1 mJ/m^2 for PDMS-glass. The JKR results showed that for PDMS self-adhesion, PDMS-mica, and PDMS-hydrophobic mica a negligible hysteresis was observed whereas, PDMS-cellulose and PDMS-glass systems displayed a relatively large hysteresis. The adhesion hysteresis of clean glass surfaces was larger than cellulose surfaces. This was attributed to the stronger H-bonds formed between PDMS and glass. The adhesion hysteresis of cellulose surfaces was attributed to the interpenetration of PDMS chains and the outer layers of cellulose.

Eriksson and co-workers [72] performed JKR measurements on three different cellulose surfaces, one crystalline (cellulose I) and two surfaces with lower degrees of crystalline order (cellulose A and B). Self-adhesion of PDMS samples made out of Sylgard 182 was also included for comparison. Cellulose I was prepared from a northern softwood, dissolving grade pulp by acid hydrolysis. The thin film of cellulose I was then spin-coated on a silicon wafer. The second

type of cellulose surface (cellulose A) were prepared by dissolving the wood pulp in NMMO (N-methylmorphine N-oxide) at 115ºC for 2 h. DMSO (Dimethyl sulfoxide) was then added to the solution to decrease the viscosity before spin coating. Thin films of cellulose were then formed on silicon wafer surfaces by means of spin-coating. The third process used for cellulose preparation (cellulose B) was based upon acetone-extracted pulp in Milli-Q water and dissolving the pulp in LiCl/DMAc (Lithium chloride/N, N, dimethylacetamide). The cellulose solution was then spin coated onto a silicon wafer. This preparation procedure was previously shown to reduce the degree of crystalline order [72]. The JKR measurements between PDMS and cellulose films showed that the work of adhesion obtained from the loading portion was similar for all three surfaces and close to that of PDMS self-adhesion while the adhesion hysteresis was inversely proportional to degree of cellulose crystallinity. The difference in adhesion hysteresis of cellulose surfaces was attributed to the ability of surface groups to re-orient for developing specific or non-specific interactions at the interface, where for surfaces with a lower degree of crystalline order there is a higher possibility for reorientation of surface groups [72]. Moreover, the JKR results of cellulose adhesion showed a dependency on relative humidity. According to the JKR measurements, the hysteresis was increased by increasing the RH from 30% to 50%, whereas the work of adhesion was greater in 30% RH. This was associated with the possibility of the surface to take up water and hence, increasing the mobility of surface molecules and the fact that water acts as a plasticizer contributing to stronger interactions. The value of W was 51 ± 2 mJ/m^2 for PDMS self-adhesion; 49 ± 6 mJ/m^2 for adhesion of PDMS and cellulose I at 30% relative humidity (RH) and 45 ± 4 mJ/m^2 at 50% RH; W was 47 ± 3 mJ/m^2 for cellulose A at both 30% and 50% RH; and W was 40 ± 4 mJ/m^2 for cellulose B at 30% RH and 46 ± 4 mJ/m^2 at 50% RH.

Kallio et al. [47] studied the spreading kinetics of liquid wood extracts on surfaces of materials occurring in paper machines by means of contact angle measurements and the JKR technique. The contact angles were used to determine the surface energies for a variety of polymers used for pitch control and paper machine surfaces as well as studying the spreading kinetics. Moreover, a model wood resin composition was chosen as well as cellulose and lignin. The cellulose and lignin surfaces were prepared by spin-coating or LB deposition and were only used in contact angle measurements. Using the surface energy of lignin obtained from contact angle measurements, the thermodynamic work of adhesion for these surfaces was reported as 61 ± 1.4 mJ/m^2 in air and 4.7 ± 0.5 mJ/m^2 in an aqueous solution with pH 4.6. For cellulose the thermodynamic work of adhesion, derived from contact angle measurements, was reported as < 0.4 mJ/m^2 in an aqueous solution with pH 4.6 and > 62 mJ/m^2 in air. The JKR measurements were only used between the wood resin and either native PDMS hemispheres or PDMS hemispheres that were spin-coated with a fluoropolymer solution. The JKR value of W for adhesion between the wood resin to native PDMS was 54.5 ± 0.7 mJ/m^2 and 33.5 ± 0.9 mJ/m^2 to fluoropolymer surfaces. These values were close to the values obtained for these surfaces using contact angle measurements.

Johnasson [73] investigated adhesion interactions between wood biopolymers using model surfaces of cellulose, lignin, and hemicellulose by means of the JKR method under ambient condition. Model surfaces of these wood biopolymers were deposited on silicon wafer by means of layer-by-layer (LbL) technique and used as substrates in the JKR experiments. PDMS hemispheres were also coated with LbL films of nanofibrillated cellulose (NFC). The JKR measurements between cellulose/cellulose, cellulose/lignin, and cellulose/glucomannon (to represent hemicellulose in softwood) surfaces showed no significant differences in the

interactions. The work of adhesion (W) obtained from the loading data was 47 ± 4 mJ/m^2 for cellulose/cellulose, 51 ± 5 mJ/m^2 for cellulose/glucomannon, and 49 ± 5 mJ/m^2 for cellulose/lignin. The adhesion hysteresis was also similar for these systems. Based on these results, the author concluded that the interactions between cellulose, lignin, and glucomannon were equivalent in magnitude although lignin surfaces are hydrophobic while cellulose is hydrophilic. The author claimed that the results are reasonable considering that wood biopolymers need to interact well with each other to give strength to woods and plants [73]. Contact angle measurements were also performed to evaluate the surface energy of cellulose, lignin, and hemicellulose surfaces. The results of these experiments showed that surface energies of cellulose, lignin, and glucomannon (as the hemicellulose representative) were comparable although water formed a lower contact angle on cellulose and glucomannon surfaces compared to lignin surfaces. The higher contact angles of water on lignin were associated with the smaller polar component of lignin surface energy compared to that of cellulose and hemicellulose while the non-polar (or dispersive) component was similar for all three surfaces [73].

Underwater JKR

Very few studies have been performed to evaluate the application of the JKR theory underwater for any material system. Chaudhury and Whitesides [52] studied the interactions between a PDMS hemisphere and a PDMS flat sheet in water-methanol mixtures of different concentrations by using what is referred to as the zero load approach. In the zero load approach, hemispheres of different sizes are brought into contact with flat sheets under their own weight and the work of adhesion is determined from the modified JKR relationship where the applied load is set to zero. The results showed that adhesion between PDMS surfaces was the largest (W≈ 75 mJ/m^2) in pure water but decreased when methanol was added. In pure methanol there

was still a small adhesion (W≈ 6 mJ/m^2) between PDMS surfaces. Haidara et al. [74] used the same zero load approach to study the adsorption of a non-ionic surfactant at the solid-liquid interface. They used PDMS surfaces that were modified with mono-layers of decyltrichlorosilane and [$H(CH_2)_{12}(OCH_2CH_2)_7OH$] as the non-ionic surfactant.

Loskofsky et al. [51] designed and evaluated an underwater full loading/unloading JKR system and evaluated silicon/silicon and silicon/silanized silicon wafers. They showed that the thermodynamic work of adhesion obtained from loading measurements underwater is comparable to the values estimated using surface energies and contact angles of water on the surfaces studied [51]. To determine the stability of G underwater, Loskofsky et al. [51] observed the development of the contact area as a function of time during a single increment (both during loading and unloading) for 3600 s. They showed that the value of G underwater, for a system consisting of extracted PDMS hemispheres in contact with a silane-modified silicon wafer, reached a plateau (G ≈ 62 mJ/m^2) at 1200 s, after which it decreased slowly. This value of G agreed reasonably well with the values estimated from contact angle measurements. For their JKR loading/unloading measurements, however, they used a waiting time of 30 s between each increment which resulted in a value of G ≈ 54 mJ/m^2, which was ca. 70% of its plateau value. Therefore, they divided the values they obtained from loading measurements by the average ratio of 0.7 to determine the work of adhesion at the equilibrium state for all other material systems they studied. Using this correction, they calculated the W for PDMS self-adhesion underwater to be in the range of 67-84 mJ/m^2. This range was similar to the results they obtained from zero load measurements (W=72 ± 4 mJ/m^2) and values determined from the static contact angle of water on PDMS surfaces (W=74-78 mJ/m^2).

In another study, the JKR method was used to investigate the adhesion between PDMS hemispheres coated with layer-by-layer (LbL) assemblies of polyelectrolytes and rigid, planar substrates [19]. Rigid substrates used in this work were amine-functionalized glass slides while PDMS hemispheres were coated with a carboxylic acid group. The JKR experiments were performed in both air and in aqueous solutions of controlled pH (3 and 5.5). The results of their study were only reported in terms of adhesion hysteresis (not W). For the uncoated PDMS hemispheres/amine-treated glass a larger adhesion hysteresis was observed in air compared to that measured in aqueous solutions [19]. The hysteresis was dependent on the pH of the solution, where at a pH=5.5 the hysteresis was larger than that of pH=3. The coated PDMS hemispheres showed a lower adhesion hysteresis compared to the uncoated hemispheres both in air and aqueous solutions despite the fact that interactions should raise when the acid in PDMS (COOH) makes contact with the base (amine) on functionalized slides. The authors attributed this to the combined effect of surface roughness and high elastic modulus of the coating that prevented intimate contact at the interface. Annealing LbL-coated hemispheres in low concentration of NaCl solutions showed that surface roughness could be reduced and therefore, the adhesion hysteresis could be increased.

Defante et al. [17] used the underwater JKR approach in combination with the surface sensitive sum frequency generation (SFG) spectroscopy to study the contact between hydrophobic surfaces underwater. In their study, PDMS hemispheres were used to probe other hydrophobic surfaces, including PDMS flat sheets, surfaces coated with octadecyltri-chlorosilane (OTS), and a layer of poly(vinyl-n-octadecyl carbamate) (PVNODC). The work of adhesion (W) underwater for PDMS-PDMS and PDMS-OTS systems was greater than that obtained in air. For the PDMS-PVNODC system, however, the value underwater was smaller than the other two

systems and close to the value obtained in air although contact angles of water and hexadecane were the same for the three systems. The values of W obtained from the JKR experiments in air were also close for the three surfaces. The difference between the value of W for PDMS-PDMS and PDMS-OTS compared to PDMS-PVNODC underwater was related to the rearrangement of water around the contact area.

Results of SFA and AFM Studies

In some studies, adhesion of smooth model surfaces under various surface and solution conditions has been studied by means of a surface force apparatus (SFA) or an atomic force microscopy (AFM). These studies mostly report surface forces between two surfaces as a function of distance in dry or humid air, aqueous environments or electrolyte solutions.

Using SFA, Faghihnejad and Zeng investigated the interaction mechanism between two hydrophobic surfaces [75] or a hydrophobic-hydrophilic system [76] underwater. They probed the force-distance profiles between two model systems consisting of two hydrophobic polystyrene (PS) surfaces [75] and PS-mica surfaces [76] in different electrolyte solutions (including NaCl, $CaCl_2$, HCl, and CH_3COOH) of various concentrations. The results showed that for two hydrophobic surfaces long range attractive interactions, referred to as hydrophobic interactions, were present and dependent on the electrolyte concentration [75]. For the hydrophobic-hydrophilic system a long-range repulsion was observed which was also dependent on the electrolyte concentration [76].

By means of an AFM, Kokkoli and Zukoski studied the interaction forces between self-assembled monolayers (SAM) of two hydrophobic surfaces [77] and a hydrophilic system [78] in an aqueous environment. They showed that for two hydrophobic surfaces underwater the interactions were purely attractive [77]. Also, the addition of an electrolyte (NaCl) to the solution

increased the attractions between the hydrophobic surfaces [77]. For a hydrophilic-hydrophobic system (an ionizable acid functional group (COOH) and a methyl-terminated (CH_3) surface) the interactions were repulsive upon approaching; whereas, upon the retraction a small adhesive interaction was observed [77]. For the hydrophilic system including two COOH surfaces [78] a pH-dependent trend was observed for force vs. distance profiles. At low pH a large attraction (no repulsion) was seen; whereas for pH larger than 4.7 the system experienced an exponentially decaying repulsion.

The adhesion of model cellulosic surfaces under various surface and solution conditions has also been studied by means of SFA [79, 80] or AFM [81, 82]. The nature of the surface forces between cellulose surfaces or cellulose and other materials in air has been described as attractive, whereas in an aqueous environment the interactions have been described as either repulsive due to steric effects [79, 80] or alternating between attractive and repulsive due to double layer interactions [83]. In the presence of a cationic electrolyte, an electrostatic repulsion was observed between cellulose surfaces [84].

Chapter 5 - Research Strategy

The fundamental objective of this research was to characterize how surface chemistry alters adhesion or surface interactions of polymeric materials in the presence of water. For this purpose the JKR experimental approach of contact mechanics was used to evaluate a variety of surfaces with different chemical structures. The JKR experimental technique reveals the thermodynamic work of adhesion, which is indicative of the surface interactions, and the specific/non-specific interactions that are developed at the interface of the two surfaces or frictional behavior of the surfaces that are in contact. As mentioned before, one of the basic requirements of the JKR experiment is that at least one of the two contacting surfaces is compliant. Based upon previous studies and the fact that we used model surface in this research as substrates, PDMS was chosen as the probe in order to assess how surface chemistry affects surface interactions underwater.

To achieve the aim of this study, this research was divided into two complementary phases, which are discussed in the following paragraphs. In brief, the first phase used native PDMS probes to investigate two different sets of model surfaces. The first set of surfaces was chemically functionalized glass substrates to obtain a basic understanding of the interactions in air and underwater in a systematic manner. These functionalized surfaces showed a diverse wetting behavior ranging from hydrophobic to hydrophilic. The second set consisted of a bio-polymeric system based upon wood-derivatives, namely cellulose and lignin.

In the second phase PDMS probes were chemically modified with a non-hydrophobic group. The modified PDMS hemispheres were used to probe a number of key surfaces introduced in the first phase. These surfaces were chosen based on their wetting behavior and their adhesion results obtained in the first phase to further advance our understanding of the

adhesion interactions underwater. The results obtained for the chemically modified glass surfaces in the first part of the first phase were used as a basis to interpret the results of the bio-polymeric system (second part of the first phase), as well as the results obtained in the second phase. This chapter discusses the two phases of this study in detail.

Although previous studies have shown contradictory results for hysteresis of 10:1 extracted PDMS samples in the JKR experiments, no hysteresis difference was seen in the current study for 5:1 PDMS samples before and after extraction. Therefore, non-extracted 5:1 PDMS hemispheres are used in the first and second phase.

Phase I

In the first part of this phase, several key functional groups were identified with distinguishing chemistry and wetting behavior. These functional groups were picked so that a wide spectrum ranging from hydrophobic to hydrophilic behavior is evaluated. These functionalities, which were applied to glass slide surfaces, included methyl (an aliphatic hydrocarbon), cyclohexyl (a cyclic hydrocarbon), and fluorocarbon as hydrophobic groups; polyethylene oxide (PEO) as a hydrophilic group; amine, carbomethoxy, and mercapto (thiol) groups with intermediate wetting behavior. These functional groups were selected for the following reasons: (1) the selected groups have a simple structure while ranging from hydrophilic to hydrophobic. This would allow us to study the interactions of a wide variety of surfaces to determine the overall trend as a function of chemistry; (2) it is relatively straightforward to use commercially available chemicals to apply these functional groups on the surface of glass or silica. In this study, silanization, with specific alkyl-silane coupling agents, is used to chemically functionalize the glass slides. Details of this process are provided in the next chapter. Ultrapure water is used as the probe in contact angle measurements to examine the

nature of the treated slides. In addition to the aforementioned functional groups, native PDMS flat sheets and clean glass (referred to as bare glass) were also evaluated for means of comparison. Since PDMS self-adhesion has been widely evaluated using the JKR technique, these tests were used to verify the JKR set-up accuracy and data reduction, too.

In the second part of phase I, three model surfaces were evaluated. These surfaces included two cellulosic surfaces and one lignin surface coated on glass slides. The cellulosic surfaces were prepared from wood pulp, while the lignin surface was prepared from ball milled hardwood. Cellulose and lignin surfaces were used for two fold. The first is to verify whether the results of the basic model surfaces used in the first part of this phase can be used to predict and/or interpret the behavior of a more advanced system. The second is the application of cellulose and lignin in paper making industries as well as composites and hydrogels. The interactions of cellulose or lignin with water can affect the efficiency of the final product in these systems. Therefore, it is important to gain an understanding of the interactions between these materials in the presence of water. As mentioned earlier, native PDMS probes were used to evaluate the silanized glass surfaces as well as cellulose and lignin surfaces in air and underwater using the JKR approach.

Phase II

As was mentioned, the main goal of this study was to determine the effects of surface chemistry on interfacial interactions underwater. In the first phase several model surfaces were probed with native PDMS, which is hydrophobic in nature. In order to further advance our understanding of the interfacial interactions underwater, for the second phase PDMS probes were functionalized to show a non-hydrophobic behavior. The results that were obtained in the first phase as well as the ubiquitous existence of the amine functional group in biology, e.g. in amino

acids, and the application of the amine group in personal care products, dyes, adhesives, and drugs inspired the selection of amine for functionalizing PDMS in the second phase. A previous study [85] has shown marine creatures, such as mussels, oysters, and barnacles, use lysine (an amino acid with amine side chain) as an underwater adhesive to attach to slippery surfaces.

For surface modification of PDMS samples, several approaches were carried out. These included surface oxidation (by oxygen plasma and UV/ozone) followed by silanization, UV-induced polymerization, and hydrosilylation techniques [86]. The UV-induced polymerization resulted in milky surfaces that could not be used in the JKR technique since they were not transparent. The hydrosilylation technique, based upon the reactions of a surface rich in silane group (Si-H) and vinyl-containing molecules in the presence of a Pt catalyst, showed a promising method at first. The results that were obtained from the JKR technique, however, showed that further cautions may need to be considered to prepare functionalized surfaces with this method. The JKR results showed that the Pt catalyst existing in the treated PDMS samples could take part in the interactions with the opposing native PDMS surface showing a hysteresis that was not caused solely by the surface interactions. No catalyst-based hysteresis was observed when a glass slide was used, nor when the Pt catalyst was poisoned. The JKR results for the samples treated with the hydrosilylation technique and the results for poisoned and non-poisoned samples are presented in Appendix A.

With the PDMS samples oxidized with both oxygen plasma and UV/ozone there is a concern that PDMS recovers its hydrophobic nature in a short duration. The silanization process followed by the oxidation has shown to decrease the hydrophobic recovery of PDMS to some extent (for several days). For the current study both the UV/ozone and oxygen plasma were tried prior to the silanization process. The plasma treatment, however, showed to be a more time

effective approach (30 sec compared to the 80-90 min UV/ozone exposure in the current study). In this study, "effectiveness" was defined as the exposure time needed to produce water sheeting on the surface. Experience has shown, however, that care must be taken with the plasma treatment as over-exposure can cause wrinkles and roughness on the surface. In addition, 1 minute plasma exposure followed by silanization resulted in smaller than the typical values of W in air (~42-44 mJ/m^2). This could be attributed to the rough and wrinkled surfaces caused by plasma exposure reducing the intimate contact. For this study the plasma oxidation (30 seconds) followed by the silanization is used to functionalize PDMS samples. The details of the silanization technique along with the chemicals used for this method are presented in the next chapter.

The substrates for the second phase were chosen to include functionalities representing hydrophilic, hydrophobic, and intermediate characteristic. PEO was used as a hydrophilic group, amine as an intermediate group, and native PDMS as a hydrophobic surface. Similar to phase I, PEO and amine functionalities were applied to glass surfaces. Amine-treated PDMS sheets were also evaluated. Flat sheets of native PDMS were also evaluated both as a hydrophobic surface and for the means of comparison.

For both phases, the JKR experiments were performed between PDMS probes (native PDMS in the first phase and amine-treated PDMS in the second phase) with the corresponding surfaces in air and underwater according to the experimental protocol discussed earlier. The following chapter provides more details regarding the materials used in this study and the specimen preparation techniques related to the two phases discussed here.

Chapter 6 - Experimental Section

As discussed in the previous chapter, two complementary phases are used to accomplish the goals of this study. This chapter first discusses the materials used in these two phases, including PDMS, the functional groups, cellulose, and lignin. Then it gives an overview of the techniques that are used to prepare the "samples" (functionalized glass surfaces, native and functionalized PDMS samples, cellulose and lignin substrates.

Materials

This section introduces the materials used in this study including PDMS, the functional groups that are selected, cellulose, and lignin. The preparation of PDMS hemispheres/flat sheets, functionalized surfaces, and cellulosic/lignin surfaces are discussed later in this chapter in the "Sample Preparation" section.

PDMS

Polydimethylsiloxane (PDMS) is a silicon-based organic polymer with repeating units of silicon and oxygen. The chemical structure of PDMS is $(Si(CH3)_2O)_n$, depicted in Figure 6.1(a), where n is the number of the repeating unit. PDMS is a commonly used polymer with many applications such as emulsions, compounds, resins, and elastomers due to its customizable viscous and mechanical properties. PDMS is optically clear, and is generally considered to be inert, non-toxic and non-flammable. It is also elastic, durable, and stable over a wide range of temperatures. PDMS forms silicone rubber when cross-linked. The excellent biocompatibility of PDMS makes these materials have a wide range of applications from contact lenses and medical devices to food additives to soft lithography and micro-fluidic channels.

Cross-linked PDMS has widely been used as a model material in adhesion studies in the JKR experiment. The Young's modulus of PDMS is in the range of 1-10MPa, depending on the amount of cross-linker and the curing temperature. This suggests that PDMS deforms relatively large with small loads. This makes PDMS an appropriate material within the load range of the JKR experiments (1-20 mN). Another advantage of using PDMS is that it is transparent. As a result, PDMS can be used in the JKR experiment to view the contact area, even if the other surface is not clear. Moreover, PDMS has a smooth and homogeneous surface that can be modified without affecting other physical properties of the bulk PDMS. These properties of PDMS make it a suitable material to probe adhesion behavior of other surfaces in the JKR framework as discussed in Chapter 4.

Functional Groups

As stated earlier, the objective of this work was to investigate the effect of surface chemistry on adhesion interactions underwater. In order to determine that, for the first phase a discriminating set of functional groups with different wetting behaviors was chosen. These surface functionalities were applied to glass surfaces and included hydrophobic, hydrophilic, and intermediate characteristics. Hydrophobic groups include two hydrocarbon groups (methyl and cyclohexyl), and fluorocarbon; whereas amine, carbomethoxy, and mercapto (thiol) functionalities show intermediate wetting behavior. PEO was also used as a hydrophilic group. In addition to these groups, clean glass slides rich in hydroxyl groups (hydrophilic) and flat sheets of PDMS (hydrophobic) were also evaluated as references.

For the second phase, as was mentioned earlier, only amine group was selected to functionalize PDMS surfaces (both hemispheres and flat sheets). Here, it should be noted that the silanization process was used in this study to introduce functional groups on the surface of glass

and PDMS surfaces. As mentioned earlier, the hydrosilylation technique was also carried out to functionalize PDMS surfaces with amine, methyl and carboxylic acid groups. The procedure, chemicals, and the JKR results obtained for this technique are presented in Appendix A. this technique, however, was not pursued for functionalizing PDMS in the second phase.

Table 6.1 shows the functional groups and the respective reactive chemical for each as well as the surface that the functional group was introduced to. Following Table 6.1 a brief discussion of each functional group is provided. The chemical structures of the silane agents used in this study are also depicted in Figure 6.1(b)-(h). The silanization process is discussed later in the "Sample Preparation" section of this chapter.

Table 6.1 Functional groups used in this study to treat glass and PDMS

Functionality		Reactive Chemical (treated surface)	Supplier
Amine		3-aminopropyl triethoxysilane (Glass and PDMS)	Gelest
Carbomethoxy		2-carbomethoxy ethyltrichlorosialne (Glass)	Gelest
Fluorocarbon		1H,1H,2H,2H-perfluorodecyl trichlorosialne (Glass)	Gelest
Hydrocarbons	**Cyclohexyl**	Cyclohexyl trichlorosilane (Glass)	Gelest
	Methyl	4-Decyltrimethoxysilane (Glass)	Alfa Aesar
Mercapto (Thiol)		3-mercaptopropyl trimetoxysilane (Glass)	Gelest
Polyethylene oxide (PEO)		2-[Methoxy(polyethyleneoxy)propyl]trimethoxysilane (Glass)	Gelest

Hydroxyl is a functional group containing oxygen and hydrogen (OH). The hydroxyl group is highly reactive showing polar behavior. It is also able to form strong hydrogen bonds (H-bonds). Hydrogen bonds are typically formed between the lone pair of a small electronegative

atom such as nitrogen, oxygen, and fluorine, of one molecule with the slightly positive hydrogen atom of another molecule.

Primary Amine (NH_2) is an organic compound of nitrogen with a lone pair and two hydrogen atoms. Amines are polar (hydrophilic) charged molecules showing basic properties. They also have the ability to develop H-bonds.

Carbomethoxy is a methyl ester of carboxylic acid. Carboxylic acid is any compound containing the COOH group. Because of the hydrogen in the COOH group, carboxylic acid is a polar charged group showing weakly acidic behavior with the capability of developing H-bonds. The carbomethoxy functionality, however, is incapable of developing H-bonds since a methyl group replaces the hydrogen of the carboxylic acid group.

Fluorocarbon is an organic compound that only contains fluorine and carbon. Fluorocarbons are highly hydrophobic molecules with small surface tension. Because of that, fluorocarbons are typically used as water repellent coatings.

Thiol is an organic compound containing sulfur with the formula SH. Because of the small electronegativity difference between sulfur and hydrogen in the SH bond, thiol is not considered a polar molecule as opposed to the hydroxyl group (OH).

Hydrocarbons are organic compounds consisting only of hydrogen and carbon. Hydrocarbons have different molecule structures depending on the bonds that are formed between the carbon and hydrogen atoms. Because of that, there is not a unified chemical formula describing hydrocarbons. Regardless of the structure, however, hydrocarbons are hydrophobic (non-polar) compounds that only react with other molecules through van der Waals forces. The hydrocarbons used in this study included an aliphatic type (methyl) and a cyclic type (cyclohexyl).

Polyethylene Oxide (PEO) is a polyether monomer consisting of ethylene oxide (C_2H_4O). Polyethylene oxide is a polar (hydrophilic) molecule which is used as a lubricating coating or surfactant to decrease adhesion at the interface of two surfaces.

Figure 6.1 Chemical structures of (a) PDMS and the silane agents with the tail groups of (b) methyl, (c) cyclohexyl, (d) fluorocarbon, (e) amine, (f) mercapto, (g) carbomethoxy, and (h) PEO

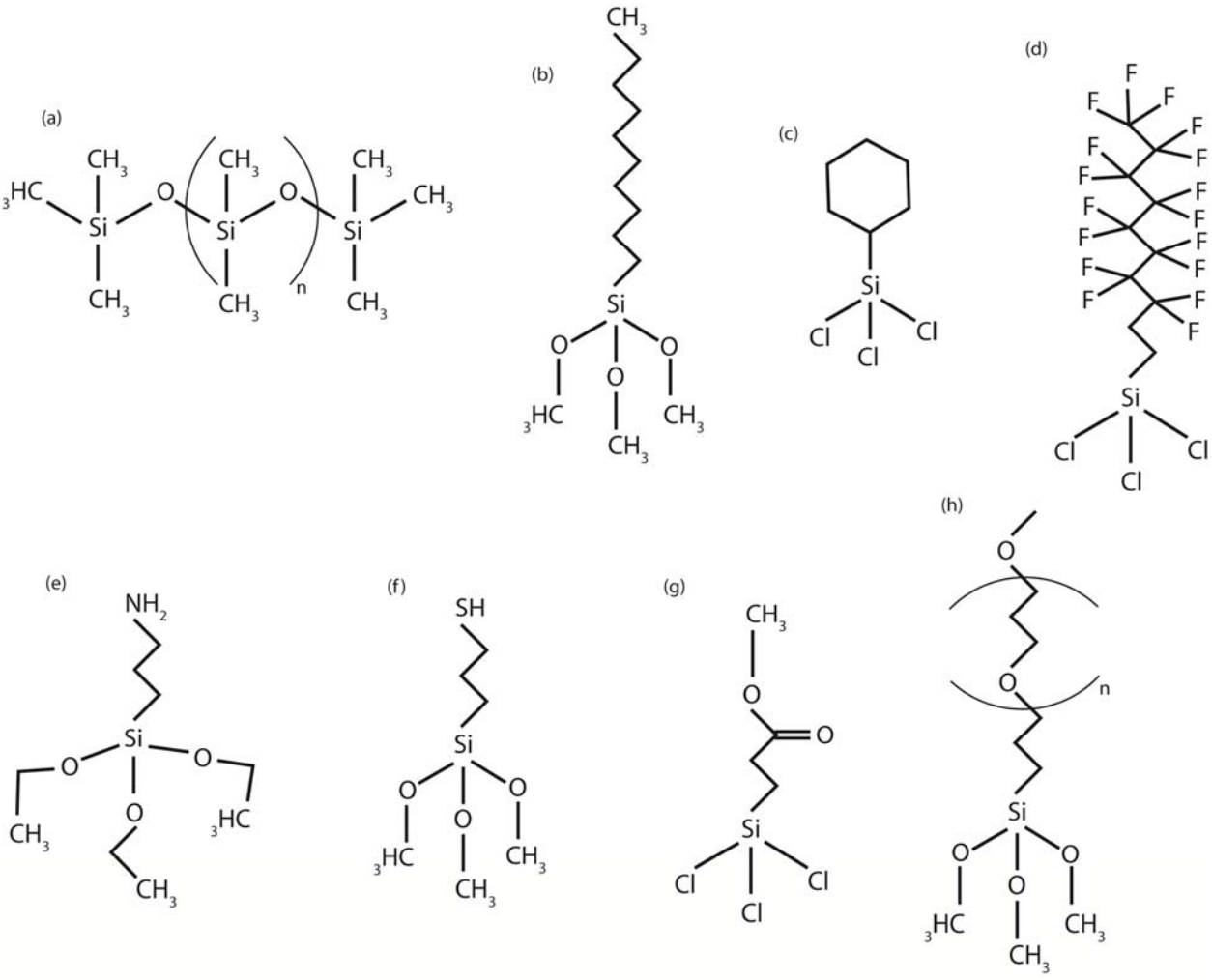

Cellulose

Cellulose is the most abundant natural organic polymer and has the formula $(C_6H_{10}O_5)_5$. The chemical structure of the cellulose chain is shown in Figure 6.2. Cellulose is the elemental building block of the cell wall of plants and trees and gives them their strength and integrity. About 90% of cotton and 40-50% of wood is comprised of cellulose. Cellulose is also used in a

wide range of applications from textile and paper to polymer reinforcement in the composite industries. The structure of the cell wall in a plant or the properties of the final product (such as paper) is dependent on the interactions of cellulose chains and other molecules.

Figure 6.2 Cellulose chain structure (reproduced from [87])

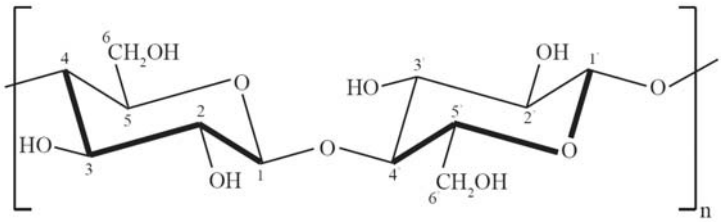

Cellulose may be found in four different crystalline structures (or forms) depending on the location of hydrogen bonds between and within cellulose molecules. These four cellulose structures are denoted as cellulose I, II, III, and IV. The natural form of cellulose is cellulose I with the highest order of crystalline arrangement. Cellulose II is referred to as regenerated cellulose and is typically obtained by regeneration of cellulose in solution. Cellulose III can be prepared from chemical treatment of either cellulose I (which leads to cellulose III_I) or cellulose II (which leads to the form III_{II}) by means of liquid ammonia or certain amines such as ethylene diamine (EDA) [88]. Cellulose IV is obtained when cellulose III is treated at high temperature in glycerol. Depending on the type of cellulose III that is used, cellulose IV can be in the form of IV_I and IV_{II} [88]. Cellulose I and II are the most studied cellulose surfaces, hence in this study cellulose I and II are used as model cellulosic surfaces. Here, it should be noted that both cellulose I and II have the intra-molecular hydrogen bonding at (OH)3-O5 [88]. The difference between cellulose I and II, however, appears in their inter-chain bonding (see Figure 6.3). In cellulose I the dominant inter-chain hydrogen bond is at (OH)6-O3, whereas for cellulose II it is at (OH)6-O2 for corner chains and (OH)6-O3 for center chains [89-92]. For cellulose II there is also an inter-sheet interaction at (OH)2(corner chain)-(O)2(center chain) which is absent in

cellulose I [93]. Moreover, cellulose I has a parallel chain structure, while cellulose II has an anti-parallel form [94].

It has been shown that physical or chemical properties of cellulose are significantly reliant on its hydrogen bonding capability [72]. According to [72], cellulose A (a variation of cellulose II based on the preparation used in the current study) showed a higher adhesion hysteresis compared to cellulose I in the JKR experiments. This was attributed to the lower crystalline order of cellulose II and hence, its ability to form hydrogen bonds with PDMS in the JKR experiments.

Figure 6.3 Hydrogen bonding for (1) cellulose I and (b) cellulose II [93]

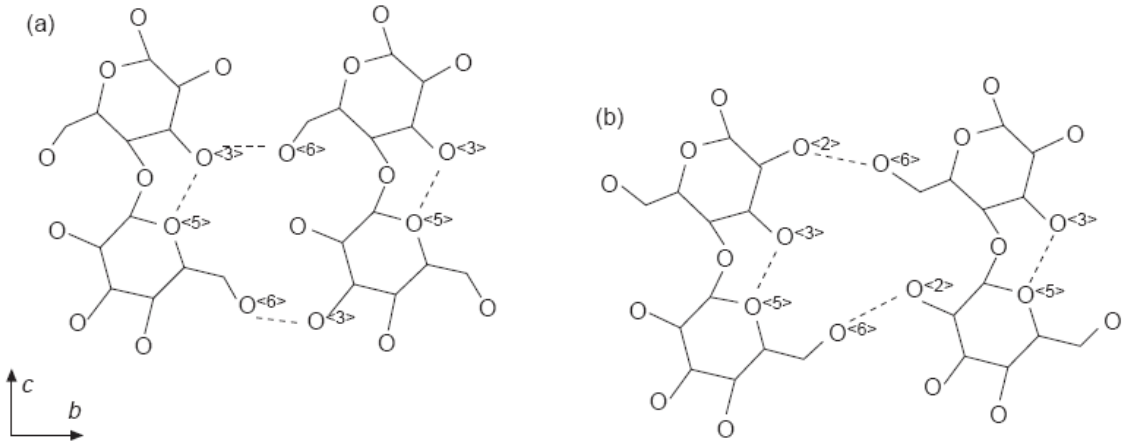

Lignin

Lignin is the second most abundant biopolymer on Earth after cellulose. Lignin plays an important role by binding wood compounds and strengthening wood. It also regulates water transport in plant stems. Lignin has a heterogeneous, complicated chemical structure which consists of many complex three-dimensional phenolic polymers. The lignin structure may vary from softwood to hardwood and even among different species. The chemical makeup and form of lignin also depends on the procedure that is used to isolate lignin from wood. Because of all these, it is difficult to define the chemical structure of lignin. A hypothetical lignin structure,

however, is illustrated in Figure 6.4. Milled wood lignin is thought to be a good approximation for the lignin occurring in wood. A recent study using contact angle measurements with three different test liquids, however, shows that the surface energy of lignin is insensitive to the origin of the lignin (whether it's a kraft lignin, a hardwood milled wood lignin or a softwood milled wood lignin [95]).

Figure 6.4 A hypothetical structure of lignin [96]

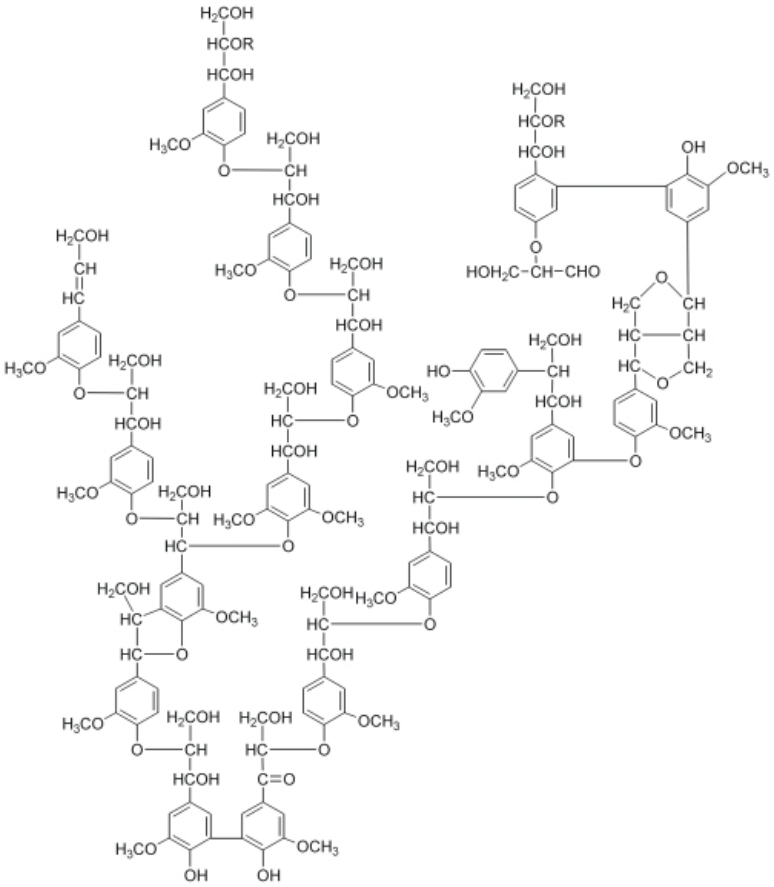

Sample Preparation

In order to accomplish the goal of this project, as discussed earlier, two complementary phases are carried out. This section focuses on the techniques that are used in these phases to modify glass and PDMS surfaces. It also explains the preparation procedure of PDMS hemispherical probes as well as cellulosic and lignin films.

Surface Modification of Glass

The most commonly used method to modify inorganic surfaces that contain hydroxyl groups (such as glass or silica) is to use alkylsilane solutions, referred to as silanization. Alkylsilanes, with the general formula of $RSiX_3$, are silicone based molecules with two end reactive groups on the molecule (R and X). One reactive group (X) is a sensitive center that can react with the inorganic substrate (the silica surface in this case). The other end contains specific functional groups (R) and is chosen in a way to promote or demote the interactions of the substrate with the opposite surface (or the polymer of the interest). Silanes tend to deposit a polymeric layer on the substrate with functional groups thrusting upward on the surface. In general, trialkoxysilanes (most commonly triethoxy and trimethoxy-silanes) and trichloroislanes are utilized to modify glass surfaces. Methoxy and ethoxy groups in alkoxysilanes are converted to methanol and ethanol during the reaction as byproducts whereas, the chloro group in chlorosilanes is converted to hydrochloric acid. Because of harmful effects of hydrochloric acid, chlorosilanes are used less than alkoxysilanes in surface treatments. Silanes with trialkoxy or trichloro maximize surface coverage of functional groups compared to mono or dialkoxy/chlorosilanes [97]. The general procedure for modifying inorganic surfaces by this method (depicted in Figure 6.5) involves four steps [97]: (1) hydrolysis of X groups; (2) condensation to oligomers; (3) hydrogen bonding with OH groups of the substrate; and (4) bond formation. The hydrolysis produces silanol groups (Si-OH) on the surface which can condense with other silanol groups on the surface to form siloxane linkages (Si-O-Si). The siloxane oligomers then hydrogen bond with OH groups of the substrate. In the last step a covalent bond is formed with the substrate during drying or curing.

Figure 6.5 Reaction of silanes with a substrate (reproduced from [97])

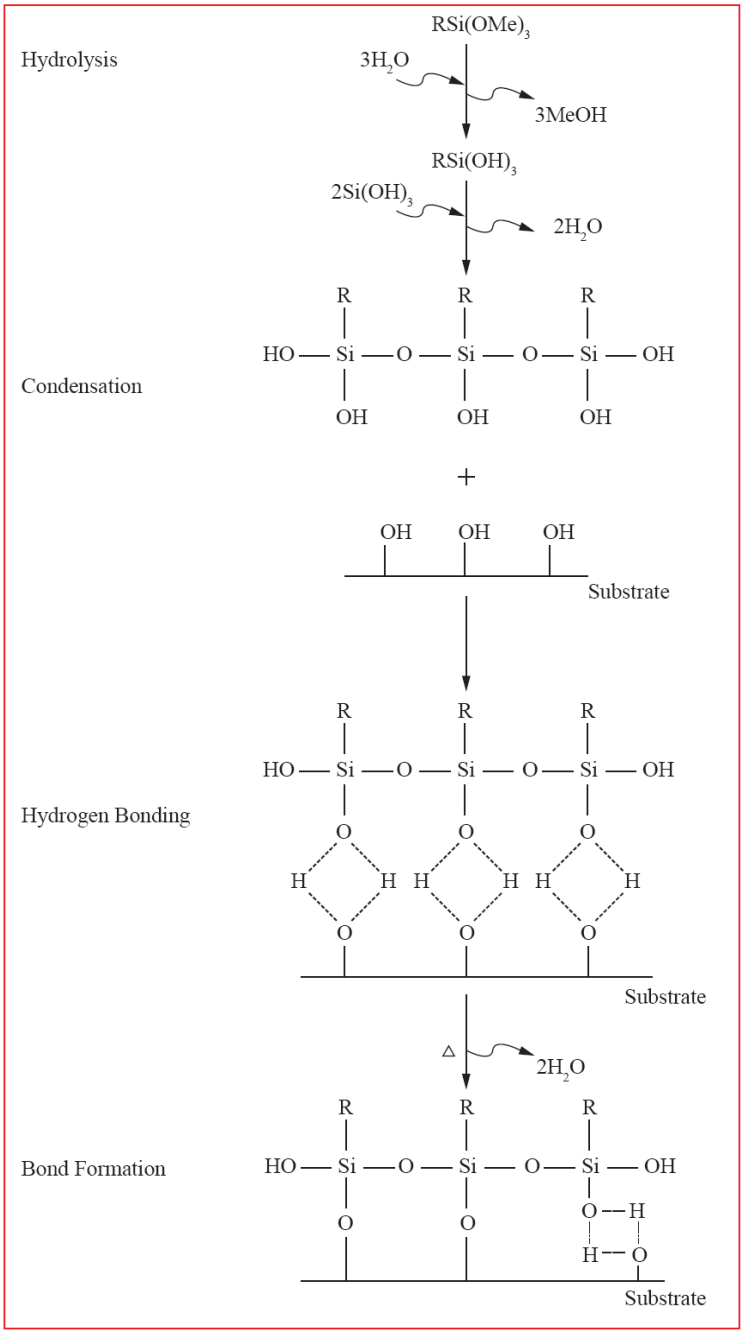

The most convenient method to prepare functional groups from silane agents is deposition from aqueous alcohol solutions [97]. In this method a reactive silane solution listed in Table 6.1 is added to the 95% ethanol solution to obtain a 2% (v/v) concentration of that particular silane. The glass surfaces were then placed into that solution for 2 min. Following that,

the glass surfaces were briefly dipped in ethanol to remove any excess silanes. The glass surfaces were then cured at 110°C for 7 min. It should be noted that prior to the treatment process, glass surfaces were cleaned according to the RCA-1 cleaning procedure. The cleaning process produces surfaces that are covered with reactive silanol groups (Si-OH). The RCA-1 cleaning procedure for glass slides was as follows:

1. Glassware was dipped in 5M sulfuric acid for 10 min.
2. Glassware was removed from sulfuric acid and rinsed with ultrapure water.
3. Glassware was rinsed with acetone, ethanol, and ultrapure water and dried under nitrogen.
4. Slides were dipped in a bath of Versa-Clean solution for 10 min and dried under nitrogen.
5. Glass slides were dipped in a bath of acetone for 15 minutes and dried under nitrogen before they are dipped in NH_4/HF for 20 sec.
6. After removing the glassware from the etching solution, they were rinsed with ultrapure water and immediately immersed in a solution of peroxide mixed with ultra-pure water and ammonium hydroxide (with a ratio of 1/2/1, respectively) at 60°C for 12 min to hydrolyze the glass surfaces.
7. The slides were then rinsed with ultrapure water and dipped in a running water bath.

A few freshly cleaned slides (referred to as bare glass) were stored in a covered Petri dish and used as references for means of comparison with the silane modified glass slides. Contact angles of ultrapure water were measured on clean and modified slides for the purpose of quality control.

Preparation of PDMS Samples

PDMS samples were prepared from Sylgard 184. Sylgard 184 contains two liquid parts, one called the base and the other the curing agent. In Sylgard 184 the base mixture is dimethylvinyl-terminated dimethyl siloxane whereas, the curing agent is dimethyl methylhydrogen siloxane. The vinyl groups have the ability to cross-link and form a solid rubber structure. Regardless of specimen type being made, PDMS samples were prepared by mixing the liquid Sylgard 184 base and the curing agent at a ratio of 5:1 by mass (in a plastic cup) and stirring the mixture (by a glass rod) for a few minutes at room temperature. The air bubbles introduced during the process of mixing were eliminated by letting the mixture rest in air for 20 minutes according to the PDMS data sheet [98]. PDMS samples were then cured in an oven at 100ºC for 2.5 h.

To prepare flat pieces, the degassed mixture was poured into an aluminum foil sheet molded onto the bottom of a small beaker. After curing, the flat sheet was cut into a few strips and removed from the foil. Each strip was taped on a glass slide by means of a strip of double sided tape with the "bottom side" down. The bottom side is the surface which was contacting the foil during curing time.

Hemispherical PDMS lenses were prepared by placing small drops of the degassed mixture by means of a needle on a glass slide pretreated with fluorosilane. This pre-treatment deteriorates the adhesion between PDMS and glass and lets the drop bead up as a hemisphere. The fluorinating material is 1H,1H,2H,2H perfluorodecyltrichlorosilane (PFDTCS), from Gelest, added to hexane with a 0.5% mixing ratio. PDMS lenses and flat sheets were then cured in an oven for the indicated time. It should be noted here that the radius of curvature of the lens (R) is calculated from the side image of the cured lens on a glass slide taken with the microscope from the equation (26) given in Chapter 3 after an experiment.

As a side note, flat pieces of PDMS were used to perform self-adhesion measurements to determine the mechanical properties of PDMS in JKR experiments in the first phase. They were also used as standards in the second phase to carry out contact angle measurements in order to verify the wettability of the modified PDMS surfaces. Moreover, amine-modified and native flat PDMS sheets were used as part of the surfaces in the second phase.

Surface Modification of PDMS

As mentioned earlier, for the second part of this study PDMS hemispheres were modified chemically to probe other surfaces. PDMS flat sheets were also modified for further evaluations. Since the JKR experiments fit best the materials with low elastic modulus, we were interested to modify PDMS in a way so that the bulk mechanical properties remain unchanged. There are various techniques reported in the literature to modify surface properties of PDMS [86]. These techniques include plasma or UV/ozone oxidation typically followed by silanization, using surfactants, chemical vapor deposition, layer-by-layer deposition, UV-induced graft polymerization, and hydrosilylation. For this study, the UV/ozone oxidation method followed by silanization was chosen due to its stability and ease-of-use approach. The same curing conditions mentioned in the PDMS preparation section of this chapter are used to cross-link 5:1 PDMS surfaces (hemispheres and flat sheets). After curing, the following procedure was used to modify PDMS surfaces with the silane compound listed in Table 6.1 to introduce the end functional groups selected.

1. PDMS surfaces were exposed to oxygen plasma (PDC-32G Plasma cleaner from Harrick PLASMA) for 30 sec on the high power setting.
2. The samples were then dipped in the silane solution (prepared according to the procedure described in the glass treatment section of this chapter) for 5 min.

3. PDMS samples were sonicated in a bath of ethanol for 5 min to remove any excessive silane or any residues on the surface.
4. The samples were rinsed with deionized water and baked in an oven for 7 min at 110°C.

Cellulose and Lignin Surfaces

In this study two different cellulose structures and one lignin type were used. Cellulose surfaces included cellulose I (with a high degree of crystallinity) and a cellulose type with a lower crystallinity degree denoted as cellulose A by Eriksson et al. [72]. Eriksson et al. [72] used this terminology because they were concerned the regeneration method of the cellulose could affect the degree of ordering, although it has been shown previously [81, 99] that the cellulose solution they prepared resulted in cellulose type II. This section gives the details of the procedures used to prepare thin smooth surfaces of these materials.

Cellulose I

Edgar and Gray [100] are believed to be the first authors reporting the preparation of native cellulose (cellulose I) smooth surfaces from cellulose nano-crystals. Using XPS, they have shown that morphology and composition of the prepared cellulose surfaces are very close to pure cellulose. Using the preparation method described by Edgar and Gray [100] as a guide, smooth surfaces of cellulose I are prepared in the current work from a dissolving grade softwood pulp (from Domsjo Fabriker, Sweden) as follows:

1. The softwood pulp was cut into small pieces.
2. Small pieces were ground in a coffee grinder.
3. The ground pulp was hydrolyzed with 64% sulfuric acid at 45ºC for 45 min (4 g of pulp treated with 70 ml of acid).
4. After hydrolysis, the suspension was diluted 10-fold to stop the reaction.

5. The suspension was then washed with water and NaCl is added so that the pH of the suspension is greater than 1.
6. The suspension was filtered through hardened ashless filter paper (Whatman 541).
7. The cellulose solution was filtered through a 0.45-µm membrane.
8. The solution was then dialyzed against water for two days.
9. The solution was allowed to stand over a mixed bed resin for 48 h.
10. Cellulose was filtered through hardened ashless filter paper.
11. Cellulose was spin-coated on clean glass slides pre-treated with Poly(diallyldimethylammonium chloride) (PDADMAC) at 4000 rpm for 1 min.

According to Edgar and Gray [100], a thermal treatment (overnight at 105°C or for 24 hr at 35°C) is necessary to stabilize cellulose films and preventing the films to disperse underwater. For this study, the cellulose I films were heat treated at 100°C for ~16 hrs to remove the sulfate groups [72] and also to stabilize these surfaces for underwater measurements [100]. Edgar et al. [100] (using essentially the same procedure) stated that the thickness of the cellulose films prepared by their technique was approximately 120 nm.

Cellulose A

Cellulose II was the other form of cellulose studied in this project. Instead of cellulose II, however, the terminology of "cellulose A" is used hereafter as it was used by Eriksson et al. [72] to indicate that the crystallinity of this type of cellulose was not measured in this study. Eriksson et al. [72] used this terminology to differentiate this type of cellulose with cellulose II although the study performed later by Aulin et al. [81] confirmed that the cellulose films prepared with the following technique possess the structure of cellulose II. Thin films of cellulose A used in this study were prepared according to [72] as following:

1. The softwood pulp was cut into small pieces.
2. Small pieces were ground in a coffee grinder.
3. 0.1 g of the ground pulp was dissolved in 5 g of NMMO at 115°C for 90 min.
4. 15 g of DMSO was added to the solution to decrease the viscosity.
5. The mixture was filtered with an ashless filter paper.
6. Cellulose films were spin coated at 3500 rpm for 30 sec on clean glass slides pretreated with PDADMAC .
7. The films were then soaked in ultrapure water overnight to remove NMMO.

According to Edgar and Gray [100], this procedure produces clear cellulosic films with a thickness of approximately 30 nm.

Lignin

The hardwood milled wood lignin (HMWL) (from sugar maple wood) was received from the USDA Forest Products Laboratory. Model lignin thin films were prepared by spin coating a 1.5% w/w solution of HMWL in NH_4OH [101]. The lignin was allowed to dissolve in NH_4OH for 24 hr. Lignin films were then spin coated at 1500 rpm for 1 min on a clean glass slide [101]. The thickness of the lignin films prepared in this study was ~40 nm, measured by a stylus-based profilometer. This thickness was close to the ca. 45 nm thickness for the lignin films reported by Norgen et al. [101] for the combination of lignin concentration and the spin coating speed.

Chapter 7 - Results of Phase I (Native PDMS Probes)

This chapter presents and discusses the results of the first phase of this research. As mentioned earlier, in this phase two sets of model surfaces were evaluated. The first set included glass slides chemically functionalized with a variety of functional groups with disparate wetting behavior. The second set included the wood-based biopolymers, namely cellulose and lignin. For both sets the JKR experiments were used to evaluate the adhesion interactions both in air and underwater. In addition to the JKR results (both W and adhesion hysteresis), static contact angles of ultrapure water were also measured and reported for means of comparison. In the following sections the results of the chemically modified glass surfaces are reported first followed by the results of the cellulose and lignin surfaces.

Chemically Modified Glass Surfaces

This section reports the results obtained for the first set of model surfaces used in this study. First, the wetting behavior of these chemically modified glass slides are reported and compared to the published values. The JKR results are then presented in Table 7.1 in terms of reduced bulk modulus (K), thermodynamic work of adhesion (W), the energy release rate calculated from the peak value of the unloading force, denoted by G_{MFUL}. The difference between G_{MFUL} and W is an indicative of adhesion hysteresis during the loading and unloading portions. Typical JKR results in the form of a^3-P curves are also demonstrated for each surface.

Wettability

Contact angles were measured on all surfaces using ultrapure water in air at room temperature. For all the surfaces contact angles were averaged from the left and right angles of a total of 6-9 droplets on different locations of at least 2 slides. For the amine-treated surfaces used

in this study the water contact angle decreased as a function of the time the droplet spent on the surface. Such behavior has been previously reported by Zeng et al. [102], and is associated with the formation of hydrogen bonds between water molecules and amino groups, surface roughness, and the ability of water molecules to penetrate the film structure. Therefore, the angles reported here for amine-treated surfaces were measured within less than 15 sec after the droplet was placed on the surface. For all other surfaces, measurements were taken within 1 min of droplet placement and no time-dependent behavior was observed. The results of the contact angle measurements are listed in Table 7.1.

As can be seen, PDMS flat sheets, methyl-, cyclohexyl-, and fluorocarbon-treated surfaces were hydrophobic, while clean glass and PEO-treated surfaces were highly hydrophilic. Amine-, mercapto-, and carbomethoxy-treated surfaces were intermediate in their wetting behavior. The value of contact angles on PDMS surfaces matched favorably to those reported in literature (106° [17]). The value for contact angle of water on methyl-terminated surfaces in the current study (98°) are close to those reported from vapor phase deposition, specifically 98.2° ± 0.3 [103], 100° [104], or 103° [105] although slightly larger angles of 108° [17] or 111° from solution [106] have also been reported. Contact angles of water on surfaces treated with FDTS in ethanol in the current study (~ 95°) were lower than the values reported in [103, 105] for surfaces treated with FDTS from vapor phase deposition (109.6 ± 0.4° or 103°). Although no comparisons were found in the literature, contact angles of water on cyclohexyl-terminated surfaces were about 91°, which is an acceptable value for a hydrophobic surface. Contact angles of water on amine-modified surfaces in the literature range from 52° [107] to 57° from vapor deposition [105], and 58° from solution [103] which was in good agreement with the current results (59°). The contact angle values for surfaces functionalized with mercapto (thiol) in this

study (57°) were close to those reported previously, ~52° [108] and ~67° from vapor phase [109] but higher than 40.3° ± 0.3 measured by Janssen et al. [103]. The values of contact angle for carbomethoxy-terminated surfaces show a relatively wide range from ~42° on glass surfaces treated with the silane solution in toluene [110] to ~71° obtained on surfaces prepared with vapor deposition [105]. The average values obtained in this study (57°) lie in the reported range. Contact angles of water on clean glass surface (~10°) were also in good agreement with the values obtained for the plasma treated glass slides (~13.5°) [110], which is expected for a clean glass surface rich in hydroxyl groups. The contact angles of water on PEO-treated surfaces in this study (20°) are, however, smaller than those reported earlier (33 ± 3° [111] or 35.8° ± 1.0 [103]) but close to the value of 25° for PEO-grafted surfaces [112]. The differences between the published values and those found in the current study for methyl, amine, and clean glass were minimal. However, the contact angles in the current study as compared to the values for the FDTS, carbomethoxy, and PEO surfaces varied to a larger extent, and this is most likely due to the different methods of deposition. The relative hydrophobicities of the surfaces, however, are consistent with previous results and so should still provide good insight into the behavior of such surfaces.

Table 7.1 Results of contact angle and JKR measurements of native PDMS hemispheres and functionalized glass surfaces in air and underwater

Surface	Static Contact Angle of Water (°)	Air			Underwater		
		K (MPa)	W (mJ/m^2)	G_{MFUL} (mJ/m^2)	K (MPa)	W (mJ/m^2)	G_{MFUL} (mJ/m^2)
PDMS	105.3 ± 2.22	1.67 ± 0.05	43.09 ± 0.59	48.65 ± 2.84	1.70 ± 0.07	78.70 ± 4.73	119.88 ± 8.05
Methyl	97.8 ± 2.71	3.40 ± 0.11	46.33 ± 1.66	56.44 ± 6.68	3.42 ± 0.13	78.49 ± 2.87	118.98 ± 6.11
Cyclohexyl	91.1 ± 1.80	3.20 ± 0.15	45.62 ± 2.93	57.10 ± 5.16	3.57 ± 0.34	80.94 ± 3.10	121.42 ± 7.52
Fluorocarbon	95.3 ± 1.74	3.52 ± 0.07	32.37 ± 1.01	128.91 ± 14.6	3.49 ± 0.27	67.05 ± 2.65	170.90 ± 16.87
Amine	59.2 ± 1.4	3.26 ± 0.13	47.85 ± 0.95	112.13 ± 6.56	3.60 ± 0.15	30.26 ± 2.22	269.02 ± 29.64
Mercapto	57.1 ± 1.62	3.37 ± 0.08	46.87 ± 1.21	103.58 ± 4.68	3.70 ± 0.08	35.91 ± 2.36	116.88 ± 17.76
Carbomethoxy	57.4 ± 1.08	3.26 ± 0.19	43.62 ± 0.25	67.24 ± 8.42	3.39 ± 0.15	36.78 ± 2.17	101.31 ± 9.26
Clean Glass	≈ 10	3.27 ± 0.12	46.53 ± 1.44	126.81 ± 11.35	3.55 ± 0.15	24.43 ± 2.20	86.80 ± 5.13
PEO	≤ 20	3.27 ± 0.04	47.19 ± 1.92	52.25 ± 3.35	2.92 ± 0.13	0.16 ± 0.10	26.06 ± 6.03

JKR Results

Typical JKR loading/unloading behavior of the adhesion between PDMS hemispheres and all surfaces in air and underwater are shown in Figure 7.1 to Figure 7.5 in the form of the a^3-P curves. Using a^3-P data obtained during loading, the reduced bulk modulus (K) and work of adhesion (W) were calculated from the linearized form of equation (3). In the linearized form, K is the slope of the line whereas, W is found using the x-intercept once K is determined. The results of K and W for each system, averaged for 4-5 samples with standard deviation, are reported in Table 7.1. The values of W for PDMS self-adhesion in air were in good agreement with previous studies [52]. The value of W in air for all surfaces except fluorocarbon was also

nearly the same as that for PDMS self-adhesion. The point that all surfaces, except fluorocarbon, show very similar results to that of PDMS self-adhesion can be attributed to the fact that native PDMS is strongly hydrophobic and only interacts with other materials through London dispersive forces in air. The lower value of W between PDMS and fluorocarbon-treated surfaces was related to the even lower surface energy of the fluorocarbon compared to PDMS because the highly polar C-F bond reduces the magnitude of the London dispersion forces.

The values of W underwater were, however, different for each system and varied from ~0 for PEO to ~80 mJ/m^2 for hydrophobic systems, such as PDMS contacting PDMS, methyl-, and cyclohexyl-terminated surfaces. As can be seen in Table 7.1, the values of W underwater could be directly related to the hydrophilicity/hydrophobicity of a surface where hydrophobic surfaces exhibited higher W's underwater compared to in air and hydrophilic surfaces exhibited smaller W's underwater compared to in air. For PEO where W was very small, K was smaller than that in air while for other systems K underwater was slightly higher than that in air. Overall, however, there was no remarkable difference between the values of K underwater with those obtained in air.

Although Table 7.1 provides values of W and K for each system, it does not provide any information regarding the hysteretic behavior, which might be indicative of specific/non-specific interactions. The adhesion hysteresis and frictional behavior of different surfaces have also been shown to be correlated [10-12, 113]. A typical JKR loading/unloading behavior for PDMS self-adhesion is depicted in Figure 7.1(a). As can be seen, no hysteresis was observed between loading and unloading in air. Underwater, however, there was a slight difference between loading and unloading, as seen before [17]. It can also be seen that at maximum force the contact radius was higher underwater compared to that in air. This indicates that a higher W would be

expected underwater. The higher W underwater has been attributed to the change in the entropy of the system when the hydrophobic surface interacts with water. This interaction is entropically unfavorable as the introduction of the hydrophobic surface disrupts the water H-bonding causing the water molecules to rearrange (gain order) to minimize their contact with the hydrophobic surface. This is referred to as hydrophobic effect. Previous studies [17, 52, 114] have shown that the value of thermodynamic work of adhesion (W) for PDMS self-adhesion underwater is in the range of 70 – 85 mJ/m^2. The results obtained for PDMS/PDMS in this study (~ 80 mJ/m^2) matches favorably with these results.

Figure 7.1 (a) JKR loading/unloading behavior of native PDMS self-adhesion in air and underwater, (b) JKR loading/unloading behavior of native PDMS/methyl-treated surface in air and underwater

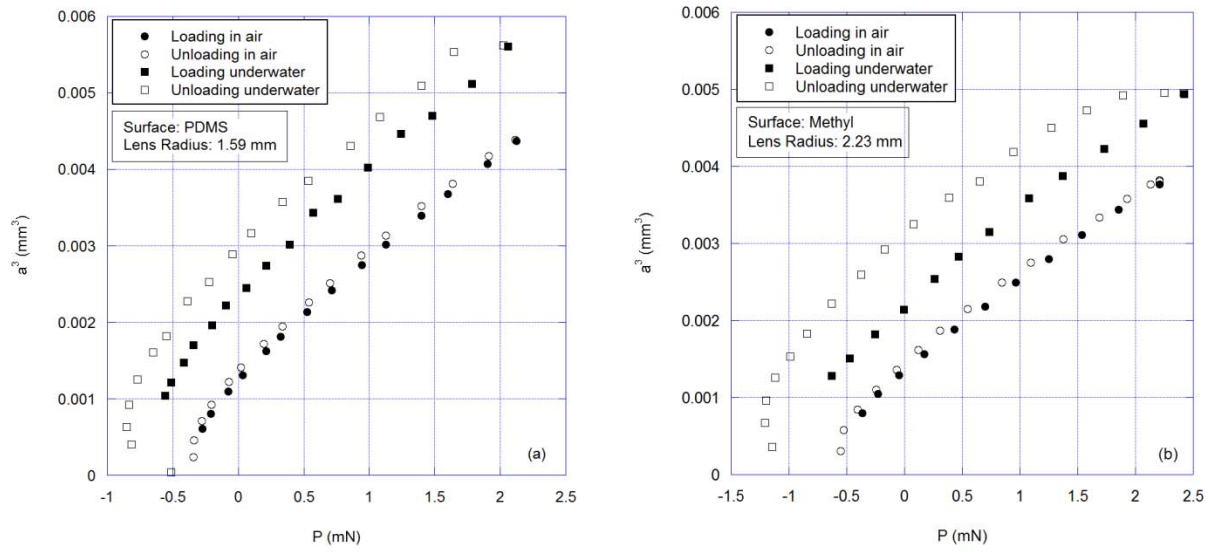

The value of W for the contact between PDMS hemispheres and methyl- or cyclohexyl-treated surfaces in air was similar to PDMS self-adhesion, as can be seen in Table 7.1. The similar value of W for these surfaces can be attributed to the fact that PDMS reacts only through London dispersive forces in air. The values of W underwater for these two groups were close to PDMS self-adhesion underwater (~ 80 mJ/m^2) and larger than that in air (~78 mJ/m^2 for methyl and ~81 mJ/m^2 for cyclohexyl). A previous study [17], has also reported similar values of W

underwater for PDMS self-adhesion (~71.6 mJ/m^2) and PDMS-methyl surfaces (~70.4 mJ/m^2). The results of sum frequency generation spectroscopy underwater [17] showed that for PDMS-PDMS and PDMS-OTS (methyl functionality) all water molecules were expelled from the contact region and no water was present between these surfaces. As discussed previously, this was due to entropic effects and arrangement of water molecules around the hydrophobic surfaces to minimize their contact with hydrophobic molecules. The similar values of W for the methyl- and cyclohexyl-treated surfaces showed that the structure of the hydrophobic surface (aliphatic vs. cyclic) minimally affected the hydrophobic interactions underwater. The adhesion hysteresis of methyl- and cyclohexyl-treated surfaces underwater was almost the same as that for PDMS self-adhesion, as can be seen in Table 7.1 and Figure 7.1(b) or Figure 7.2(a). In the study performed by Defante et al. [17] the methyl surfaces that were prepared from octadecyltrichloro-silane (OTS) showed no adhesion hysteresis in air or underwater. The larger adhesion hysteresis observed in the current study for methyl- or cyclohexyl-treated surfaces underwater could be attributed to the chain length of the silanes that were used to prepare these surfaces. It has been shown that for the self-assembled monolayers (SAMs) prepared from long carbon chains friction is lower than those prepared from short carbons chains [115, 116]. Because of the correlation between the friction and adhesion hysteresis [10, 11], the larger hysteresis for methyl- and cyclohexyl-treated surfaces in the current study was associated with the shorter-carbon-chains of the silane agents that were used.

Figure 7.2 (a) JKR loading/unloading behavior of native PDMS/cyclohexyl-treated surface in air and underwater, (b) JKR loading/unloading behavior of native PDMS probing fluorocarbon-treated surface in air and underwater

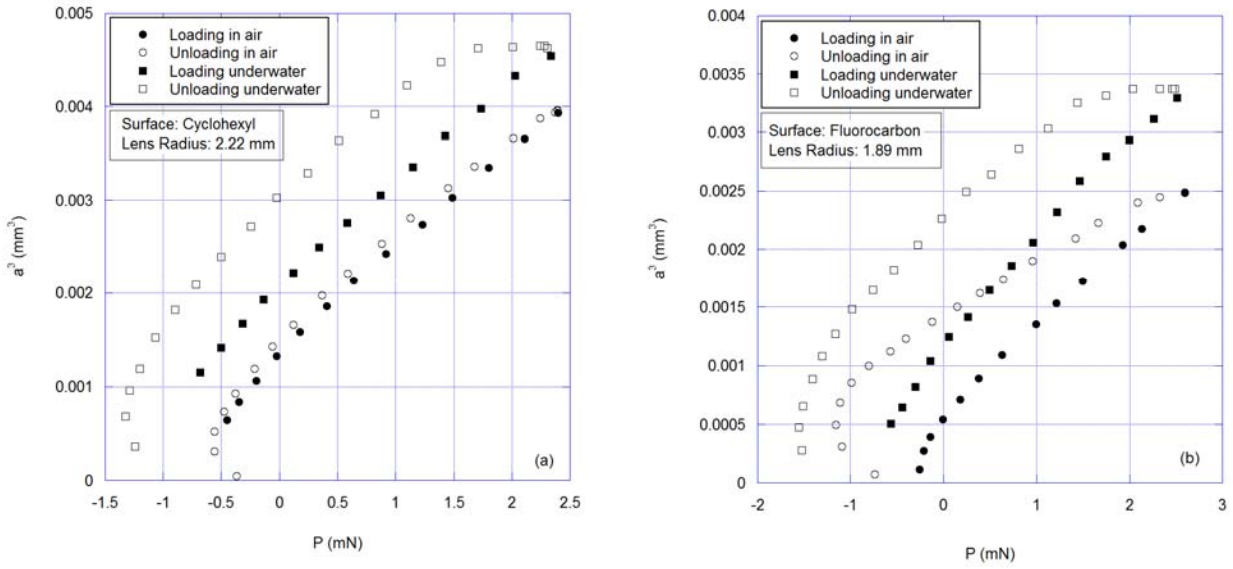

As can be seen in Table 7.1, the work of adhesion between PDMS and fluorocarbon in air was smaller than the other surfaces because of the lower surface energy of fluorocarbon. Underwater, however, similar to other hydrophobic surfaces, the value of W was increased compared to that in air. Because of the higher hydrophobicity of fluorocarbons compared to hydrocarbons one might expect to get a higher W for fluororcarbons underwater. This, however, was not the case. The first reason for this behavior is that the polarized C-F bonds show a higher dipole moment compared to the C-H bonds. Hence, fluorocarbons are more hydrophilic than hydrocarbons and show stronger interactions with water [117]. Moreover, it has been shown that fluorocarbons are capable of breaking hydrogen bonds of, for example, OH---O or NH---N type [118]. Therefore, it is anticipated that the arrangement of water molecules near fluorocarbon surfaces is not as ordered as their arranegement near hydrocarbon surfaces. As a result, a lower value of W underwater (compared to hydrocarbon surfaces) is expected. The second is that the lower surface energy of fluorocarbon surface results in weaker interactions between the PDMS

and fluorocarbon surfaces [119] compared to the PDMS – hydrocarbon (PDMS, methyl, and cyclohexyl) surfaces. Since the hydrophobic interactions between PDMS and fluorocarbon underwater are not as strong as the the interactions developed between PDMS and other hydrocarbons, a lower W underwater was obtained for PDMS/fluorocarbon system. But because the fluorocarbon surface is still hydrophobic and water would rearrange to minimize its contact, a higher W undewater would be expected (compared to that in air). A typical a^3-P curve between PDMS and a fluorocarbon-treated surface is shown in Figure 7.2(b). As can be contrasted with PDMS self-adhesion or PDMS/methyl-treated system, fluorocarbon showed a noticeable hysteresis in air. The adhesion hysteresis upon unloading in air was related to restructing of PDMS under pressure and formation of dipole interactions [9]. Previous studies on frictional behavior of fluorocarbon- and methyl-treated surfaces with PDMS hemispheres [10, 11] have shown that for the fluorocarbon surface, with larger adhesion hysteresis in air, the frictional force is greater compared to the methyl-treated surface, which shows no adhesion hysteresis.

In the current study, the same amount of hysteresis in air and underwater was observed for fluorcarbon surfaces, see Table 7.1. It was anticipated that because of this hysteresis underwater, the fluorocarbon-treated surfaces show a higher friction force compared to methyl-treated surfaces. It should also be noted that underwater for the fluorocarbon surfaces at the final few steps of unloading a bubble would form that encompassed the contact area. This behavior was not seen for other hydrophobic surfaces. The formation of bubble was asscoiated with the high solubility of oxygen and other gases, such as carbon dioxide and nitroegn in fluorcarbons [120]. The gas-dissolving capacity of fluorcarbons are attributed to their weak intermolecular forces, which facilitates the formation of cavities that encompass gas molecules [121]. The contact areas that were formed in a bubble were not included in the a^3-P graph.

For the surfaces with an intermediate wetting nature (amine, mercapto, and carbomethoxy), as can be seen in Table 7.1, the values of W in air were close to that for PDMS self-adhesion. Once again, this was attributed to the ability of PDMS to only form London dispersive forces in air. The work of adhesion underwater for all these surfaces, however, was lower than that in air. The values of W underwater were very close to each other, although amine showed the smallest W of this group. A previous study [17] has shown that if water is present in the contact region, the value of W underwater decreases compared to hydrophobic surfaces, such as PDMS or methyl-treated surfaces. It has also been shown that for esters, ketones, and large nitrogen-containing molecules [122], with intermediate wetting behavior, the hydration number is ca. zero. Therefore, no hydrogen bond is expected between water and the functional groups with intermediate wetting behavior, except amine, which can form H-bonds with water molecules because of its small size and the lone pair electron of nitrogen.

For the PDMS-PVNODC system [17], as mentioned earlier, the value of W underwater was comparable to that obtained in air. For this system only van der Waals forces were present in the contact region [17]. It was anticipated that the lower values of W underwater for the intermediate groups in this study were also indicative of weaker van der Waals forces developed underwater between PDMS and the other surface compared to those in air. The lower value of W underwater for amine was associated with a short-ranged hydration repulsion force of the steric origin [123] developed between water molecules and the amine group because of the H-bonds formed between water and amine. This repulsion force would reduce the interactions between PDMS and the amine-treated surfaces to a larger extent resulting in a lower value of W underwater for this system.

Figure 7.3 (a) JKR loading/unloading behavior of native PDMS in contact with amine-treated glass slide in air and underwater, (b) JKR loading/unloading behavior of native PDMS in contact with mercapto-treated glass slide in air and underwater

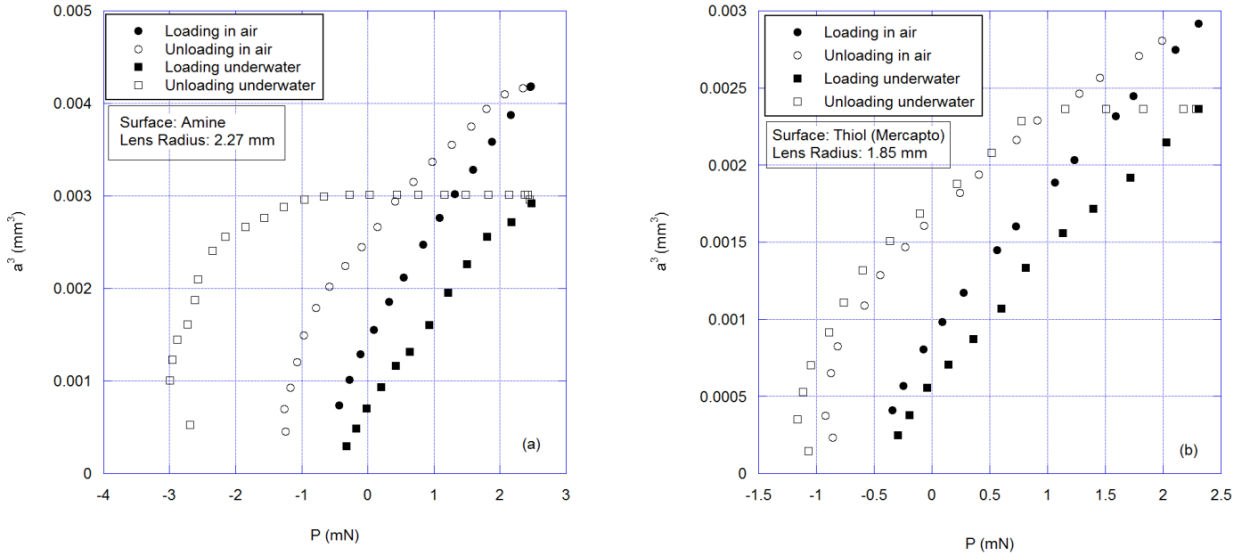

Although W for the intermediate wetting group underwater showed close values for air and underwater, they displayed a distinct hysteresis behavior both in air and underwater. Amongst these groups, amine showed the largest hysteresis both in air and underwater followed by mercapto and carbomethoxy, see Figure 7.3(a) and (b), as well as Figure 7.4(a). The slight hysteresis for the carbomethoxy surface was related to the ability of PDMS chains to rearrange under pressure and form dipole interactions upon unloading [9].

As can be seen in Figure 7.3 (a), the loading/unloading behavior for the PDMS/amine-treated surface in air showed a noticeable hysteresis. This hysteresis was attributed to the ability of PDMS chains to rearrange under pressure and form hydrogen bonds (H-bonds) with the other surface upon unloading [9]. During unloading underwater a significantly larger hysteresis was observed. Upon unloading underwater the load decreased noticeably while the contact area remained constant for almost half of the unloading duration. This was associated with the presence of hydration layers that form around charged ions and the ability of the hydration layers to sustain a large normal load [123]. The formation of these hydration layers are related to the

formation of ionic H-bonds between positively-charged amine (in neutral water) and water molecules [124]. According to [125], the ionic H-bonds are much stronger than the H-bonds formed between neutral species. This, in combination with the less-ordered packing of APTES, gives amine chains the ability to dissipate more energy before they lose their contact with rearranged PDMS chains during unloading. The hydration layers formed around charged ions have been the basis of several studies in the area of boundary lubrication and their application in biomedical devices [126, 127]. This behavior (the plateau and large adhesion hysteresis) is analogous to the stick-slip friction [128] in boundary lubrication. The stick-slip motion in the presence of a lubricant is affected by the thickness as well as properties of the confined lubricant film and the film transition between solid-like and liquid-like states [128]. The properties of the confined liquid film might be different from the bulk properties because of the ordering of the film between the surfaces. The film acts like a liquid at low sliding velocities, and hence friction is low [128]. When the sliding velocity is high the lubricant has no time to inter-digitate and the film behaves like a solid giving rise to the friction force [128]. At the intermediate regime, the inter-digitation of lubricant chains occurs but the bonds do not break, which results in a large energy dissipation [128, 129]. The plateau region upon (the quasi-static) unloading of this system (where the contact size remained the same implying that the bonds were either not broken or broken but healed at the same rate) is comparable to the scenario that occurs at the intermediate velocity regime in sliding situations. A recent study [130] has shown that for a thin layer of water confined between two mica surfaces, with potassium ions (K^+) on the surface capable of adsorbing water molecules, the stick-slip condition is observed, while the water molecules confined between two hydrophobic surfaces (graphene) demonstrated smooth friction [130]. For

thicker layers of water confined between two mica surfaces no stick-slip condition was observed [130].

Figure 7.4 (a) JKR loading/unloading behavior of native PDMS in contact with carbomethoxy-treated glass slide in air and underwater, (b) JKR loading/unloading behavior of native PDMS in contact with clean glass slide in air and underwater

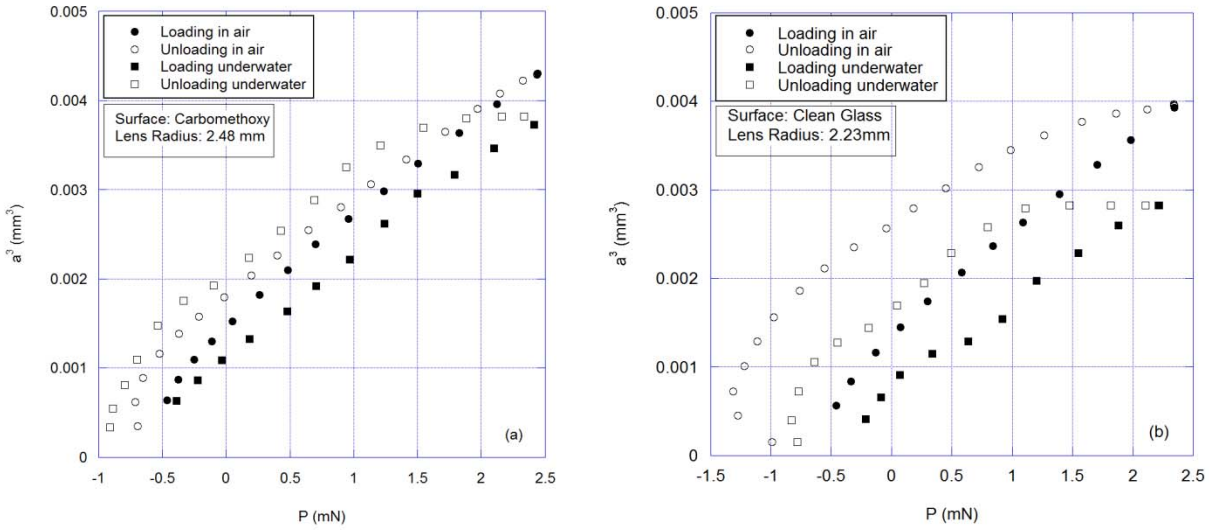

For the adhesion between PDMS and a clean glass slide, as can be seen in Table 7.1, the value of W in air was close to that of PDMS self-adhesion. For this system, a noticeably smaller W was obtained underwater. This was attributed to the ability of hydroxyl groups on the surface of clean glass to form stronger H-bonds with water, compared to amine, as evidenced by the higher number of H-bonds the hydroxyl group develops with water compared to the amine group [131]. The stronger H-bonds between the hydroxyl group and water could form a thicker layer of adsorbed water on the surface to reduce the interactions between PDMS and the clean glass surface further. Therefore, a smaller W underwater was obtained. A previous study using AFM has also shown that the adhesion energy between PDMS and glass decreases underwater compared to that in air [132]. A noticeable hysteresis, see Figure 7.4(b), was observed for this system both in air and underwater. The hysteresis in air was somewhat larger than that observed for amine because of the stronger H-bonds that could form between PDMS and the hydroxyl

group on the clean glass slide surface. The underwater hysteresis, however, was much smaller compared to that seen for amine. This was attributed to the stretching of the bonds on a silane treated surface compared to a rigid surface.

As can be seen in Table 7.1, once again the value of W in air for PEO-treated surfaces was essentially that of PDMS self-adhesion. However, the value of W underwater decreased to essentially zero. As mentioned earlier, if water is present in the contact region, a lower W is expected [17]. The zero value is due to the formation of a hydration layer near the surface [133]. This water layer impedes the contact between PDMS and PEO-treated surfaces by forming a physical and energetic barrier [133] leading to a W that is essentially zero. Previous studies [134-136] have also shown that for PEO-based hydrogels, H-bonds are formed between the hydrogen of the water molecule and the oxygen of the ether group on the PEO network. Binding of water molecules to ether groups cause PEO molecules to achieve minimum free energy while gaining a random conformation (high entropy). Mono and trihydrates of water are formed with each ether oxygen on the PEO backbone [134-136]. This is why PEO surfaces exhibit low protein adsorption behavior underwater as the water molecules bind to the ether group in PEO network and hence, repel proteins due to entropic effects [137].

Although PEO and clean glass surfaces showed a similar wetting behavior, as seen in Table 7.1, no hysteresis was observed in air when PDMS was in contact with PEO, as depicted in Figure 7.5. This was in contrast to the hysteresis that was observed for clean glass in air and due to the fact that the PEO functionality is solely an H-bond acceptor. This is unlike the behavior of the clean glass with hydroxyl groups on the surface, which can be H-bond donors or acceptors depending on the other surface they are interacting with. Therefore, the clean glass surface can

provide H-bonding sites for rearranged PDMS chains upon unloading, whereas PEO lacks that characteristic.

Another fact that should be pointed out is that although the hydroxyl group has a higher hydration number than PEO, the hydroxyl-rich surface shows a higher W underwater compared to PEO-treated surfaces. This is associated with the chain conformation and flexibility of the PEO network that allows the water molecules to penetrate into the PEO network and produce a brush-like structure [127], whereas the hydroxyl groups lack this characteristic. The absorption of water into the PEO film and the brush structure produces an electrostatic repulsive force that hinders the contact between the PEO film and another surface [133]. A previous study [3] has shown that this repulsive force is largest for PEO SAMs, where water can form a higher number of H-bonds, followed by hydroxyl and methyl SAMs.

Figure 7.5 JKR loading/unloading behavior of native PDMS in contact with PEO-treated glass in air and underwater

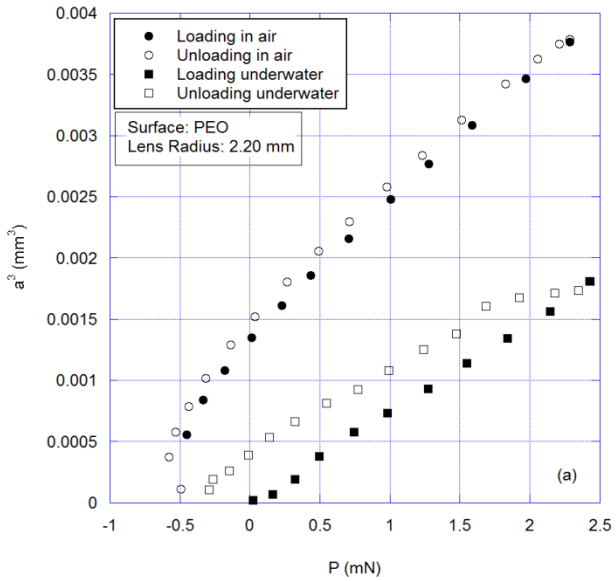

Cellulose and Lignin

This section presents the results that were obtained for the cellulose and lignin surfaces in terms of wettability and the JKR results. As before, these results (K, W, and G_{MFUL}) are found in

Table **7.2** and are shown in the form of a^3-P plots.

Wettability

Similar to the previous section, contact angles of ultrapure water were measured against the cellulosic and lignin surfaces. These results are shown in Table 7.2. The results of contact angles for cellulose I and cellulose A surfaces in this study (≤ 20°) were close to those previously reported for cellulose surfaces where the contact angles ranged from 17° to 22° [138, 139]. Cellulose surfaces are typically rich in hydroxyl groups, and therefore, small contact angles were expected. Water droplets also showed small angles on surfaces coated with lignin in the current study. Previous studies [101, 140] have reported significantly higher contact angles (46-56°) for isolated Kraft lignin coated on silicon wafers. Potential reasons for this discrepancy include the fact that: 1) lignin structure is dependent on the substrate upon which it is deposited [141], 2) the chemical composition of lignin varies from tree species to species, and 3) the chemical composition depends upon the extraction process [142]. Lee and Luner [143] also reported that the contact angle of water on lignin surfaces decreased rapidly with time from 60° to 0°. This was associated with the highly porous nature of the lignin films prepared [140]. No change, however, was observed in the contact angle of water on lignin surfaces in this study over time.

Table 7.2 Results of contact angle and JKR measurements of native PDMS hemispheres with cellulose and lignin in air and underwater

Surface	Static Contact Angle of Water (°)	Air			Underwater		
		K (MPa)	W (mJ/m^2)	G_{MFUL} (mJ/m^2)	K (MPa)	W (mJ/m^2)	G_{MFUL} (mJ/m^2)
Cellulose I	≤ 20	*3.63 ± 0.06	45.85 ± 0.69	50.89 ± 3.20	3.26 ± 0.18	0.17 ± 0.15	8.59 ± 2.73
Cellulose A	≤ 20	3.50 ± 0.30	43.66 ± 1.34	48.41 ± 4.24	3.66 ± 0.36	18.22 ± 1.18	71.87 ± 3.12
Lignin	≤ 20	3.30 ± 0.10	50.0 ± 0.90	50.32 ± 3.36	2.8 ± 0.20	0.4 ± 0.10	6.80 ± 3.40

* The PDMS samples that were used to probe cellulose I surfaces were made out of a different Sylgard184 kit compared to other surfaces of phase I. For this PDMS kit K was in the range of 1.75-1.8 MPa.

JKR Results

The JKR results for W and K for the cellulosic and lignin surfaces, both in air and underwater, are shown in Table 7.2. For adhesion between PDMS and a surface coated with cellulose I the a^3-P data is given in Figure 7.6(a). No hysteresis is observed between loading and unloading in air. This is in contrast to the large hysteresis reported in a previous study [139]. Since the wettability measurements on the cellulose I surfaces prepared for this study showed a very hydrophilic nature for these surfaces, the small adhesion hysteresis in air may be attributed to either the difference in the wood pulp used or the inability of the polar groups in the cellulose to provide H-bond donating sites on the surface level. Underwater, the work of adhesion was essentially zero for the samples that were heat treated. For the samples that were tested with no heat treatment a slightly higher W in air (48.5 ± 2.5 mJ/m^2) and a non-zero value of W underwater (14-18 mJ/m^2) was obtained. No hysteresis was observed for the heat treated samples in air, too. For non-heat-treated surfaces some hysteresis similar to that observed for clean glass or mercapto-treated surfaces was seen (a plateau in the beginning of the unloading portion). This

was associated with the presence of sulfate in the cellulose I structures before the heat treatment, which was also verified by X-ray fluorescence (XRF) measurements.

The zero value of W between PDMS and cellulose I underwater is attributed to the penetration of water into the 3D micro-porous structure of cellulose I [144] and swelling of this surface, similar to that observed for PEO-treated surfaces in the preceding section. Aulin et al. [81] has shown that cellulosic surfaces made out of nanocrystals (cellulose I) swell by a high degree in the presence of water. According to the work performed by Mueller et al. [145], Aulin et al. [81] mentioned that water cannot penetrate cellulose crystalline structure, and concluded that the swelling is due to the water uptake via penetration between the crystals and not the swelling of individual crystals [81]. They mentioned that the water penetration causes a separation of the crystals and allowing for a further water imbibition into the film. They also noted that the nanocrystalline cellulose contained sulfonic groups from the dissolution process, which aided in creating an osmotic pressure separating the crystals in the film [81]. The water penetration between crystals of cellulose I hydrate and swell these surfaces. Therefore, a zero value of W was obtained for PDMS/cellulose I. Several studies [144, 146-148] have used cellulose nanocrystals, as a superabsorbent material, and their variants (e.g. functionalized ones) to produce hydrogels for different applications.

Figure 7.6 (a) JKR loading/unloading behavior of native PDMS in contact with cellulose I in air and underwater, (b) JKR loading/unloading behavior of native PDMS in contact with cellulose A in air and underwater

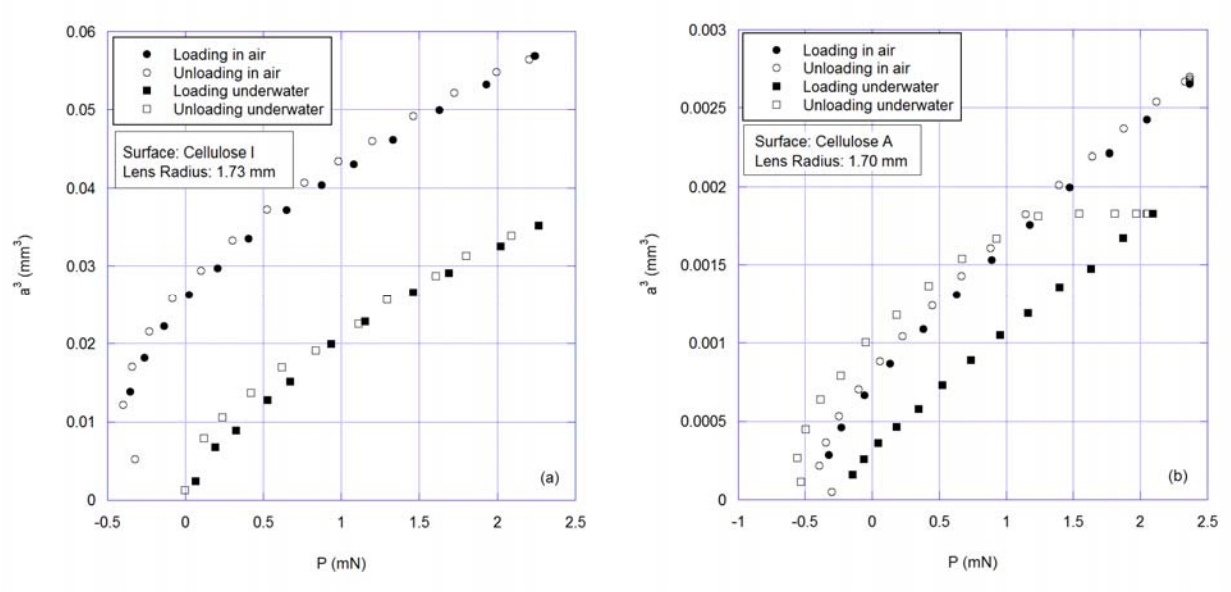

The results of a^3-P data for PDMS and a surface coated with cellulose A for in air and underwater measurements are compared in Figure 7.6(b). No hysteresis was displayed in air between loading and unloading indicating that only dispersive forces were formed between PDMS and cellulose A in air. Underwater a non-zero value of W was obtained with a noticeable hysteresis although a smaller W was obtained in air for cellulose A compared to cellulose I. The low value of W between PDMS and cellulose A underwater is attributed to the absorption of water between the fibrils of the NMMO-based cellulose, and hence swelling of the cellulosic A surfaces [81]. As Aulin et al. [81] reported previously, the swelling degree for cellulose I is higher than the cellulose prepared from NMMO. Therefore, a non-zero W was expected between PDMS and cellulose A surfaces. It is anticipated that the difference between the swelling and/or the value of W underwater for cellulose I and cellulose A is associated with the difference in their crystalline order (which is affected by the dissolving process [72]), surface area, as well as

the parallel (as in cellulose I) vs. anti-parallel (as in cellulose II) chain arrangements of these surfaces [149].

The results for adhesion between PDMS and a surface coated with lignin are displayed in Figure 7.7. As can be seen, no hysteresis was observed in air possibly because of the inability of PDMS and lignin to form any specific bonds. The work of adhesion in air was also close to the value of W for other surfaces. Underwater, however, the work of adhesion dropped to ≈ 0 similar to that observed for PEO-treated surfaces and cellulose I. The zero value of W indicated swelling of the lignin film [150]. The swelling can be attributed to the reactions between ether linkages, which are dominant among all the linkages of lignin, and water molecules, as mentioned before for PEO surfaces. Therefore, similar to PEO or many types of hydrogels, formation of hydration shell around ether groups significantly reduces the interactions between PDMS and lignin-coated surfaces.

Figure 7.7 JKR loading/unloading behavior of native PDMS in contact with lignin in air and underwater

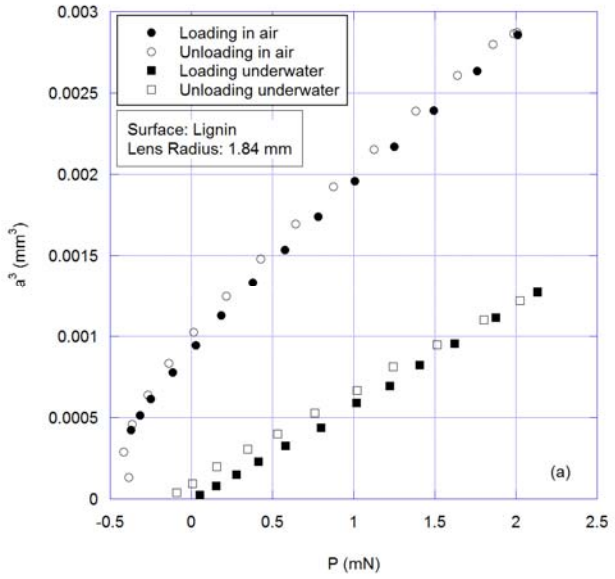

Chapter 8 - Results of Phase II (Functionalized PDMS Probes)

This chapter presents the JKR results related to the second phase of this study. As was mentioned earlier, in the second phase the PDMS hemispheres were chemically functionalized with the amine functionality to probe numerous functionalized surfaces in air and underwater.

In order to perform the experiments for the second phase, the PDMS hemispheres were functionalized according to the procedure described in Chapter 6. The glass surfaces were also treated in the same way as in phase I and according to the procedure mentioned in preceding chapters. The surfaces that were tested included native PDMS sheets, amine-treated PDMS sheets, amine-treated glass surfaces, and PEO-treated glass surfaces. Since the amine-treated PDMS sheets and amine-treated glass surfaces showed similar results, only the results of one of these systems are shown and discussed in this chapter. Here, it should be noted that although it is believed that the silanization process slows the hydrophobic recovery of PDMS for several days [151], all the functionalized PDMS samples were used within less than 14 hr of the treatment to minimize any effects related to hydrophobic recovery of PDMS.

JKR Results

The first system that was studied in the second phase was amine-treated PDMS hemispheres in contact with native PDMS sheets. This was assumed to be equivalent to the native PDMS probe/amine-treated glass surfaces evaluated in the first part of phase I. The amine-treated PDMS probes were then used to probe amine-treated PDMS flat sheets and amine-treated glass surfaces. The two systems showed similar values of W and hysteresis both in air and underwater. Therefore, only the results of one of these systems (amine-treated PDMS flat sheets) are shown here. The other surface that was probed in this phase was PEO-treated glass surfaces. The results of the JKR experiments (K, W, and G_{MFUL}) for amine-treated PDMS

hemispheres probing these selected surfaces are listed in Table 8.1. The tabulated results show the average of the corresponding values obtained for 4 samples and their standard deviation both in air and underwater. The typical a^3-P curves for these surfaces are also depicted in Figure 8.1and Figure 8.2.

Table 8.1 Results of the JKR measurements of amine-treated PDMS hemispheres with various surfaces in air and underwater

Surface	Air			Underwater		
	K (MPa)	W (mJ/m^2)	G_{MFUL} (mJ/m^2)	K (MPa)	W (mJ/m^2)	G_{MFUL} (mJ/m^2)
Native PDMS Flat Sheets	*1.75 ± 0.07	49.41 ± 1.46	125.33 ± 17.28	1.89 ± 0.14	40.10 ± 2.95	207.20 ± 20.88
Amine-treated PDMS Flat Sheets	*1.72 ± 0.04	48.85 ± 3.24	67.60 ± 3.34	1.94 ± 0.08	19.00 ± 4.61	166.76 ± 5.75
PEO-treated Glass	*3.72 ± 0.17	77.88 ± 4.58	83.57 ± 3.89	3.57 ± 0.08	1.55 ± 0.99	7.64 ± 1.31

*A different Sylgard184 kit was used in the second phase. The values of K obtained from self-adhesion of samples made out of this kit were in the range of 1.7-1.8 MPa.

As can be seen in Table 8.1, the values of W for the native and amine-treated PDMS flat sheets in air are similar to the value of W obtained for native PDMS probe/amine-treated glass surfaces in the first phase (~ 47 mJ/m^2). For the PEO-treated surfaces, however, a noticeably larger W was obtained in air. The higher value of W is attributed to the donor-acceptor bonds formed between the ether groups of the PEO network with the amine group. The ether groups are dipolar and act as H-bond acceptors, whereas the nitrogen atoms of the amine group with lone pair electrons are, at the same time, H-bond donors or acceptors, depending on the molecule they are interacting with. The donor-acceptor interactions are stronger than van der Waals forces. Therefore, a larger work of adhesion is expected for a system showing donor-acceptor bonds compared to the systems with only van der Waals forces. The value of W underwater, as seen in

the first phase, was vastly dependent on the system, ranging from very small values for a hydrophilic surface to 40 mJ/m^2 for a system involving an intermediate group.

A typical JKR loading/unloading curve for the amine-treated PDMS probe in contact with native PDMS sheet is depicted in Figure 8.1(a). As mentioned earlier, this system was evaluated as a reference and its similarity to the native PDMS/amine-treated glass system. The value of W for the amine-treated PDMS/native PDMS sheet was close to its analogous system (native PDMS probing amine-treated glass surfaces). As can be seen in Figure 8.1(a) and Table 8.1, for the treated probe/native sheet an adhesion hysteresis comparable to its corresponding system was also observed. The value of W underwater for the amine-treated PDMS probing the native PDMS sheet was, however, larger than that for the equivalent system (~ 30 mJ/m^2). In order to verify whether or not this was caused by the arrangement of the probe/substrate, native PDMS hemispheres were used to probe amine-treated PDMS sheets. The results of W underwater for this system were also in the range of 35-41 mJ/m^2, which indicated that the arrangement of the probe/substrate did not influence the value of W. The difference between the values of W for these two systems (amine-treated PDMS probes/native PDMS and native PDMS probes/amine-treated glass surfaces), which are considered to be similar in surface chemistry, was attributed to the impact of PDMS and its hydrophobic nature on the arrangement of amine groups on oxidized PDMS surfaces as compared to their arrangement on glass surfaces. The static contact angle of water on amine-treated glass in the first phase of the current study was ~ 59°, which was in agreement with the published results. The contact angles of water on amine-treated PDMS sheets were, however, larger than that in the current study (~ 70°), which is close to the previously published results of oxidized PDMS surfaces treated with APTES (~75° [151]). The adhesion hysteresis for the amine-treated PDMS probes in contact with native PDMS sheets

underwater were also significantly smaller than that observed for the native probe/amine-treated glass surface underwater; for the difference, please refer to Table 7.1 and Table 8.1. This was also attributed to the hydrophobic nature of PDMS substrates and arrangement of amine groups on these surfaces as compared to clean glass surfaces. The trend of the hysteresis, the plateau region at the beginning of the unloading and a large difference between the loading and unloading parts, reveal that a relatively large amount of energy could be dissipated for this system and the stick-slip friction could be expected, too. As discussed earlier, this was associated with the positively-charged nature of the amine surface in neutral water and its capability to adsorb water (the hydration layer).

Figure 8.1 (a) JKR loading/unloading behavior of amine-treated PDMS hemisphere in contact with native PDMS sheet in air and underwater, (b) JKR loading/unloading behavior of amine-treated PDMS probe in contact with amine-treated PDMS sheet air and underwater

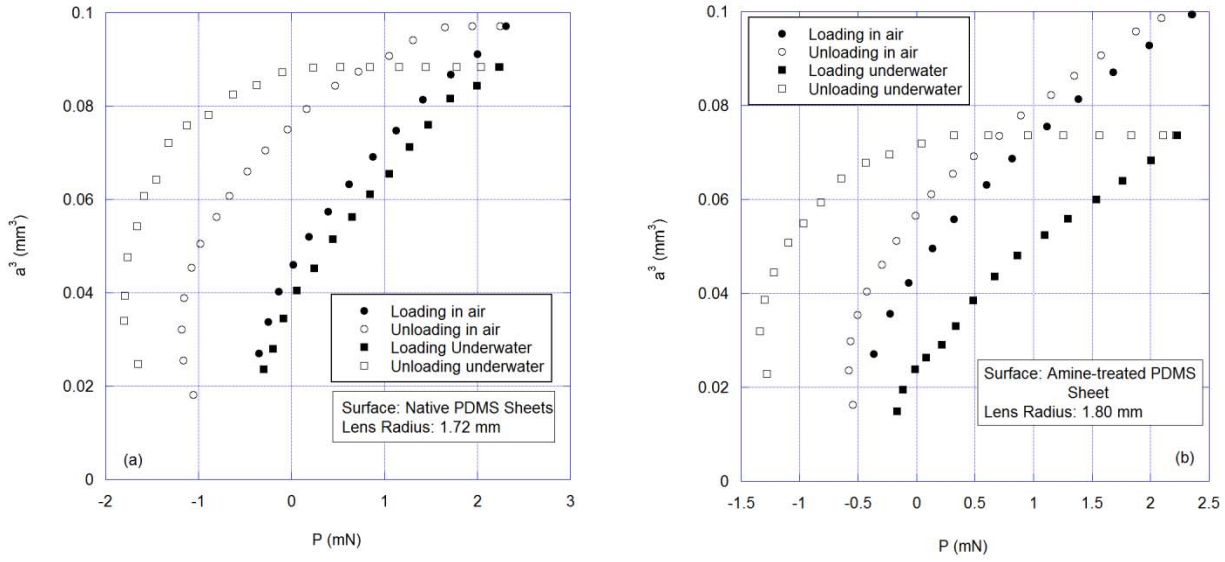

The contact between an amine-treated PDMS probe with the amine-treated PDMS flat sheet is depicted in Figure 8.1(b). As mentioned earlier, no difference in the value of W in air was seen for this system compared to the other systems discussed earlier with amine-treated glass or PDMS surfaces. The amount of hysteresis in air, however, was noticeably smaller for

this system compared to the other systems involving amine-treated surfaces. The reduction of the hysteresis amount shows that the bonds formed between amine-amine during unloading were not as strong as the interactions formed between rearranged PDMS chains and amine as seen in native PDMS surfaces against amine-treated (glass or PDMS) surfaces. For two amine-treated PDMS surfaces underwater the value of W was significantly lower than the values obtained for the native PDMS/amine-treated glass surfaces or amine-treated PDMS probes in contact with native PDMS sheets. As stated earlier, the steric repulsion of the hydration layer of water was the main reason the value of W for native PDMS probe/amine-treated glass surfaces was lower than the other intermediate groups in the first phase. The further reduction of W underwater for amine-amine surfaces was attributed to the surface charges on these surfaces underwater. The combination of the electrostatic double-layer repulsion (caused by two similarly charged surfaces) and the steric repulsion of the hydration layer of the water molecules bound to the amine surfaces [152] further decreased the interactions of amine surfaces, and hence a low value of W was obtained. Regardless of this, however, the adhesion hysteresis was close to that obtained for the amine-treated PDMS probe in contact with native PDMS sheet although slightly smaller, see Table 8.1. Based upon the large energy dissipation, the stick-slip condition could be predicted for this system as well.

The a^3-P curve for the amine-treated PDMS hemisphere probing a PEO-treated glass surface is shown in Figure 8.2. As noted earlier, a higher value of W was obtained for this system in air compared to the other surfaces studied in the current study. This was associated with the formation of donor-acceptor bonds upon contact of amine and PEO. Very small hysteresis was also observed for this system in air. Underwater the value of W was very small, similar to that observed in the first phase. This indicated that the interactions between water

molecules and PEO chains were still more favorable than the interactions between PEO and amine. Therefore, a water layer was formed on the PEO surface, which impeded the interactions between amine-treated PDMS and PEO surfaces.

Figure 8.2 JKR loading/unloading behavior of amine-treated PDMS hemisphere in contact with a PEO-treated glass surface in air and underwater

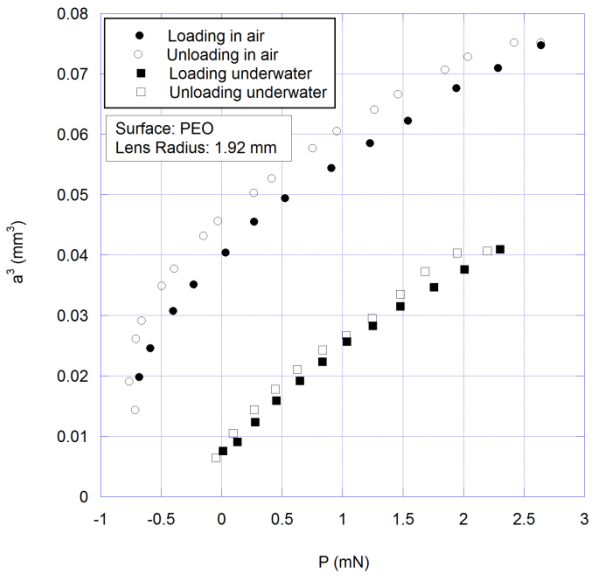

Chapter 9 - Summary

This chapter provides a detailed summary of the work performed and the results obtained in this study. As stated previously, the aim of this study was to evaluate how surface chemistry influences the adhesion behavior of polymeric systems underwater. For this means, the JKR theory of contact mechanics and its associated experimental approach was used. The JKR experiment utilizes a hemispherical probe made out of a compliant polymeric material (typically PDMS) to probe other surfaces (referred to as substrates). In the JKR experiment the polymeric probe is brought into contact and pressed on the substrate during the loading process. After reaching a pre-determined load, the motion is halted and reversed to start the unloading process until separation occurs. During both the loading and unloading parts the amount of the load and the images of the contact region are captured for later processing. The relationship formulated by Johnson-Kendall-Roberts between the size of the contact area and the amount of the load determines the thermodynamic work of adhesion (W), which is indicative of the bonds that are formed at the interface of the probe and substrate upon contact. The JKR relationship was developed for a system where loading and unloading were identical. For some systems, however, there might be a difference between the loading and unloading processes, referred to as adhesion hysteresis. Several explanations given for the adhesion hysteresis include formation of specific/non-specific bonds, viscoelastic nature of a system, or surface roughness. It has been shown that since the mechanism of the molecular relaxation during normal separation and friction are similar; the frictional behavior of a system is correlated to the adhesion hysteresis of that system. Namely, the higher the adhesion hysteresis for a system, the larger the friction forces are.

Research Strategy

In the current study the JKR experiments were performed to determine the effect of surface chemistry on both W and adhesion hysteresis underwater. The JKR experiments were also conducted in air for means of comparison. In order to accomplish the overall goal of this study, the experiments were divided into two phases. In brief, native PDMS probes were used in the first phase to evaluate a variety of model surfaces with disparate surface chemistries. The first phase itself was divided into two parts. In the first part several model surfaces ranging from hydrophilic to medium to hydrophobic were first evaluated. The model surfaces included (flat) glass surfaces that were chemically modified by several functional groups through the silanization process. The functional groups were PEO as a hydrophilic group; amine, carbomethoxy, and mercapto with intermediate wetting behavior; cyclohexyl, fluorocarbon, and methyl with hydrophobic characteristics. PDMS flat sheets and bare glass surfaces were also evaluated for means of comparison. In the second part of this phase three model surfaces based upon wood-derived biopolymers were evaluated. These surfaces included two cellulosic surfaces (natural and regenerated cellulose) and one lignin surface (from hardwood). In the second phase the PDMS probes were functionalized to show a non-hydrophobic characteristic. Because of its wide existence in nature, the amine functionality was chosen to treat PDMS hemispheres. For this means the PDMS samples were oxidized and then silanized, similar to the procedure that was carried out for treating glass surfaces. The surfaces that were probed in the second phase included native and amine functionalized flat sheets of PMDS, amine- and PEO-treated glass surfaces.

Phase I

The results of the JKR experiments in the first part of phase I showed that for all the chemically modified glass surfaces the value of W in air was similar and close to that obtained for PDMS self-adhesion. The only exception was fluorocarbon-treated surfaces, which showed a noticeably smaller W in air. This was attributed to the weaker van der Waals forces formed between native PDMS and fluorocarbon because of the lower surface energy of fluorocarbon. For other surfaces the similar values of W in air indicated that the interactions were dominated by PDMS and London dispersion forces. The adhesion hysteresis in air was greatly affected by the functionality that was deposited on the surface. Bare glass surfaces, rich in hydroxyl groups, and those treated with amine, mercapto, and fluorocarbon were the surfaces that showed a noticeable hysteresis. The carbomethoxy surfaces also displayed a small hysteresis. The adhesion hysteresis for bare glass, amine-, mercapto-, carbomethoxy, and fluorocarbon-treated surfaces was associated with the ability of PDMS chains to rearrange under pressure and form either H-bonds or dipole interactions with the aforementioned surfaces during unloading. For PDMS probes in contact with PDMS flat sheets, methyl-, cyclohexyl-treated surfaces no adhesion hysteresis was observed. These hydrophobic systems only interact with London dispersion forces and hence, no hysteresis was expected. Although clean glass and PEO-treated surfaces were both highly hydrophilic a large adhesion hysteresis was seen for clean glass but not for PEO. The highly hydrophilic characteristic of PEO was attributed to the dipolar characteristic of the ether groups of the PEO network which render these groups as merely H-bond acceptors, whereas the hydroxyl groups can be H-bond donors or acceptors depending on the surface they are interacting with.

Underwater, both the values of W and adhesion hysteresis for the chemically modified surfaces were considerably different from the corresponding property in air and also amongst

each surface type. In general, for hydrophobic substrates (PDMS, cyclohexyl-, methyl-, and fluorocarbon-treated surfaces) the value of W underwater was larger than that in air and other surfaces underwater. This was attributed to the hydrophobic interactions and rearrangement of water molecules near the hydrophobic surfaces to minimize their contact with these surfaces.

Amongst the hydrophobic surfaces, fluorocarbon showed the smallest value of W underwater although it is more hydrophobic than the other surfaces. The lower value of W for fluorocarbon surfaces compared to hydrocarbons underwater was attributed to the polarity of fluorocarbon and its potency to break hydrogen bonds of water. This could perturb the ordered structure of water molecules in the vicinity of fluorocarbons compared to hydrocarbon surfaces. Another reason for the smaller value of W underwater was the weaker interactions that could be formed between PDMS and fluorocarbon-treated surfaces. The weaker interactions would make it less favorable for these surfaces to interact underwater, too.

The values of W for the intermediate groups (amine, carbomethoxy, and mercapto) were smaller than those in air. Amongst these surfaces amine showed the smallest value of W underwater although all these surfaces showed similar wetting behavior. For the other two surfaces the value of W was closer to those obtained in air. The smaller value of W for amine surfaces underwater was associated with the formation of H-bonds between water molecules and amine groups although this is not as favorable as strong hydrogen bonds between water molecules. The H-bonds formed between amine and water molecules would result in a hydration repulsion of steric origin that demotes the interactions between the PDMS probe and the amine-treated surfaces. The higher value of W or the other two groups with medium wettability (carbomethoxy and mercapto) underwater reflected that such hydration repulsion, if present, was

not as strong as that for the amine surface. Therefore, the interactions were not affected as much as for the amine surfaces.

For bare glass surfaces rich in hydroxyl groups the value of W underwater was further reduced compared to the intermediate groups. The small W underwater was once again attributed to the hydration repulsion between the probe and the substrate. The smaller value of W compared to the amine surfaces indicated that the hydration repulsion was stronger than that for amine surfaces. This was expected considering that the hydrogen bonds formed between hydroxyl groups and water molecules were stronger than those formed between amine and water.

For PEO-treated surfaces no interactions were observed between the PDMS probe and the substrate, as evidenced by W that was essentially zero. The zero value was attributed to the strong H-bonds formed between hydrogen atoms of water molecules and the oxygen of the ether group on the PEO network. This resulted in formation of a hydration layer near PEO surfaces, which impeded the contact between PDMS and these substrates.

It was shown by the wettability measurements that water droplets sheeted both bare glass and PEO-treated surfaces. Underwater, however, a hydration layer was only formed on PEO-treated surfaces and not on hydroxyl rich surfaces although the hydroxyl group has a higher hydration number than PEO. The superiority of the PEO substrates underwater was associated with the flexibility of the PEO network and formation of a brush-like structure as water molecules penetrate into the PEO network. This brush structure produces an electrostatic repulsive force that hinders the contact between the PEO film and another surface.

The unloading portion of the JKR experiments showed no significant adhesion hysteresis for the hydrophobic substrates underwater, except for fluorocarbon surfaces. The higher adhesion hysteresis for fluorocarbon surfaces in air was correlated to the larger frictional forces

of these surfaces in air. It was anticipated that because of the larger adhesion hysteresis of fluorocarbon underwater, this surface would show a larger friction force compared to hydrocarbon surfaces underwater, too.

For the intermediate groups the amine-treated surfaces displayed the highest adhesion hysteresis not only amongst the medium groups but also amongst all the surfaces that were evaluated in this study. The high adhesion hysteresis for amine surfaces was associated with the positively-charge characteristic of amine underwater and its ionic hydrogen bonds with water molecules in the confined water layer. The high adhesion hysteresis of the amine-treated surfaces believed to be correlated with the stick-slip friction condition in boundary lubrication, previously seen for positively charged surfaces. The adhesion hysteresis underwater was also seen for mercapto-treated surfaces followed by clean glass surfaces, and carbomethoxy-terminated surfaces.

The JKR results of the second part of phase I on two cellulosic and one lignin surfaces also showed that the values of W for cellulose I and lignin surfaces were close in air and higher than that for cellulose A surfaces. The smaller value of W for cellulose A was attributed to its lower surface energy compared to cellulose I. No adhesion hysteresis was observed for any of these surfaces indicating that they were highly ordered. Although all these three surfaces were completely wetted by water droplets, they showed disparate values of W underwater. Cellulose I and lignin surfaces showed almost no interactions with PDMS probes underwater ($W \sim 0$), whereas cellulose II showed a small non-zero value ($W \sim 18$ mJ/m^2). It was anticipated that similar to PEO surfaces, cellulose I and lignin surfaces swelled in water and formed a brush-like structure that completely obstructed the contact between the probe and the substrate. The value

of W obtained for cellulose A surfaces was close to (but smaller than) those obtained for the hydroxyl-rich surfaces in the first part of phase I of the current study.

Phase II

In the second phase PDMS probes were chemically treated with the amine functionality to probe native PDMS sheets, amine-functionalized PDMS sheets and glass surfaces, as well as PEO-treated surfaces. The JKR results showed different values of W in air and underwater for these surfaces. The adhesion hysteresis was also significantly influenced by the surface chemistry. The system involving amine-treated probes in contact with native PDMS was assumed to be analogous to the native PDMS probe/amine-treated glass surfaces in terms of surface chemistry. The value of W and amount of adhesion hysteresis in air for these two systems were similar. The amount of W underwater was, however, larger for the amine-functionalized PDMS probe in contact with native PDMS sheet. This was attributed to the arrangement of the amine groups on PDMS substrates compared to that on clean glass surfaces, as evidenced by the difference in static contact angles of water. The amount of hysteresis for the amine-treated probe/native PDMS sheet underwater was much smaller than that observed for its twin system, but still higher than other surfaces evaluated in the current study. This was also attributed to the arrangement of amine groups on hydrophobic PDMS substrates as compared to hydrophilic glass surfaces. Regardless of this, however, the trend that was observed for the amine-treated probe/native PDMS sheet could also point to the stick-slip condition observed for the native PDMS probe/amine-treated system.

When amine-treated PDMS hemispheres probed amine-treated PDMS sheets and amine-treated glass surfaces the value of W in air was close to the value of W obtained in air for native PDMS in contact with amine-treated glass surfaces in the first phase. The value of W

underwater, however, was smaller than that for the amine-treated probe/native PDMS sheet or native PDMS probe/amine-treated system. The reduction in W underwater was attributed to the combination of electrostatic repulsion and steric repulsion of the hydration layer formed on amine-treated surfaces at both sides of the contact, which further demoted the interactions underwater. Even though a lower value of W was obtained for this system underwater, the amount of hysteresis was close to that obtained for the amine-treated probe/native PDMS sheets, specifying that a stick-slip condition would be expected for this system as well because of the positively charged surfaces.

For PEO-treated surfaces in contact with amine-treated probes a larger value of W in air was obtained. The larger value was attributed to the formation of stronger donor-acceptor bonds between PEO and amine. No significant hysteresis was also observed in air, similar to phase I. The value of W underwater was very low and close to zero. This showed that the interactions between PEO and water molecules were still more favorable than the interactions between amine and PEO.

References

1. B.P. Lee, P.B. Messersmith, J.N. Israelachvili, J.H. Waite. Mussel-inspired adhesives and coatings. Annual review of materials research 2011;41:99-132.

2. V.L. Andolina. **Influence of elastomeric seal plate surface chemistry on interface integrity in biofouling-prone systems: Evaluation of a hydrophobic "easy-release" silicone-epoxy coating for maintaining water seal integrity of a sliding neoprene/steel interface**. 2012.

3. J. Zheng, L. Li, H. Tsao, Y. Sheng, S. Chen, S. Jiang. Strong Repulsive Forces between Protein and Oligo (Ethylene Glycol) Self-Assembled Monolayers: A Molecular Simulation Study. Biophys J 2005;89(1):158-166.

4. C.W. McCutchen. The frictional properties of animal joints. Wear 1962;5(1):1-17.

5. A.Y. Stark, I. Badge, N.A. Wucinich, T.W. Sullivan, P.H. Niewiarowski, A. Dhinojwala. Surface wettability plays a significant role in gecko adhesion underwater. Proceedings of the National Academy of Sciences 2013;110(16):6340-6345.

6. S. Lee, N.D. Spencer. Poly(L-lysine)-graft-poly(ethylene glycol): A versatile aqueous lubricant additive for tribosystems involving thermoplastics. Lubr Sci 2008;20(1):21-34.

7. G. Sudre, L. Olanier, Y. Tran, D. Hourdet, C. Creton. Reversible adhesion between a hydrogel and a polymer brush. Soft matter 2012;8(31):8184-8193.

8. K.L. Johnson, K. Kendall, A.D. Roberts. Surface energy and the contact of elastic solids. Proceedings of the Royal Society of London.Series A, Mathematical and physical sciences 1971;324(1558):301-13.

9. S. Kim, G.Y. Choi, A. Ulman, C. Fleischer. Effect of chemical functionality on adhesion hysteresis. Langmuir 1997;13(25):6850-6856.

10. M.K. Chaudhury. Adhesion hysteresis and friction. Langmuir 1993;9(1):29-31.

11. S. Yamada, J. Israelachvili. Friction and adhesion hysteresis of fluorocarbon surfactant monolayer-coated surfaces measured with the surface forces apparatus. The journal of physical chemistry.B 1998;102(1):234-244.
12. R. Szoszkiewicz, B. Bhushan, B.D. Huey, A.J. Kulik, G. Gremaud. Correlations between adhesion hysteresis and friction at molecular scales. American Institute of Physics. 2005.
13. K.L. Mittal. ADHESION MEASUREMENT OF THIN FILMS. Electrocomponent science and technology 1976;3(1):21-42.
14. M.E. Schrader. Young-Dupre revisited. Langmuir 1995;11(9):3585-3589.
15. A. Falsafi. Contact mechanical measurement of block copolymer adhesion. 1999.
16. J. Israelachvili. Adhesion forces between surfaces in liquids and condensable vapours. Surface Science Reports 1992;14(3):109-159.
17. A.P. Defante, T.N. Burai, M.L. Becker, A. Dhinojwala. Consequences of water between two hydrophobic surfaces on adhesion and wetting. Langmuir 2015;31(8):2398-2406.
18. J. Than. Hydrophobic Interactions. http://chemwiki.ucdavis.edu/Physical_Chemistry/Physical_Properties_of_Matter/Atomic_and_Molecular_Properties/Intermolecular_Forces/Hydrophobic_Interactions ed.
19. A. Nolte, J.Y. Chung, M.L. Walker, C.M. Stafford. In situ adhesion measurements utilizing layer-by-layer functionalized surfaces. ACS applied materials & interfaces 2009;1(2):373-380.
20. H. Hertz. On the contact of elastic solids. Journal für die reine und angewandte Mathematik 1882(92):156-171.
21. B.V. Derjaguin, V.M. Muller, Y.P. Toporov. Effect of contact deformations on the adhesion of particles. J Colloid Interface Sci 1975;53(2):314-26.

22. D. Tabor. Surface forces and surface interactions. J Colloid Interface Sci 1977;58(1):2-13.

23. D. Maugis. Adhesion of spheres: The JKR-DMT transition using a dugdale model. J Colloid Interface Sci 1992;150(1):243-269.

24. D. Maugis. Contact, adhesion and rupture of elastic solids. Springer. 1999.

25. D. Maugis, M. Barquins. Fracture mechanics and the adherence of viscoelastic bodies. Journal of physics.D, Applied physics 1978;11(14):1989-2023.

26. A.A. Griffith. The phenomena of rupture and flow in solids. Philosophical transactions of the Royal Society of London 1920;221:163-198.

27. G.R. Irwin. Analysis of stresses and strains near the end of a crack traversing a plate (Translation into Ukrainian). Journal of Applied Mechanics 1957;24:361-364.

28. M.E.R. Shanahan. Adhesion and wetting. Similarities and differences. Rubber World 1991;205(1):28-28.

29. D. Ahn, K.R. Shull. Effects of substrate modification on the interfacial adhesion of acrylic elastomers. Langmuir 1998;14(13):3646-3654.

30. V. Vaenkatesan, Z. Li, W. Vellinga, W.H. de Jeu. Adhesion and friction behaviours of polydimethylsiloxane - A fresh perspective on JKR measurements. Polymer 2006;47(25):8317-8325.

31. W. Merrill, A.V. Pocius, B.V. Thakker, M. Tirrell. Direct measurement of molecular level adhesion forces between biaxially oriented solid polymer films. Langmuir 1991;7(9):1975-1980.

32. Y.L. Chen, C.A. Helm, J.N. Israelachvili. Molecular mechanisms associated with adhesion and contact angle hysteresis of monolayer surfaces. J Phys Chem 1991;95(26):10736-47.

33. K.R. Shull, A.J. Crosby. Axisymmetric adhesion tests of pressure sensitive adhesives. Journal of engineering materials and technology 1997;119(3):211-215.

34. A. Gent, J. Schultz. Effect of wetting liquids on the strength of adhesion of viscoelastic materials 1971;31(2).

35. E.H. Andrews, A.J. Kinloch. Mechanics of adhesive failure. Proceedings of the Royal Society of London Series A, Mathematical and physical sciences 1973;332:385-389.

36. M.L. Williams, R.F. Landel, J.D. Ferry. The temperature dependence of relaxation mechanisms in amorphous polymers and other glass-forming liquids. J Am Chem Soc 1955;77(14):3701-3707.

37. Y.S. Garif, W.W. Gerberich, C.W. Macosko, A.V. Pocius. Microprobing of interfacial behavior of solid polymers by means of normal mechanical contacts. Materials Research Society symposia proceedings 2002;710:81-86.

38. N. Amouroux, F. Restagno, L. Léger. Adhesion at poly(butylacrylate)-poly(dimethylsiloxane) interfaces. The journal of adhesion 2007;83(8):741-760.

39. Wettability, non-wettability, and contact angle hysteresis. http://web.mit.edu/nnf/education/wettability/wetting.html ed.

40. T. Young. An Essay on the Cohesion of Fluids. Philosophical Transactions of the Royal Society of London 1805;95:65-87.

41. C.J. Van Oss, M.J. Roberts, R.J. Good, M.K. Chaudhury. Determination of the apolar component of teh surface tension of water by contact angle measurements on gels. Colloids and surfaces 1987;23(4):369-373.

42. D. Owens, R. Wendt. Estimation of the surface free energy of polymers. J Appl Polym Sci 1969;13(8):1741-1747.

43. A. Dillow, S.E. Ochsenhirt, J.B. McCarthy, G.B. Fields, M. Tirrell. Adhesion of α5β1 receptors to biomimetic substrates constructed from peptide amphiphiles. Biomaterials 2001;22(12):1493-1505.
44. J.T. Koberstein, D.E. Duch, W. Hu, T.J. Lenk, R. Bhatia, H.R. Brown, J.P. Lingelser, Y. Gallot. Creating smart polymer surfaces with selective adhesion properties. The journal of adhesion 1998;66(1):229-249.
45. N. Amouroux, L. Léger. Effect of dangling chains on adhesion hysteresis of silicone elastomers, probed by JKR test. Langmuir 2003;19(4):1396-1401.
46. L. Li, M. Tirrell, G.A. Korba, A.V. Pocius. Surface energy and adhesion studies on acrylic pressure sensitive adhesives. The journal of adhesion 2001;76(4):307-334.
47. T. Kallio, J. Lindfors, J. Laine, P. Stenius. Spreading and adhesion of lipophilic extractives on surfaces in paper machines. Nordic pulp & paper research journal 2008;23(1):108-119.
48. N. Amouroux, L. Léger. Modulation of adhesion at acrylic adhesive-silicone elastomer interfaces. The journal of adhesion 2006;82(9):919-932.
49. K.R. Shull. Contact mechanics and the adhesion of soft solids. Materials science & engineering.R, Reports 2002;36(1):1-45.
50. E. Barthel. Adhesive contact of a compliant sphere to an elastic coated substrate: The thin film limit. The journal of adhesion 2007;83(8):729-739.
51. C. Loskofsky, F. Song, B. Zhang Newby. Underwater adhesion measurements using the JKR technique. The journal of adhesion 2006;82(7):713-730.
52. M. Chaudhury, G. Whitesides. Direct measurement of interfacial interactions between semispherical lenses and flat sheets of poly(dimethylsiloxane) and their chemical derivatives. Langmuir 1991;7(5):1013-1025.

53. M. Deruelle, L. Leger, M. Tirrell. Adhesion at the solid-elastomer interface: influence of the interfacial chains. Macromolecules 1995;28(22):7419-7419.

54. S. Perutz, E.J. Kramer, J. Baney, C.-. Hui, C. Cohen. Investigation of adhesion hysteresis in poly(dimethylsiloxane) networks using the JKR technique. Journal of polymer science.Part B, Polymer physics 1998;36(12):2129-39.

55. L. Lihua, V.S. Mangipudi, M. Tirrell, A.V. Pocius. Direct measurement of surface and interfacial energies of glassy polymers and PDMS. Proceedings of the NATO Advanced Study Institute on Fundamentals of Tribology and Bridging the Gap Between the Macro- and Micro/Nanoscales 2001:305-29.

56. R. Mason, J. Emerson, J.T. Koberstein. Self-adhesion hysteresis in polydimethylsiloxane elastomers. The journal of adhesion 2004;80(1):119-143.

57. M. Deruelle, H. Hervet, G. Jandeau, L. Leger. Some remarks on JKR experiments. J Adhes Sci Technol 1998;12(2):225-47.

58. A. Oláh, G.J. Vancso. Characterization of adhesion at solid surfaces: Development of an adhesion-testing device. European polymer journal 2005;41(12):2803-2823.

59. J. Qi, D.A. Dillard, R.H. Plaut, J.G. Dillard. Experiments on contact of a loop with a substrate to measure work of adhesion. The journal of adhesion 2003;79(6):559-579.

60. E. Degrandi Contraires, A. Beaumont, F. Restagno, R. Weil, C. Poulard, L. Leger. Cassie-Wenzel-like transition in patterned soft elastomer adhesive contacts. Europhys Lett 2013;101(1):14001-14001.

61. G.Y. Choi, S. Kim, A. Ulman. Adhesion hysteresis studies of extracted poly(dimethylsiloxane) using contact mechanics. Langmuir 1997;13(23):6333-6338.

62. P. Silberzan, S. Perutz, E.J. Kramer, M.K. Chaudhury. Study of the self-adhesion hysteresis of a siloxane elastomer using the JKR method. Langmuir 1994;10(7):2466-2470.

63. M.K. Chaudhury, G.M. Whitesides. Correlation between surface free energy and surface constitution. Science 1992;255(5049):1230-1232.

64. R. Mason, J.T. Koberstein. Adhesion of PDMS elastomers to functional substrates. The journal of adhesion 2005;81(7):765-789.

65. M.E.R. Shanahan, F. Michel. Physical adhesion of rubber to glass. Cross-link density effects near equilibrium. Int J Adhes Adhes 1991;11(3):170-176.

66. J.P. Pickering, D.W. Van Der Meer, G.J. Vancso. Effects of contact time, humidity, and surface roughness on the adhesion hysteresis of polydimethylsiloxane. J Adhes Sci Technol 2001;15(12):1429-1441.

67. D. Woerdeman, J.A. Emerson, R.K. Giunta. JKR contact mechanics for evaluating surface contamination on inorganic substrates. Int J Adhes Adhes 2002;22(3):257-264.

68. A. Falsafi, M. Tirrell, A.V. Pocius. Compositional effects on the adhesion of acrylic pressure sensitive adhesives. Langmuir 2000;16(4):1816-1824.

69. B.K. Ahn, S. Jonggeun, N. Rahmani, G. Wang, K. Namhoon, K. Lease, X.S. Sun. Uv-curable, high-shear pressure-sensitive adhesives derived from acrylated epoxidized soybean oil. The journal of adhesion 2013;89(4):323-38.

70. B. Zhao, H. Zeng, Y. Tian, J. Israelachvili. Adhesion and detachment mechanisms of sugar surface from the solid (glassy) to liquid (viscous) state. Proceedings of the National Academy of Sciences of the United States of America 2006;103(52):19624-19629.

71. M. Rundlof, M. Karlsson, L. Wagberg, E. Poptoshev, M. Rutland, P. Claesson. Application of the JKR Method to the Measurement of Adhesion to Langmuir-Blodgett Cellulose Surfaces. J Colloid Interface Sci 2000;230(2):441-447.
72. M. Eriksson, S.M. Notley, L. Wågberg. Cellulose thin films: Degree of cellulose ordering and its influence on adhesion. Biomacromolecules 2007;8(3):912-919.
73. E. Johansson. Molecular interactions in thin films of biopolymers, colloids, and synthetic polyelectrolytes. 2011.
74. H. Haidara, M.K. Chaudhury, M.J. Owen. Direct method of studying adsorption of a surfactant at solid-liquid interfaces. J Phys Chem 1995;99(21):8681-8681.
75. A. Faghihnejad, H. Zeng. Hydrophobic interactions between polymer surfaces: Using polystyrene as a model system. Soft matter 2012;8(9):2746-2759.
76. A. Faghihnejad, H. Zeng. Interaction mechanism between hydrophobic and hydrophilic surfaces: Using polystyrene and mica as a model system. Langmuir 2013;29(40):12443-12451.
77. E. Kokkoli, C.F. Zukoski. Interaction between hydrophobic self-assembled monolayers. Effect of salt and the chemical potential of water on adhesion. Langmuir 1998;14(5):1189-1195.
78. E. Kokkoli, C.F. Zukoski. Surface forces between hydrophilic self-assembled monolayers in aqueous electrolytes. Langmuir 2000;16(14):6029-6036.
79. M. Holmberg, J. Berg, S. Stemme, L. Odberg, J. Ramusson, P. Claesson. Surface Force Studies of Langmuir- "Blodgett Cellulose Films. J Colloid Interface Sci 1997;186(2):369-381.

80. M. Osterberg, P. Claesson. Interactions between cellulose surfaces: effect of solution pH. J Adhes Sci Technol 2000;14(5):603-618.

81. C. Aulin, S. Ahola, P. Joseffson, P. Nishino, Y. Hirose, M. Osterberg, L. Wagberg. Nanoscale cellulose films with different crystallinities and mesostructures - Their surface properties and interaction with water. Langmuir 2009;25(13):7675-7685.

82. J. Bastidas, R. Venditti, J. Pawlak, R. Gilbert, S. Zauscher, J. Kadla. Chemical force microscopy of cellulosic fibers. Carbohydr Polym 2005;62(4):369-378.

83. A. Carambassis, M. Rutland. Interactions of cellulose surfaces: effect of electrolyte. Langmuir 1999;15(17):5584-5590.

84. M. Osterberg. The Effect of a Cationic Polyelectrolyte on the Forces between Two Cellulose Surfaces and between One Cellulose and One Mineral Surface. J Colloid Interface Sci 2000;229:620.

85. Q. Lu, E. Danner, J.H. Waite, J.N. Israelachvili, H. Zeng, D.S. Hwang. Adhesion of mussel foot proteins to different substrate surfaces. Journal of The Royal Society Interface 2013;10(79).

86. J. Zhou, D.A. Khodakov, A.V. Ellis, N.H. Voelcker. Surface modification for PDMS-based microfluidic devices. Electrophoresis 2012;33(1):89-104.

87. J. Stiernstedt. Interactions of cellulose and model surfaces. Royal Institute of Technology. 2006.

88. E.E. Kontturi. Surface chemistry of cellulose:from natural fibres to model surfaces. Technische Universiteit Eindhoven. 2005.

89. M. Tsuboi. Infrared spectrum and crystal structure of cellulose. Journal of Polymer Science 1957;25(109):159-171.

90. C.Y. Liang, R.H. Marchessault. Infrared spectra of crystalline polysaccharides. I. Hydrogen bonds in native celluloses. Journal of Polymer Science 1959;37(132):385-395.

91. J. Mann, H.J. Marrinan. Crystalline modifications of cellulose. Part II. A study with plane-polarized infrared radiation. Journal of Polymer Science 1958;32(125):357-370.

92. R.H. Marchessault, C.Y. Liang. Infrared spectra of crystalline polysaccharides. III. Mercerized cellulose. Journal of Polymer Science 1960;43(141):71-84.

93. A.C. O'Sullivan. Cellulose: The structure slowly unravels. Cellulose 1997;4(3):173-207.

94. E. Dinand, M. Vignon, H. Chanzy, L. Heux. Mercerization of primary wall cellulose and its implication for the conversion of cellulose I → cellulose II. Cellulose 2002;9(1):7-18.

95. S.M. Notley, M. Norgren. Surface Energy and Wettability of Spin-Coated Thin Films of Lignin Isolated from Wood. Langmuir 2010;26(8):5484-5490.

96. D. Vallero.
L'Acide Cleanup Recommendation Report . http://www.onlineethics.org/cms/23119.aspx ed.

97. Hydrophobicity, Hydrophilicity and Silane Surface Modification. http://www.gelest.com/goods/pdf/Hydrophobicity.pd ed.

98. Sylgard 184 Siliocne Elastomer. http://www.dowcorning.com/DataFiles/090276fe80190b08.pdf ed.

99. S. Fält, L. Wågberg, E.-. Vesterlind, P.T. Larsson. Model films of cellulose II – improved preparation method and characterization of the cellulose film. Cellulose 2004;11(2):151-162.

100. C. Edgar, D. Gray. Smooth model cellulose I surfaces from nanocrystal suspensions. Cellulose 2003;10(4):299-306.

101. M. Norgren, S. Notley, A. Majtrenova, G. Gellerstedt. Smooth model surfaces from lignin derivatives. I. Preparation and characterization. Langmuir 2006;22(3):1209-1214.

102. X. Zeng, G. Xu, Y. Gao, Y. An. Surface wettability of (3-Aminopropyl)triethoxysilane self-assembled Monolayers. The journal of physical chemistry.B 2011;115(3):450-454.

103. D. Janssen, R. De Palma, S. Verlaak, P. Heremans, W. Dehaen. Static solvent contact angle measurements, surface free energy and wettability determination of various self-assembled monolayers on silicon dioxide. Thin Solid Films 2006;515(4):1433-1438.

104. L.L. Kosbar, C.D. Dimitrakopoulos, D.J. Mascaro. The effect of surface preparation on the structure and electrical transport in an organic semiconductor. Materials Research Society symposia proceedings 2001;665:401-406.

105. O. Noel, M. Brogly, G. Castelein, J. Schultz. In situ determination of the thermodynamic surface properties of chemically modified surfaces on a local scale: An attempt with the atomic force microscope. Langmuir 2004;20(7):2707-2712.

106. N. Tillman, A. Ulman, J.S. Schildkraut, T.L. Penner. Incorporation of phenoxy groups in self-assembled monolayers of trichlorosilane derivatives: Effects on film thickness, wettability, and molecular orientation. J Am Chem Soc 1988;110(18):6136-6144.

107. D. Kowalczyk, S. Slomkowski, M.M. Chehimi, M. Delamar. Adsorption of aminopropyltriethoxy silane on quartz: an XPS and contact angle measurements study. Int J Adhes Adhes 1996;16(4):227-232.

108. S.K. BHATIA, K.J. Shriver-Lake, J.H. Prior, J.M. Georger, R. Calvert, F.S. Bredehorst, Ligler. Use of thiol-terminal silanes and heterobifunctional crosslinkers for immobilization of antibodies on silica surfaces. Anal Biochem 1989;178(2):408-413.

109. E.L. Schmid, Z. Keller, H. Dienes, Vogel. Reversible Oriented Surface Immobilization of Functional Proteins on Oxide Surfaces. Anal Chem 1997;69(11):1979-1985.

110. J.R. Cox, L.A. Ferris, V.R. Thalladi. Selective growth of a stable drug polymorph by suppressing the nucleation of corresponding metastable polymorphs. Angewandte Chemie (International ed.) 2007;46(23):4333-4336.

111. H. Sorribas, C. Padeste, T. Mezzacasa, L. Tiefenauer, L. Leder, D. Fitzli, P. Sonderegger. Neurite outgrowth on microstructured surfaces functionalized by a neural adhesion protein. Journal of materials science.Materials in medicine 1999;10(12):787-791.

112. N.A. Alcantar, E.S. Aydil, J.N. Israelachvili. Polyethylene glycol-coated biocompatible surfaces. J Biomed Mater Res 2000;51(3):343-351.

113. W.H. Briscoe, J. Klein. Friction and Adhesion Hysteresis between Surfactant Monolayers in Water. The journal of adhesion 2007;83(7):705-722.

114. C. Loskofsky, F. Song, B. Zhang Newby. Underwater adhesion measurements using the JKR technique. The journal of adhesion 2006;82(7):713-730.

115. B. Bhushan, H. Liu. Nanotribological properties and mechanisms of alkylthiol and biphenyl thiol self-assembled monolayers studied by AFM. Physical review.B, Condensed matter 2001;63(24):2454121-24541211.

116. B. Bhushan, T. Kasai, G. Kulik, L. Barbieri, P. Hoffmann. AFM study of perfluoroalkylsilane and alkylsilane self-assembled monolayers for anti-stiction in MEMS/NEMS. Ultramicroscopy 2005;105(1-4):176-188.

117. V.H. Dalvi, V. Srinivasan, P.J. Rossky. Understanding the Effectiveness of Fluorocarbon Ligands in Dispersing Nanoparticles in Supercritical Carbon Dioxide. The journal of physical chemistry.C 2010;114(37):15553-15561.

118. T. Di Paolo, C. Sandorfy. Hydrogen bond breaking potency of fluorocarbon anesthetics. J Med Chem 1974;17(8):809-814.

119. R.P. Dalvi VH. Molecular origins of fluorocarbon hydrophobicity. Proceedings of the National Academy of Sciences of the United States of America 2010;107(31):13603.

120. A.M.A. Dias, M. Freire, J.A.P. Coutinho, I.M. Marrucho. Solubility of oxygen in liquid perfluorocarbons. Fluid Phase Equilib 2004;222-223:325-330.

121. J.G. Riess. Oxygen carriers ("blood substitutes") - Raison d'etre, chemistry, and some physiology. Chem Rev 2001;101(9):2797-2919.

122. T. Shikata, M. Okuzono. Are all polar molecules hydrophilic? Hydration numbers of ketones and esters in aqueous solution. The journal of physical chemistry.B 2013;117(25):7718-7723.

123. J. Klein. Hydration lubrication. Friction 2013;1(1):1-23.

124. B. Wang, R.D. Oleschuk, J.H. Horton. Chemical force titrations of amine- And sulfonic acid-modified poly(dimethylsiloxane). Langmuir 2005;21(4):1290-1298.

125. D.A. Smith, M.L. Wallwork, J. Zhang, J. Kirkham, C. Robinson, A. Marsh, M. Wong. Effect of electrolyte concentration on the chemical force titration behavior of ω-functionalized SAMs: evidence for the formation of strong ionic hydrogen bonds. The journal of physical chemistry.B 2000;104(37):8862-8870.

126. W.H. Briscoe, S. Titmuss, F. Tiberg, R.K. Thomas, D.J. McGillivray, J. Klein. Boundary lubrication under water. Nature 2006;444(7116):191-194.

127. U. Raviv, S. Giasson, N. Kampf, J. Gohy, R. Jéröme, J. Klein. Lubrication by charged polymers. Nature 2003;425(6954):163-165.

128. H. Zeng. Polymer Adhesion, Friction, and Lubrication. Wiley. 2013.

129. S. Das, S. Chary, J. Yu, J. Tamelier, K.L. Turner, J.N. Israelachvili. JKR Theory for the Stick–Slip Peeling and Adhesion Hysteresis of Gecko Mimetic Patterned Surfaces with a Smooth Glass Surface. Langmuir 2013;29(48):15006-15012.

130. W. Chen, A.S. Foster, M.J. Alava, L. Laurson. Stick-Slip Control in Nanoscale Boundary Lubrication by Surface Wettability. American Physical Society,. 2015.

131. J. Hladílková, H.E. Fischer, P. Jungwirth, P.E. Mason. Hydration of hydroxyl and amino groups examined by molecular dynamics and neutron scattering. The journal of physical chemistry.B 2015;119(21):6357-6365.

132. H. Kesari, J.C. Doll, B.L. Pruitt, W. Cai, A.J. Lew. Role of surface roughness in hysteresis during adhesive elastic contact. Philosophical magazine letters 2010;90(12):891-902.

133. S. Chen, L. Li, C. Zhao, J. Zheng. Surface hydration: Principles and applications toward low-fouling/nonfouling biomaterials. Polymer 2010;51(23):5283-5293.

134. N. Graham, N. Nwachuku, D. Walsh. Interaction of poly(ethylene oxide) with solvents: 1. Preparation and swelling of a crosslinked poly(ethylene oxide) hydrogel. Polymer 1981;23(9):1345-1349.

135. N. Graham, M. Zulfiqar, N. Nwachuku, A. Rashid. Interaction of poly(ethylene oxide) with solvents. 2 Water-poly(ethylene glycol). Polymer 1989;30(3):528-533.

136. N. Graham, M. Zulfiqar, N. Nwachuku, A. Rashid. Interaction of poly(ethylene oxide) with solvents. 4. Interaction of water with poly(ethylene oxide) crosslinked hydrogels. Polymer 1990;31(5):909-916.

137. W.R. Gombotz, W. Guanghui, T.A. Horbett, A.S. Hoffman. Protein adsorption to poly(ethylene oxide) surfaces. J Biomed Mater Res 1991;25(12):1547-1562.

138. J. Forsstrom, M. Eriksson, L. Wagberg. A new technique for evaluating ink-cellulose interactions: initial studies of the influence of surface energy and surface roughness. J Adhes Sci Technol 2005;19(9):783-98.

139. M. Eriksson, S. Notley, L. Wagberg. Cellulose thin films: Degree of cellulose ordering and its influence on adhesion. Biomacromolecules 2007;8(3):912-919.

140. M. Norgren, L. Gardlund, S. Notley, M. Htun, L. Wagberg. Smooth model surfaces from lignin derivatives. II. adsorption of polyelectrolytes and PECs monitored by QCM-D. Langmuir 2007;23(7):3737-3743.

141. D. Pasquini, D. Balogh, P. Antunes, C. Constantino, A. Curvelo, R. Aroca, O. Oliviera. Surface morphology and molecular organization of lignins in Langmuir-Blodgett films. Langmuir 2002;18(17):6593-6596.

142. M. Micic, M. Jeremic, K. Radotic, M. Mavers, R.M. Leblanc. Visualization of artificial lignin supramolecular structures. Scanning 2000;22(5):288-294.

143. S. Lee, P. Luner. Wetting and interfacial properties of lignin. Tappi 1972;55(1):116-122.

144. G. Chinga-Carrasco, K. Syverud. Pretreatment-dependent surface chemistry of wood nanocellulose for pH-sensitive hydrogels. J Biomater Appl 2014;29(3):423-432.

145. M. Müller, C. Czihak, H. Schober, Y. Nishiyama, G. Vogl. All Disordered Regions of Native Cellulose Show Common Low-Frequency Dynamics. Macromolecules 2000;33(5):1834-1840.

146. J. Yang, C. Han, F. Xu, R. Sun. Simple approach to reinforce hydrogels with cellulose nanocrystals. Nanoscale 2014;6(11):5934-5943.

147. X. Yang, E. Bakaic, T. Hoare, E.D. Cranston. Injectable Polysaccharide Hydrogels Reinforced with Cellulose Nanocrystals: Morphology, Rheology, Degradation, and Cytotoxicity. Biomacromolecules 2013;14(12):4447-4455.

148. D. Ciolacu, A.M. Oprea, N. Anghel, G. Cazacu, M. Cazacu. New cellulose–lignin hydrogels and their application in controlled release of polyphenols. Materials Science and Engineering: C 2012;32(3):452-463.

149. L.C. Fidale, N. Ruiz, T. Heinze, O.A. El Seoud. Cellulose swelling by aprotic and protic solvents: What are the similarities and differences?. Macromolecular chemistry and physics 2008;209(12):1240-1254.

150. S. Notley, M. Norgren. Measurement of interaction forces between lignin and cellulose as a function of aqueous electrolyte solution conditions. Langmuir 2006;22(26):11199-11204.

151. P.C.H. Li. Microfluidic Lab-on-a-Chip for Chemical and Biological Analysis and Discovery. CRC Press. 2006.

152. J.N. Israelachvili. Intermolecular and Surface Forces. Academic Press. 2011.

153. W. Hu, H.R. Brown, J.T. Koberstein, R. Bhatia, J. Lingelser, Y. Gallot. Adhesion enhancement of polymer blend interfaces by reactive block copolymer brushes. Comptes rendus.Chimie 2006;9(1 SPEC. ISS.):45-59.

154. K. Kishi, T. Ishimaru, M. Ozono, I. Tomita, T. Endo. Development and application of a latent hydrosilylation catalyst. IX. Control of the catalytic activity of a platinum catalyst by polymers bearing amine moieties. Journal of polymer science.Part A, Polymer chemistry 2000;38(5):804-809.

Appendix A - Hydrosilylation Technique

This appendix presents the JKR results obtained for PDMS samples treated with a number of different functional groups via the hydrosilylation technique. It also describes the procedure that was used to functionalize PDMS samples using the hydrosilylation technique and the chemicals that were exploited. The functional groups selected for the hydrosilylation treatment in this study included methyl, carboxylic acid, amine, and hydroxyl groups. Amongst these four groups the results of the three former are shown here because the samples that were treated with hydroxyl showed inconsistent behavior.

In the hydrosilylation-based treatment, a surface rich in silane group (Si-H) reacts with unsaturated compounds (e.g. a vinyl group) in the presence of a platinum (Pt) catalyst. In order to functionalize PDMS surfaces by this approach, a 5:1 mixing ratio, which produces Si-H rich PDMS surfaces, was used. The following procedure was followed to functionalize 5:1 PDMS samples:

1. Cured samples were immersed in a solution of xylene (99% v/v), the vinyl-based chemical compound (0.5% v/v) (see Table A.1), and Pt catalyst (0.5% v/v) for 1h.
2. PDMS samples were rinsed with xylene and stored in a petri dish that was allowed to be air ventilated.

Table A.1 The vinyl-based chemicals used for the hydrosilylation technique

Functionality	Reactive Chemical	Supplier
Amine	1-amino-10-undecene	GFS Chemicals
Carboxylic acid	Undecylenic acid	Sigma Aldrich
Hydroxyl	10-Undecen-1-ol	Sigma Aldrich
Methyl	1-Undecene	Sigma Aldrich

Because of the similarity between the chemistry of the methyl group and native PDMS, the methyl group was selected as a basis to verify the effect of the hydrosylilation technique on

PDMS properties (compliance, color, etc.). As is shown in Figure , PDMS functionalized with the methyl group showed a large hysteresis when contacting a native PDMS flat sheet (in air); whereas no hysteresis was observed when a clean glass surface or methyl-treated PDMS sheet was used as the substrate (in air). This was attributed to the interactions between the chains of the native PDMS substrate and the Pt catalyst in the methyl-treated hemisphere [153]. No hysteresis was observed (in air) between the methyl-treated PDMS hemispheres and native PDMS sheets after poisoning the Pt catalyst using a thiol-based agent (1-dodecanethiol) [54]. No significant difference was seen in the bulk modulus of PDMS after methyl treatment, although PDMS samples turned yellowish after the treatment. The color change, however, did not affect the transparency of the PDMS probes. The results obtained from the methyl treatment highlighted the effects of the Pt catalyst and further poisoning of that on the interactions in air.

Figure A.1 The effect of catalyst poisoning in the adhesion hysteresis of methyl-treated PDMS hemisphere in contact with native PDMS sheet

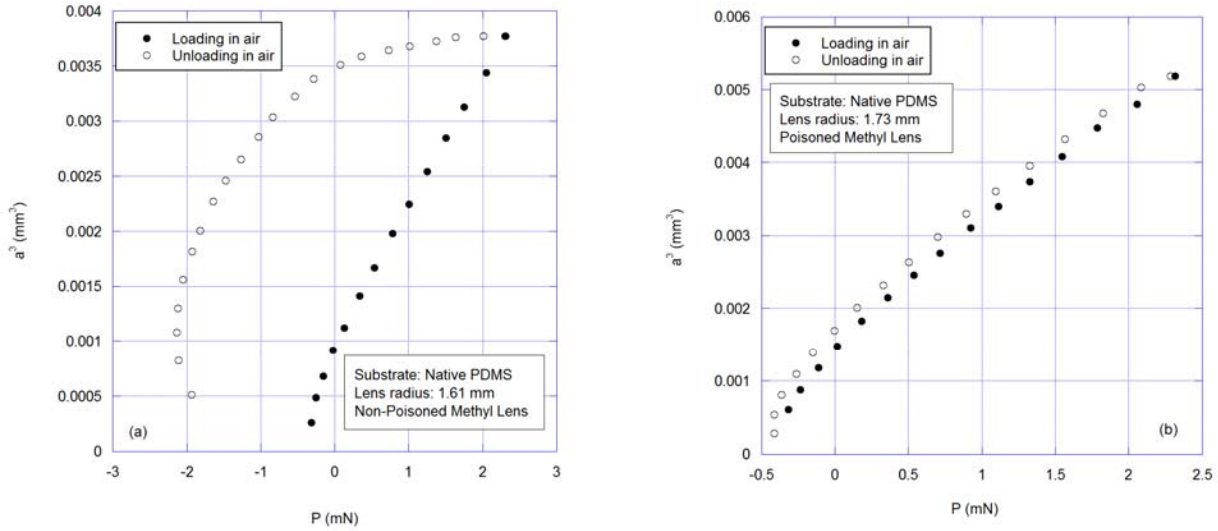

Such behavior in hysteresis difference, but to a much smaller extent, was observed for PDMS hemispheres treated with carboxylic acid in contact with native PDMS flat sheets in air, see Figure . It was anticipated that the carboxylic acid group does poison the Pt catalyst to some extent. The hysteresis (in air) was further reduced when treated hemispheres were poisoned with

the thiol agent. For the samples treated with the carboxylic acid group, there was also a color change after the treatment, although PDMS still remained transparent.

Figure A.2 The effect of catalyst poisoning in adhesion hysteresis of carboxylic acid-treated PDMS hemisphere in contact with native PDMS sheet

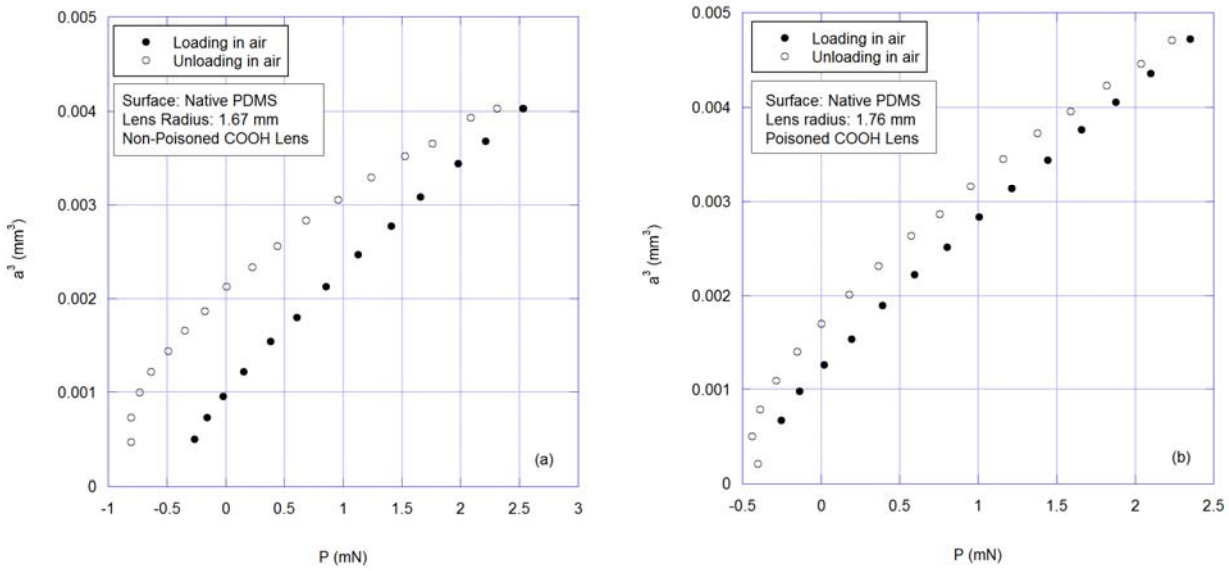

When the hydroxyl-treated PDMS probes were in contact with native or hydroxyl-treated PDMS sheets, no consistent results (in terms of adhesion hysteresis) were obtained before or after the Pt catalyst poisoning. Therefore, no results are shown here. This was associated to the incomplete reactions between PDMS and the agent used for the treatment.

As can be seen in Figure A.3, the amine-treated hemispheres in contact with PDMS flat sheets showed no remarkable differences before and after poisoning of the Pt catalyst. It has been shown that the effect of the Pt catalyst is suppressed in the hydrosilylation technique if amine-bearing moieties are utilized [154].

Figure A.3 The effect of the catalyst poisoning in adhesion hysteresis of amine-treated PDMS hemisphere in contact with native PDMS sheet

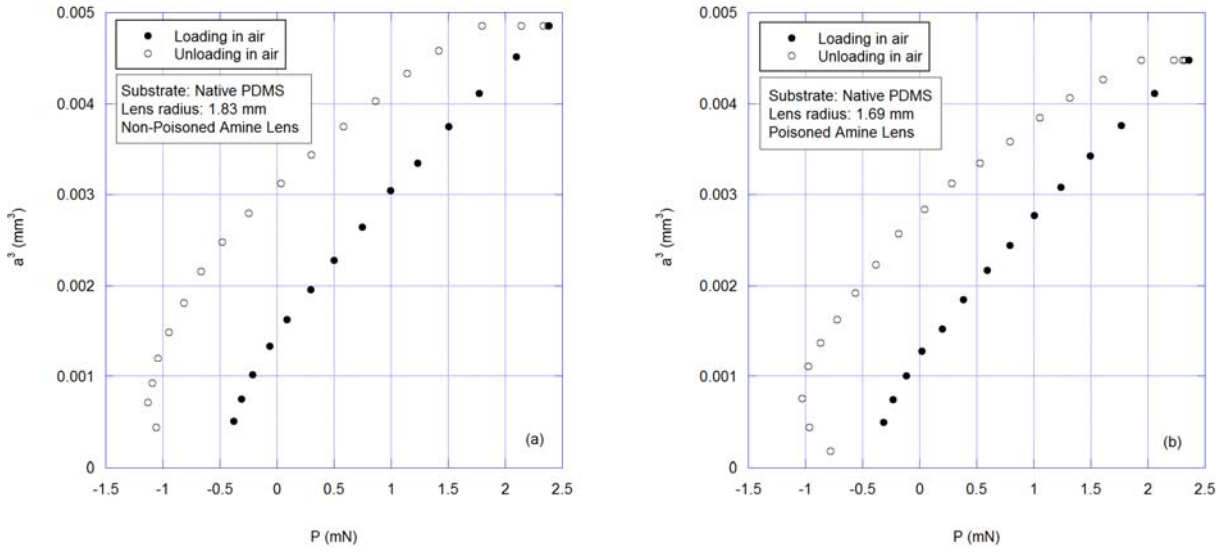

Here it should be noted that amine-treated PDMS hemispheres were poisoned and used in contact with native PDMS sheets for the JKR experiments. The results showed consistent hysteresis in air. Underwater, however, the hysteresis was significantly different from one sample to another. When amine-treated hemispheres were in contact with amine-treated PDMS sheets (both poisoned) consistent hysteresis was seen both in air and underwater. This discrepancy could not be explained. Therefore, this method was not pursued for PDMS modification.